EVALUATION OF THE STRUCTURAL PERFORMANCE OF BRIDGE MSE RETAINING WALLS

by

ZAID MOMANI

Presented to the Faculty of the Graduate School of

The University of Texas at Arlington in Partial Fulfillment

of the Requirements

for the Degree of

DOCTOR OF PHILOSOPHY

THE UNIVERSITY OF TEXAS AT ARLINGTON

December 2019

Acknowledgments

First and foremost, I acknowledge my gratitude to my God for giving me the strength to complete this research. My deepest appreciation goes to my advisor Dr. Nur Yazdani for his generous guidance, consistent support and advice through all stages of this research work. I am thankful to Dr. Sahadat Hossain, Dr. Suyun Ham, and Dr. Chen Kan for readily accepting to serve on my dissertation committee. I want to thank them for their support during my study. I will always be thankful to the Civil Engineering Department at UT Arlington for supporting me throughout my research work.

I am thankful to my friends Dr. Eyosias Beneberu, Dr. Santosh Timilsnia, Dr. Tariq Al Jaafreh, Dr. Natawut Chaiwino, Dr. Yazan Almomani, Towfiqul Quadir, Ikram Efaz, Mohd Rahman, Khadiza Jalal, Karzan Habeeb, Nice Kaneza, Sean Natelli, and Adams Siphanh for all the help during the research work.

I am deeply grateful to my family who stood by my side through the entirety of this research.

November 24, 2019

Abstract

EVALUATION OF THE STRUCTURAL PERFORMANCE OF BRIDGE MSE RETAINING WALLS

Zaid Momani, PhD

The University of Texas at Arlington, 2019

Supervising Professor: Nur Yazdani

Mechanically Stabilized Earth (MSE) walls have been used extensively since the first MSE wall constructed in California in the early 70's. MSE walls proved that they are reliable, cost-effective, aesthetically pleasing, and easily constructible. However, the design criteria of an MSE wall does not always incorporate the comprehensive behavior. A reasonable number of MSE walls do not perform as expected; a few experienced catastrophic failure. The current study was inspired by multiple MSE walls showing excessive movement of the precast panels in Fort Worth and Hurst, Texas. Three most critical MSE walls were selected for this study. The main focus of this research is to 1) periodically monitor the movement of the walls; 2) evaluate the effect of wall movement on earth reinforcement, precast panels, approach slab, copings and traffic barriers; 3) recommend remedial measures on the earth reinforcement to prevent rupture or pullout; 4) perform several field and lab tests on the backfill soil material to check the integrity of the backfill soil; and 5) develop a 3D Finite Element Modeling (FEM) of an MSE wall using ABAQUS software to predict the actual behavior of an MSE wall and investigate the wall

failure criteria. Several non-destructive tests were performed on the critical walls. A laser scanner was used to monitor the movement of the precast panels. Ground Penetrating Radar (GPR) was used to examine the integrity of the earth reinforcement. A subsurface investigation was conducted using Resistivity Imaging (RI) technique to investigate the presence of groundwater table or perched water zones. Regression and structural reliability analyses were carried out to investigate the effect of significant parameters on wall performance and check the integrity of MSE wall design formulas of FHWA (2009), respectively.

Table of Contents

List of Figures

List of Tables

Chapter 1
INTRODUCTION

1.1 Background

Mechanically Stabilized Earth (MSE) wall structure has become the most common type of earth retaining wall structures among the U.S. It can be used to either support bridge abutments or retain embankment fills. MSE walls are continually growing in number; approximately more than 210 acres of MSE walls are constructed in U.S. every year (Berg et al. 2009). Also, MSE walls become crucial as the height increases; this is because the cost of traditional reinforced concrete retaining walls increases rapidly while increasing the height. MSE walls have notably decreased the cost compared to traditional retaining walls.

MSE walls have been used extensively since the first MSE wall constructed in California in the early 1970's. MSE walls using metal or geosynthetic reinforcements proved that they are reliable, cost-effective, aesthetically pleasing, and easily constructible. The system of an MSE wall consists of facings, reinforced (backfill) soil, earth reinforcement, retained soil, and foundation soil, as shown in Figure 1-1. The facings are typically made of precast concrete panels (PCP), cast-in-place (CIP) panels, and modular blocks, and are used to hold the reinforced soil from falling out of the MSE wall. The retained soil is the selected fill material which is placed between the selected reinforced soil and the natural soil. The reinforced soil is the selected backfill where the

reinforcement layers are embedded and required to have good shear resistance and sufficient drainage characters (FHWA 2009).

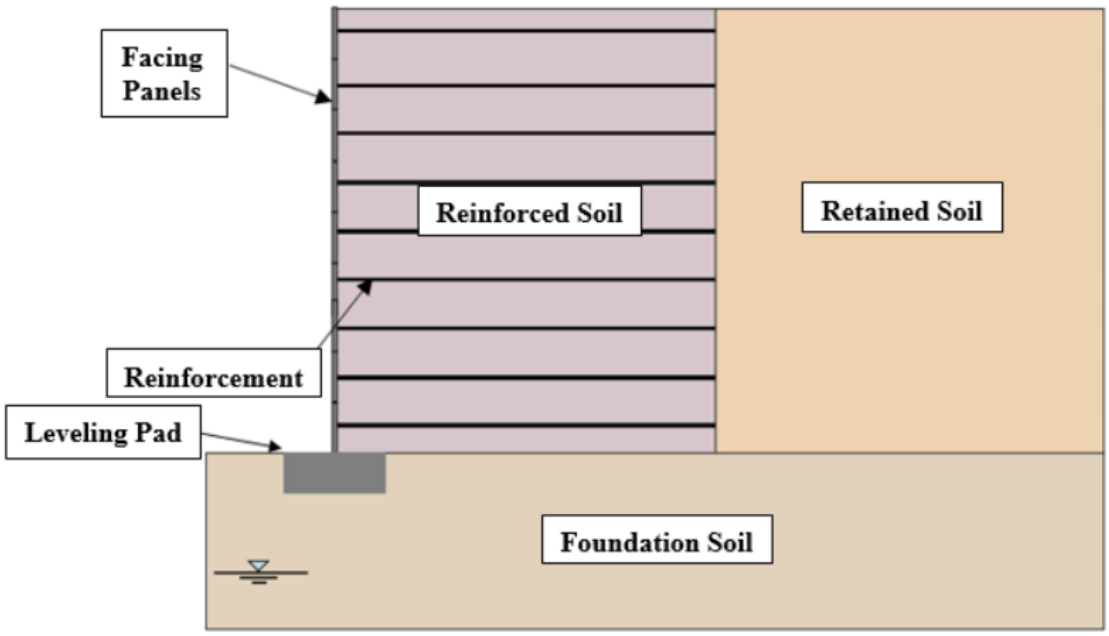

Figure 1-1 Cross-sectional view of an MSE wall

MSE walls are classified in two categories based on the extensibility of the reinforcement material. The material is considered inextensible when its strains at failure are very small comparing to the backfill soil strains, while it is considered extensible when its strains at failure are close or comparably higher than the soil strains (FHWA 2009). The first type requires the reinforcement material to have stiffness much higher than that in the soil, such as metallic reinforcement (steel strips or welded wire grids), while the stiffness of the extensible material is comparable to that of the soil, such as a polymeric materials that consist of polypropylene, polyethylene, or polyester.

The internal stability of an MSE wall depends on the reinforcement properties, such as reinforcement type, length, and spacing. The external stability relies on restraining an MSE wall from global failure modes, such as sliding, overturning, bearing, and slope stability. Adams and Nicks (2017) found that the main five factors that may lead to MSE wall failure are: design approach, backfill soil condition, coordination, existence of pore pressure, and construction. The application of an MSE wall system is to retain soil using its own self-weight. Its design relies on a series of internal and external stability checks, however, it does not always incorporate the comprehensive behavior of MSE walls.

MSE walls have notably simplified the design and construction of the bridge abutments. This is because it requires less site preparation, allows faster construction, and leads to cost saving. Tarawneh et al. (2017) performed a large-scale inspection program which consists of 339 MSE walls to identify the most frequent MSE wall problems. It was found that only 5% of the MSE walls exhibit no issues while the rest have a variety of problems, such as drainage, backfill soil leaking, exposed leveling pads, bulging of the facing panels, cracked panels, and vegetation, as shown in Figure 1- 2.

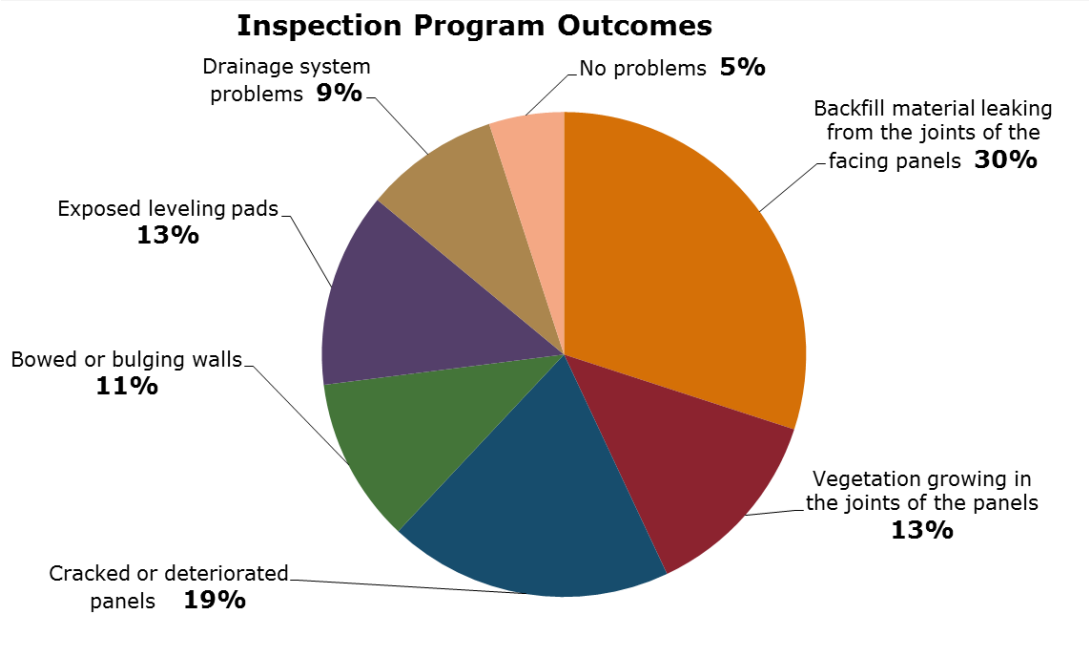

Figure 1- 2 Inspection program outcomes on MSE walls (Tarawneh et al. 2017)

Armour et al. (2004) investigated a case history of a 25 year old MSE wall that exhibited a catastrophic failure in Soda Springs, Idaho. Six precast panels fell out in 2002 (Figure 1-3). After a wide investigation, it was determined that the cause of the failure was due to corroded steel strips that sheared at the panel connections. It was found that the lateral earth pressure applied at the facing panels exceeded the connection's tensile strength.

Figure 1-3 Failed MSE wall at Soda Springs, Idaho (Armour et al. 2004)

MSE walls are often characterized by redundancy; if the failure occurs at some of the reinforcement layers, the wall may not collapse since the rest of the reinforcement layers will be responsible to carry increased loads. This aspect is typically ignored by previous models. A case study (Zevgolis and Bourdeau 2008) regards this aspect by modeling a stochastic MSE wall to assess the internal stability of an MSE wall. To account for the redundancy nature, the reinforcement layers were modeled as an individual in-series system. This means when a layer fails due to pullout or rupture, it will no longer contribute in resisting the internal forces. The results show that most of the failure modes occur due to pullout of reinforcements.

Significant wall movement may be caused by poor quality of backfill soil and poor drainage system. Hossain et al. (2011) investigated a case study of an MSE wall located at State Highway 342 in Lancaster, Texas, which showed a lateral movement ranged between 12-18 inches in only 5 years after construction. Several site and laboratory tests were performed to detect the cause of the movement. The results of the tested soil samples obtained from the backfill soil show that the soil contains high content of clayey sand according to the Unified Soil Classification System.

Bearing pads are secondary elements in an MSE structure and are used to maintain vertical and horizontal joint width, provide flexibility of the facing panels, allow permeability, and prevent intact between the concrete panels which would lead to developing distresses and spalling of concrete. On the other hand, bearing pads are not designed properly to fully withstand the stresses developed in the concrete panels. Hence, excessive stresses may lead to crushing of bearing pads and spalling of the adjacent concrete, as shown in Figure 1-4. To avoid failure of bearing pads, they should be accounted in MSE wall design (Neely and Tan 2010).

Figure 1-4 Spalling of concrete near failed bearing pads (Neely and Tan 2010)

A history case of a 45 ft high MSE wall located in Arizona was evaluated by Samtani and Alexander (2005). After performing wide investigation, it was found that the MSE wall was experiencing external stability issues. The maximum recorded differential movement between the facing panels was 5 inches at distance of 30 to 70 ft from the wall corner, as shown in Figure 1-5 (a). Also, it was noted that there was an outward movement of the traffic barrier (Figure 1-5 (b)) as well as separation between the backfill soil and the facing panels (Figure 1-5(c)). By looking at the distress pattern, it is appeared that the failure was due to bearing capacity failure of the foundation soil which has led to global stability failure. Also, it was found that the used reinforcement length is 0.7H (H is the wall height) which is the minimum recommended length by FHWA (2009). Hence, the failure may also be due to insufficient reinforcement length.

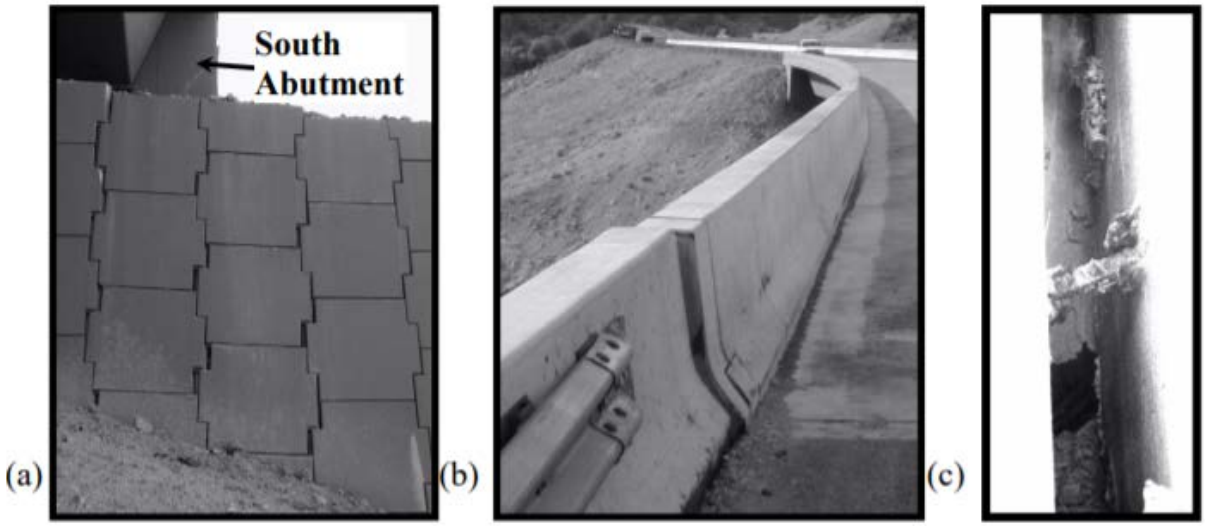

Figure 1-5 (a) Openings between the MSE wall panels, (b) Outward rotation of the railroad, and (c) Separation between the panels and backfill soil (Samtani and Alexander 2005)

Scarborough (2005) investigated two case histories of failed MSE walls. After performing several investigations, it was determined that the cause of the catastrophic failure of the first MSE wall that failed after one year of construction was most probably due to low permeability. A backfill soil with low permeability is not desired in an MSE structure as it leads to adding hydrostatic pressure on the facing panels which would significantly increase the lateral earth pressure. The failure of the second wall that occurred after nine months of construction was due to serviceability. The designer did not account properly for the global stability in the MSE wall design which has led to global failure.

1.2 Problem Statement

MSE walls offer notable technical and cost advantages over conventional reinforced concrete retaining structures. The application of an MSE wall system is to retain soil using its own self-weight. Its design relies on a series of internal and external stability checks, however, it does not always incorporate the comprehensive behavior of MSE walls. A reasonable number of MSE walls does not perform as expected; a few of them have experienced catastrophic failure. The design of reinforcements, such as metal and geosynthetic reinforcement, are based on internal stability checks of MSE walls, rupture and pullout. However, there is a lack in understanding the effect of reinforcements on comprehended behavior of MSE walls.

The current study was inspired by multiple MSE walls, showing excessive movement on the precast panels in Fort Worth and Hurst, Texas. Three of the most critical MSE walls were selected for this study as they are exhibiting several issues, including cracks on wall copings, cracks on traffic barriers, bulging of precast panels, differential movement between precast panels, opening of corner joints, and leakage of backfill soil.

Failure analysis should be conducted on the MSE wall design to investigate if there is any lack in designing precast panels and earth reinforcement. These uncertainties in the design parameters affect the internal stability of MSE walls. Also, a method should be developed to monitor the movements of an MSE wall to determine whether these movements are ongoing or they cease to have further movements.

1.3 Objectives

This study investigates the performance of MSE wall structures that have experienced significant deformations and distresses. It aims to improve the public safety by ensuring the MSE wall structures are strong and safe in carrying the anticipated traffic loading by detecting the causes of the severe deformations and recommend remedial measures on the MSE wall design guidelines. Due to lack of research regarding fully understanding the behaviour of MSE wall structures, the performance of these structures is evaluated by analytical models and field measurements. A significant improvement in MSE structures is expected through the developed knowledge, guidelines, analytical and test methods for MSE structures. The proposed research involves non-destructive evaluation, movement monitoring, backfill soil testing, FE modeling, and regression and structural reliability analyses. This research was conducted with the following main objectives:

- Develop a strategy to monitor MSE wall movement.
- Evaluate the effect of wall movement on reinforcements, panels, abutment, approach slab, and barriers.
- Investigate the design considerations of earth reinforcement.
- Perform several site investigations on the backfill soil material to check if it agrees with TxDOT specifications.
- Conduct a finite element modeling using ABAQUS software to predict the actual MSE wall behavior.

- Perform a parametric study using ABAQUS software to investigate the effect of the main parameters of MSE walls that may potentially lead to a failure of MSE walls. The parametric study is initiated using the Design of Experiment (DOE) by using Minitab software.
- Analyze the outcomes of the parametric study through comparing the maximum out-of-plane movement of precast panels, maximum stresses developed in earth reinforcement and their respective locations, and crack propagations on precast panels, copings, traffic barriers, and approach slab.
- Perform a regression analysis to assess the effect of the wall parameters of the parametric study on the lateral wall movement.
- Perform a structural reliability analysis to investigate the accuracy of the most recent code used for MSE wall design by FHWA, and check if any recommendations are needed to improve the overall performance of MSE walls.

1.4 Organization of the Dissertation

The dissertation is organized into seven different chapters. The content of the chapters is described below.

Chapter 2- Literature Review

This chapter presents a review of previously carried out research on the following areas: 1) history cases of failed MSE walls; 2) MSE wall design methodology; 3)

experimental and numerical evaluation of MSE walls; 4) internal stability checks of MSE walls; and 5) MSE wall types.

Chapter 3- Background of the Investigated MSE Walls

A precise description and inspection on the three investigated MSE walls are presented in this chapter.

Chapter 4- Evaluation of MSE Walls

Non-destructive evaluation, backfill soil testing, and movement monitoring techniques are talked about in detail in this chapter.

Chapter 5- Finite Element Modeling

Material properties, contact properties, modeling techniques, and analysis procedure for obtaining a full-scale baseline model in ABAQUS of an MSE wall structure are presented in this chapter. Material testing, mesh refinement, applying simulated geostatic pressure on backfill soil, and steps to obtain a calibrated finite element model are detailed. Results of a parametric study obtained on the numerical model are presented in this chapter to investigate the effect of varying MSE wall parameters on the performance of the MSE wall.

Chapter 6- Regression and Structural Reliability Analyses

The results obtained from the parametric study are compared in this chapter. Developing correlations and generating charts between the parameters are also

presented by performing regression analysis. Structural reliability analysis is carried out on the FHWA (2009) formulas used for designing MSE walls and presented in this chapter.

Chapter 7- Conclusions and Recommendations

The summary of the research conducted is presented. The conclusions drawn from MSE wall's evaluation, FE modeling, parametric study, regression analysis, and structural reliability analysis are mentioned. Recommendations for further research is finally made.

Chapter 2
LITERATURE REVIEW

2.1 Introduction

This chapter covers previously carried out research on the following areas: 1) history cases of failed MSE walls; 2) MSE wall design methodology; 3) experimental and numerical evaluation of MSE walls; 4) internal stability checks of MSE walls; and 5) MSE wall types.

2.2 History Cases of Failed MSE Walls

Nowadays, earth reinforcement structures usually indicate soil stabilization throughout the use of embedded reinforcements. These reinforcements are made of steel or polymer materials and placed between compacted soil layers to provide confinement to the backfill soil. The concept of reinforced earth structures was introduced by Henri Vidal (1969) in France, and in 1971 it was brought to the U.S. for a major landslide repair on Highway 39 in the Angeles National Forest, CA. Soil reinforced structures using geosynthetic reinforcement were initially introduced in the 1980's. Afterwards, this MSE wall type raised in number dramatically in the 1990's when the segmental facings became popular (Mahmood 2009).The retaining walls that were built before 1960s were mainly made of rigid reinforced concrete. These types of structures perform as expected for a long service-life; however, they become costly as the wall height increases (Ambauen 2014). Vidal's new theory involved retaining the backfill soil through the use of embedded steel strips connected to facing units, resulting in significant cost savings compared to the

traditional retaining walls. The use of tensile reinforcement in a retaining wall system, referred to as mechanically stabilized earth (MSE) wall, increases significantly the backfill soil's internal shear resistance, which generates a self-supporting structure through transferring shear forces to the adjacent reinforcements as yielding occurs (Mitchell and Villet 1987). The major advantage of using MSE wall system is the inherent variety and the aesthetic of their components, with different facing and reinforcement types, and wall configurations (Ambauen 2014).

A finite element numerical modeling was conducted on a failed 38 ft high MSE wall. The MSE wall failure criteria was compared along with the numerical modeling results (Kim et al. 2010). The MSE wall consisted of segmental precast panels, selected compacted backfill soil, and reinforcing steel strips. Some of the precast panels were installed atop caissons which were previously built for an adjacent project. It was found that the reinforcement-panel connections sheared at 10 of the caisson locations as a result of differential movements. The differential movements led to developing extra stresses which exceeded the connections' tensile strength; thus, the connections collapsed and the attached panels fell out of the MSE wall and had to be replaced (Figure 2-1).

Figure 2-1 MSE wall repair (Kim et al. 2010)

The Texas Department of Transportation (TxDOT) was concerned about an MSE wall as its approach slab exhibited cracks as well as an observed loss of backfill soil at the locations of the cracks, as shown in Figure 2-2. TxDOT was trying to correlate whether the cracks are related to the backfill soil loss or not. Chen et al. (2007) conducted several destructive and non-destructive tests to determine the causes of these cracks. Based on the data analysis, the cracks occurred shortly after constructing the MSE walls due to temperature variation; therefore, the cracks that appeared on the approach slab were unrelated to the loss of backfill soil.

(a)

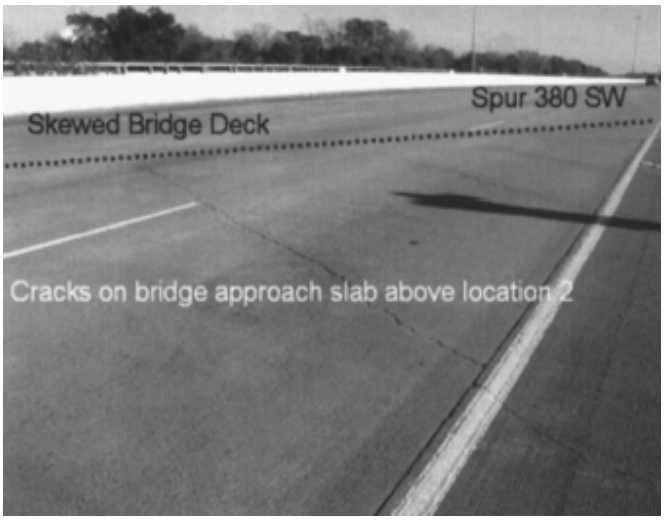

(b)

Figure 2-2 (a) Leaking sand, and (b) Cracks on the approach slab atop the MSE wall (Chen et al. 2007)

The Ohio Department of Transportation concluded that building MSE walls with acute angles (Figure 2-3) should be avoided (Alzamora et al. 2009). As the Ohio DOT explained, it becomes hard to construct the reinforcement layers because of the overlapping of reinforcements. They also explained that the overall performance will not

be at its peak because the backfill soil will lose some of its shear strength because of the overlapping of the reinforcements that caused poor confinement of the backfill soil. Also, the MSE wall will not perform well if there is any obstructions, such as drainage structures or piles, and this may increase the risk of an internal failure.

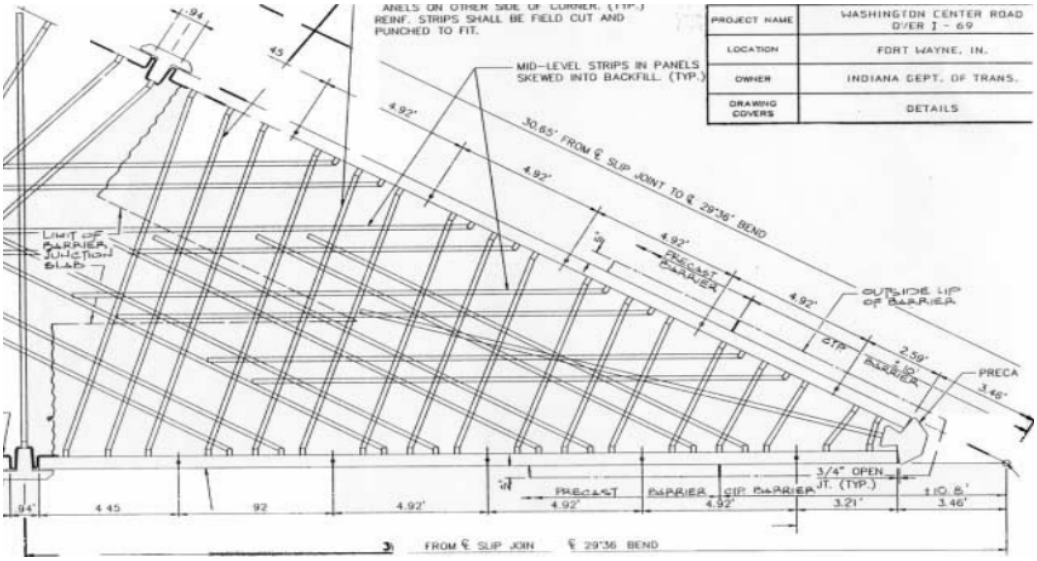

Figure 2-3 Overlapping of earth reinforcement of an MSE wall

The creep of geosynthetics plays a role in increasing the deformation of MSE walls. Liu and Won (2009) developed a finite element modeling to investigate the creep effect of clay and geosynthetic reinforcement on an MSE wall performance. A long-term analysis was carried out for a 26 ft high wall. The data was conducted along 5 years after the wall was constructed. It was found that, by comparing the results data with the creep parameters of backfill soil and geosynthetic reinforcement, the creep affects not only the wall deformation, but also the stresses among the reinforcement and backfill soil.

2.3 MSE Wall Design Methodology

2.3.1 Internal Stability Design

As mentioned in many geotechnical design methodologies, the design of an MSE wall is based on experimental observations. The internal failure of an MSE wall occurs due to shear of panel-reinforcement connection, rupture of reinforcement, or pullout of reinforcement from the reinforced soil zone. The most critical one of these failure mechanisms is the rupture for geosynthetic reinforced MSE walls as the geosynthetic reinforcement is expected to yield since it is designed as extensible material (Helwany et al. 2003). Furthermore, the geosynthetic reinforced MSE walls have better inter-locking property between the grid openings and soil particles; therefore, this type of MSE walls most likely does not fail due to pullout (Lee 2000; Yoo and Kim 2008).

When the reinforcement yields, large deformations are expected to occur; hence, the MSE wall may be at risk of reaching serviceability limits or collapse (Ambauen 2014). The maximum tensile load that is developed in reinforcement can be predicted using Equation 2.1:

$$T_{MAX} = S\,\sigma_H \tag{2.1}$$

where S is the tributary area for a single reinforcement layer and σ_H is the horizontal (lateral) earth pressure estimated at specific reinforcement layer. As stated in Equation 2.1, the lateral earth pressure is used to estimate the maximum developed tensile force in reinforcement. The calculation of the lateral earth pressure relies on the value of the

lateral earth pressure coefficient, K_r, which varies based on depth of reinforcement. Several design methodologies were developed for this purpose. These methods are empirically based, through evaluations of previously carried out research on MSE walls. However, they have small varieties in estimating the "K_r" value, as well as locating the critical slip surface of an MSE wall, which indicates the location of where the maximum tension of reinforcement occurs at each reinforcement layer. The most common design methods are:

- Coherent Gravity
- Tieback Wedge
- FHWA Structure Stiffness
- Working Stress
- AASHTO Simplified
- K-Stiffness
- Design and Construction of MSE Walls and RSS

Coherent Gravity Method (Schlosser 1978)

As stated above, these methods are empirically based from previously instrumented MSE walls. Therefore, the design procedure of each method limits its applicability to the MSE wall types that are within the range of those which were used for calibration. For instance, the Coherent Gravity method proposed by Schlosser (1978) investigated only case histories of MSE walls reinforced with steel strip reinforcements; therefore, it does not perform well for the welded wire reinforcements as well as the extensible

reinforcements. The design methodology of the Coherent Gravity Method is represented in Figure 2-4 and the bullet points below.

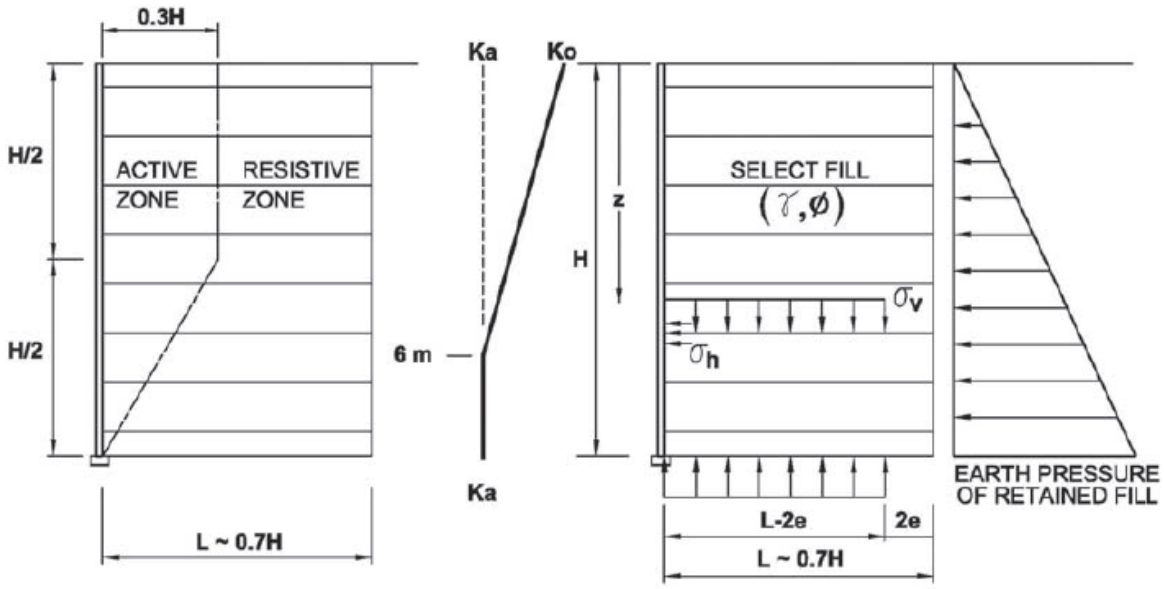

Figure 2-4 Coherent Gravity method characteristics (Schlosser 1978)

- A rectangular block is identified by the MSE wall height, H, and the reinforcement length, L, (Figure 2-4).
- The vertical and horizontal forces applied to the block create eccentric loadings.
- The vertical earth pressure developed at the reinforcement layers are calculated based on Meyerhof bearing pressure theory (Meyerhof 1953).
- The state of stress is at rest (K_o) at the top of the MSE structure, gradually decreases to active state (K_a) at a depth of 20 ft (6 m), then it becomes constant up to the bottom of MSE structure (Figure 2-4).

- Each reinforcement level is responsible to restrain the tensile forces acting on its tributary area.
- The active zone through the reinforcement length is separated from the effective zone by a bilinear envelope (Figure 2-4).
- The internal stability is maintained by the inextensibility and pullout resistance of the reinforcements.

Tie-back Wedge Method (Bell et al. 1975)

While the Coherent Gravity method accounts for both at rest and active pressure states in predicting the failure surface, the Tie-back method (Bell et al. 1975) only uses the active earth pressure to predict the pressures developed in geosynthetic reinforced soil walls. The stiffness of the geosynthetic reinforcement is low compared to that of the metal reinforcement. Thus, the geosynthetic reinforcement allows higher lateral movements of the facings, and that lowers the tensile stress developed in the geosynthetic reinforcement. The horizontal stress (σ_H) at each reinforcement level is calculated using the Tie-back method as:

$$\sigma_H = \sigma'_a = K_a \sigma'_V = K_a \gamma z \quad (2.2)$$

where σ'_a is the active lateral earth pressure, K_a is the active earth pressure coefficient, and σ'_V is the vertical effective stress (can be calculated as the unit weight of the backfill soil (γ) multiplied by the depth (z)). As stated in Equation 2.2, the Tie-back method is

based on ultimate limit states; therefore, it tends to over-predict the lateral stresses acted on the reinforcement levels which may not be safe for the MSE structures.

FHWA Structure Stiffness Method (Christopher 1993)

The Structure Stiffness method developed by the Federal Highway Administration (FHWA) was generated to suit both types of reinforcements, extensible and inextensible reinforcements, and allow for any design considerations, such as reinforcement strength and spacing. This versatility in the design made it widely accepted by the designers. The global index (S_r) of reinforcement stiffness can be calculated as:

$$S_r = \frac{J_{ave}}{(\frac{H}{n_r})} \tag{2.3}$$

where J_{ave} is the average tensile stiffness index, and n_r is the number of reinforcement layers. The calculations of the stiffness relationships were found as:

$$K_r = \begin{cases} K_a(\Omega_1\left(1 + 0.4\frac{S_r}{1000}\right)\left(1 - \frac{z}{20}\right) + \Omega_2\frac{z}{20}) & z \le 20 \text{ ft} \\ K_a\Omega_2 & z > 20 \text{ ft} \end{cases} \tag{2.4}$$

where Ω_1 and Ω_2 are geometrical factors and can be calculated as:

$$\Omega_1 = \begin{cases} 1.0 & \text{for strip and sheet reinforcements} \\ 1.5 & \text{for grid and mat reinforcements} \end{cases} \tag{2.5}$$

$$\Omega_2 = \begin{cases} 1.0 & \text{if } S_r \le 1000 \text{ ksf} \\ \Omega_1 & \text{if } S_r > 1000 \text{ ksf} \end{cases} \tag{2.6}$$

Working Stress Method (Ehrlich and Mitchell 1994)

Ehrlich and Mitchell (1994) have proposed a working stress method to predict the tensile stresses developed in reinforcement layers of MSE structures. It proved that it has better prediction for the compaction influence of the backfill soil than the other methods. However, it requires more details regarding the wall properties and compaction process, and needs long complex iterations to be performed, which makes it less desirable to be used by designers.

AASHTO Simplified Method (Allen et al. 2001)

This method is the follow up version of the Tie-back Wedge method mentioned earlier. This method was designed so it can work for both types of reinforcement, extensile and inextensible reinforcements. However, it limits the friction angle of the backfill soil to 40-degrees. Bathurst et al. (2009) found that the AASHTO Simplified method became less conservative in predicting the reinforcement stresses of mat reinforced MSE walls when the values of friction angles are high. The AASHTO Simplified method has a main contribution in predicting the lateral earth pressure coefficient relationships, as shown in Figure 2-5.

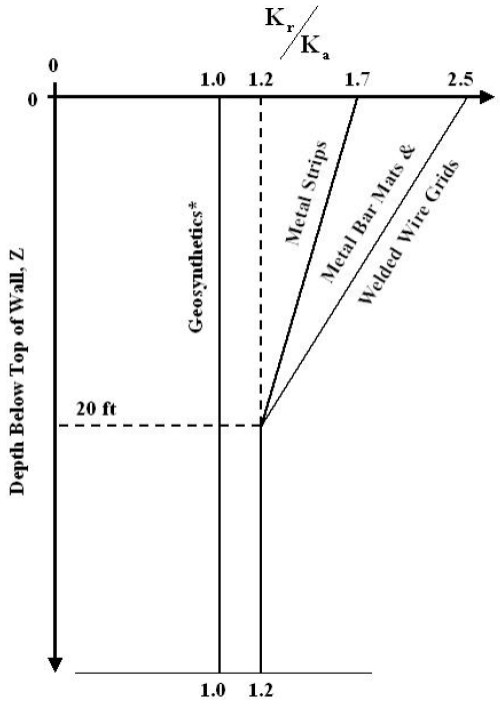

Figure 2-5 Selection of lateral earth pressure coefficients proposed by AASHTO simplified method (Allen et al. 2001)

K-Stiffness Method (Allen et al. 2003)

The K-stiffness method was introduced by Allen et al. (2003) and provided better estimations of metallic reinforced MSE structures attached to different facing types. This method intended to enhance the FHWA Structure Stiffness method so it can work for metallic reinforced MSE walls built with different geometries. Afterwards, this method was updated so that it became practical for MSE wall types that use geosynthetic reinforcement under serviceability conditions (Bathurst et al. 2008).

Design and Construction of MSE Walls and RSS (FHWA 2009)

The FHWA Structure Stiffness method mentioned earlier was developed based upon allowable stress design (ASD) procedures. However, it was updated to follow Load and Resistance Factor Design (LRFD) since many of the state DOTs follow the LRFD procedures in designing the reinforced earth structures. This method has been evolved based on the previous design methods of FHWA and AASHTO Bridge Design codes.

As this method is the most recent code that is used by DOTs for designing MSE structures, it was used in this research to check from the performance of the investigated MSE walls. The internal stability of an MSE wall was assumed in this method to be relied on restraining the wall against two internal failure modes, which are pullout and rupture of the earth reinforcement.

The critical slip surface shown in Figure 2-6 indicates the location of the maximum tensile force "T_{MAX}" that occurs at each reinforcement level throughout the length of the reinforcement. The location of the critical slip surface at each reinforcement level was determined based upon empirical MSE structures that were previously instrumented and tested. It was found that the shape and location of the critical failure surface rely on the reinforcement extensibility. The critical slip surface was assumed to follow a bilinear curve when the MSE reinforcement is inextensible (Figure 2-6(a)), and a linear curve when the MSE reinforcement is extensible (Figure 2-6(b)). It was also found that the critical surface occurs at the connection location at the base of the MSE wall for both types of reinforcement (Figure 2-6).

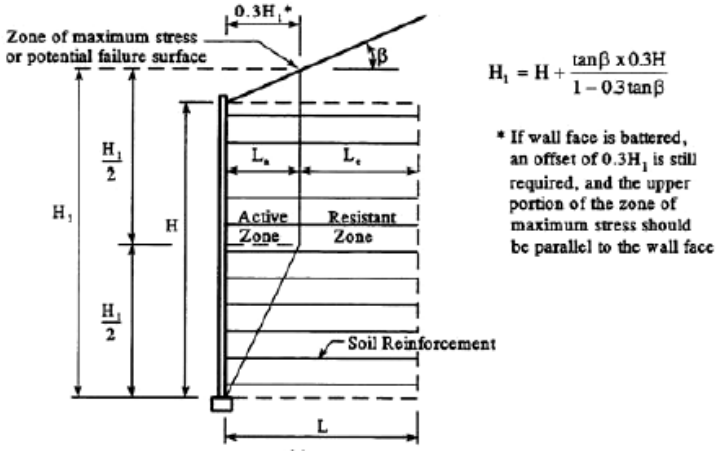

(a)

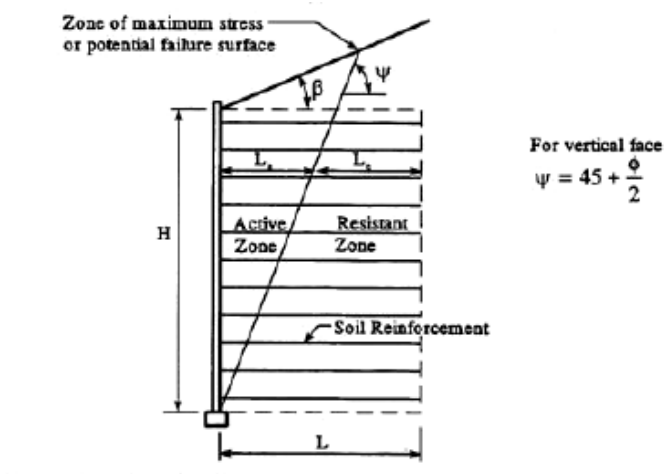

(b)

Figure 2-6 Critical failure surface for (a) inextensible reinforcement and (b) extensible reinforcement (FHWA 2009)

2.3.1.1 Rupture Stability Design

The resistance of rupture failure of reinforcement requires that (FHWA 2009):

$$T_{MAX} \leq T_r \quad (2\text{-}7)$$

where T_r is the factored tensile resistance in reinforcement. T_{MAX} can be calculated as (FHWA 2009):

$$T_{MAX} = \sigma_H S_V \quad \text{(force per unit reinforcement width (kips/ft))} \quad (2\text{-}8)$$

where σ_H is the horizontal stress and S_V is the reinforcement vertical spacing. The calculation of the horizontal stress of an MSE wall varies depending on the geometrical properties of MSE walls and load applications. For instance, when an MSE wall has uniform surcharge load and a level backfill, σ_H can be calculated by replacing the applied surcharge load with an equivalent soil surcharge layer of height of "h_{eq}" (equals to 2 ft) using the following formula (FHWA 2009):

$$\sigma_H = K_r[\gamma_r(z + h_{eq})\gamma_{EV-MAX}] \quad (2\text{-}9)$$

where γ_r is the backfill soil unit weight and γ_{EV-MAX} is the maximum load factor (equals to 1.35). The right side of Equation 2-7 represents the factored tensile resistance of reinforcement "T_r" and can be calculated as (FHWA 2009):

$$T_r = \phi T_{al} \quad (2\text{-}10)$$

where ϕ is a rupture resistance factor and can be obtained using Appendix A. T_{al} is the nominal long-term strength of reinforcement and can be calculated using one of the following two formulas depending on the reinforcement type (FHWA 2009):

$$T_{al} = \frac{F_y A_c}{b} \qquad \text{(for metal reinforcements (kips/ft))} \qquad \text{(2-11(a))}$$

where F_y is the yield tensile strength of steel, A_c is the design cross-sectional area considering the corrosion loss (can be calculated using Figure 2-7), and b is the width of reinforcement.

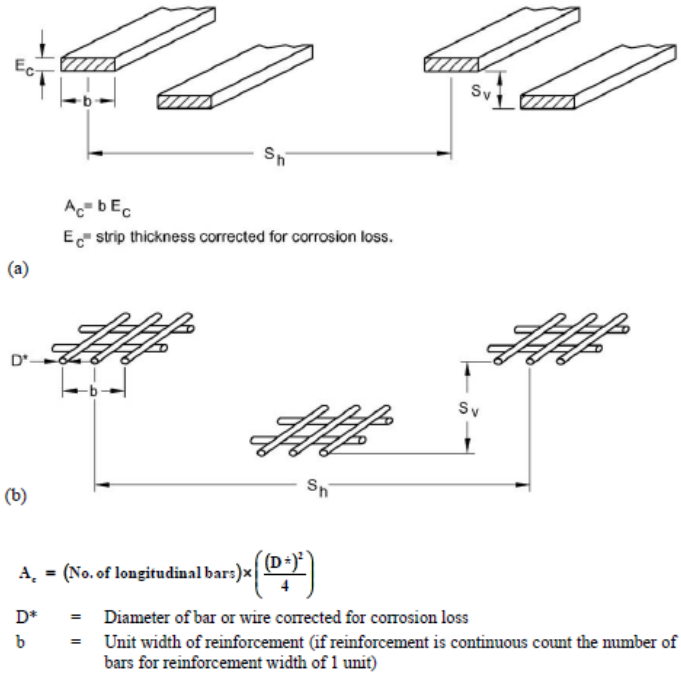

Figure 2-7 Metal reinforcement parameters (a) Steel strips, and (b) Steel grids (FHWA 2009)

$$T_{al} = \frac{T_{ult}}{RF_{ID} RF_{CR} RF_{D}} \qquad \text{(for geosynthetic reinforcement (kips/ft))} \qquad \text{(2-11(b))}$$

where T_{ult} is the geosynthetic ultimate tensile strength, and RF_{ID}, RF_{CR}, RF_{D} are reduction factors for installation damage, creep, and durability, respectively. These reduction factors represent the actual long-term strength losses, as shown in Figure 2-8. It can also be noted from Figure 2-8 that there is an immediate drop of reinforcement strength due to the installation process, and the creep affects the long-term reinforcement strength.

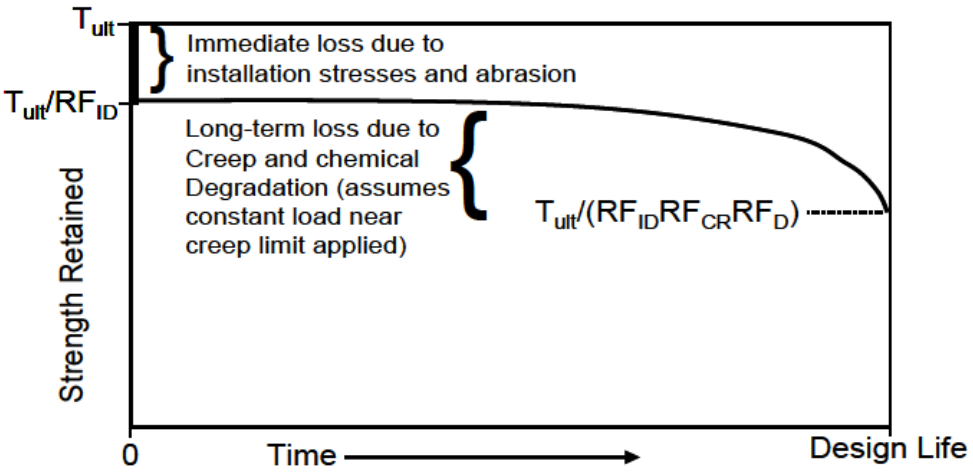

Figure 2-8 Long-term geosynthetic reinforcement strength (FHWA 2009)

2.3.1.2 Pullout Stability Design

The pullout resistance, P_r, of the reinforcement requires the effective pullout length, L_e, to be equal or greater than the factored tensile load developed in the reinforcement, T_{MAX}. Each layer must be checked according to the following formula (FHWA 2009):

$$P_r = F^* \alpha \sigma'_v L_e C \quad (2\text{-}12)$$

where F^* is a pullout resistance factor, α is a scale correction factor, σ_v' is the vertical stress at the reinforcement level, and C is the reinforcement effective unit perimeter (equals to 2 for strip, grid, and sheet reinforcements).

2.3.2 External Stability Design

The external stability of a reinforced soil wall is commonly evaluated by assuming the entire reinforced zone as a rigid body system, similar to the other traditional rigid earth retaining walls, with an active earth pressure acting behind the wall. The external stability of an MSE wall is checked against four global failure modes which are a) sliding failure; b) overturning failure; c) foundation bearing failure; and d) slope stability failure, as shown in Figure 2-9 (Elias et al. 1997).

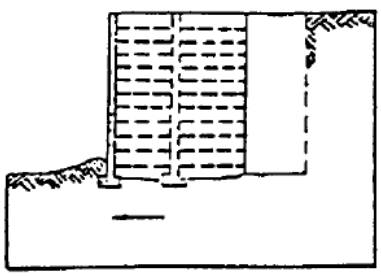

(a) Sliding

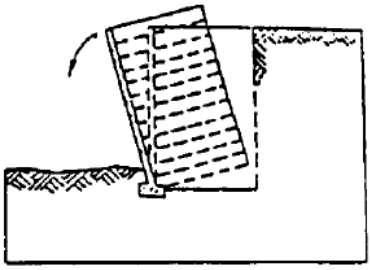

(b) Overturning

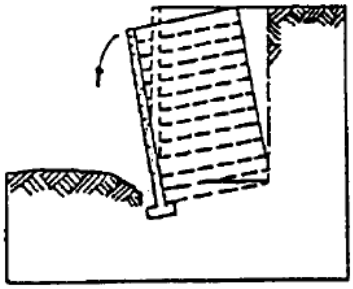

(c) Bearing capacity

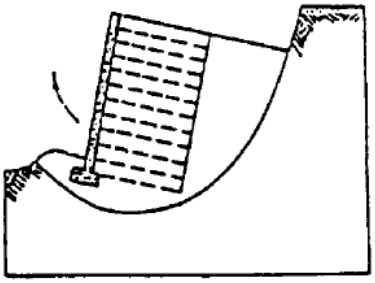

(d) Deep stability (rotational)

Figure 2-9 Global stability failure modes (Elias et al. 1997)

As the MSE wall system is considered as a rigid body system with an active thrust shown in Figure 2-10, the factors of safety for sliding (FS_S), overturning (FS_O), and bearing capacity (FS_{BC}) can be calculated as:

$$FS_S = \frac{S_t}{P_a} \tag{2-13}$$

$$FS_O = \frac{3W_t L}{2P_a H} \tag{2-14}$$

$$FS_{BC} = \frac{q_{ult}}{\frac{W_t}{L - 2e}} \quad (2\text{-}15)$$

where W_t is the total weight of the reinforced soil, P_a is the total active thrust, S_t is the total shear resistance, q_{ult} is the ultimate bearing capacity of the foundation soil, and e is the eccentricity due to active thrust ($e = P_aH/3W_t$).

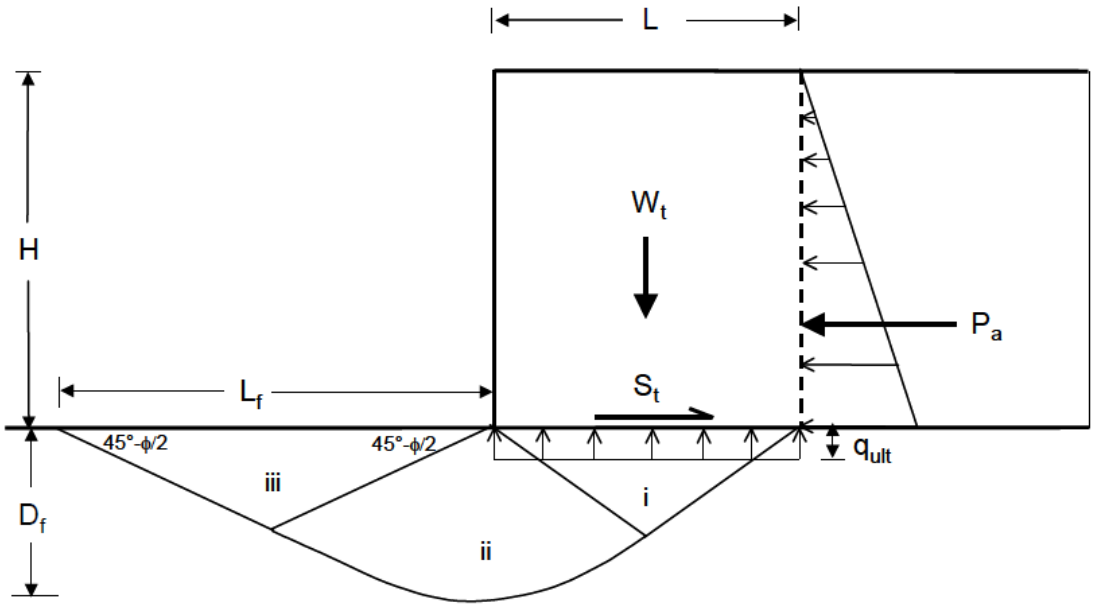

Figure 2-10 Global forces and stresses acting on an MSE wall (Elias et al. 1997)

2.4 Experimental and Numerical Evaluation of MSE Walls

A section of an MSE wall located in Salt Lake City, Utah, was subjected by a reconstruction project. The MSE wall was calibrated using 2D finite element modeling using PLAXIS software (Budge et al. 2006). The reconstruction began in May 1997 and was accomplished in July 2001. Figure 2-11 shows the MSE wall during and after

construction. The 30 ft high MSE wall was placed on foundation soil consisted of fine clay. During the reconstruction phase, the wall was instrumented with inclinometers and extensometers horizontally and vertically, respectively, to be able to monitor the overall response of the MSE wall (Figure 2-12). A vertical settlement of 1.64 ft was observed right after the completion of the construction. The conducted horizontal and vertical movements measured by the inclinometers and extensometers, respectively, were used to calibrate the numeral model. Figures 2-13 and 2-14 show comparisons between the numerical modeling deformations and the field measurements. Based on the modeling data, the excessive settlement was caused by the effect of primary consolidation of the fine clay content of the foundation soil.

Figure 2-11 MSE wall reconstruction phase (Budge et al. 2006)

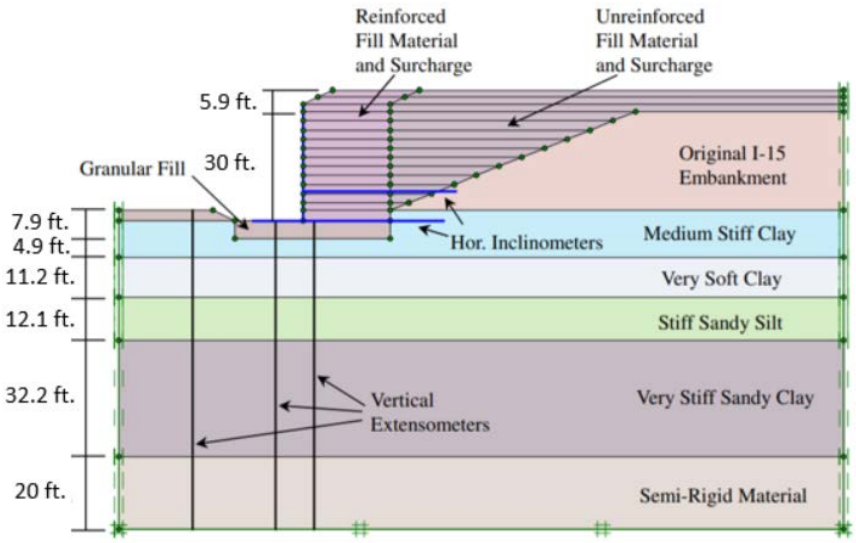

Figure 2-12 MSE wall cross-section and instrumentations (Budge et al. 2006)

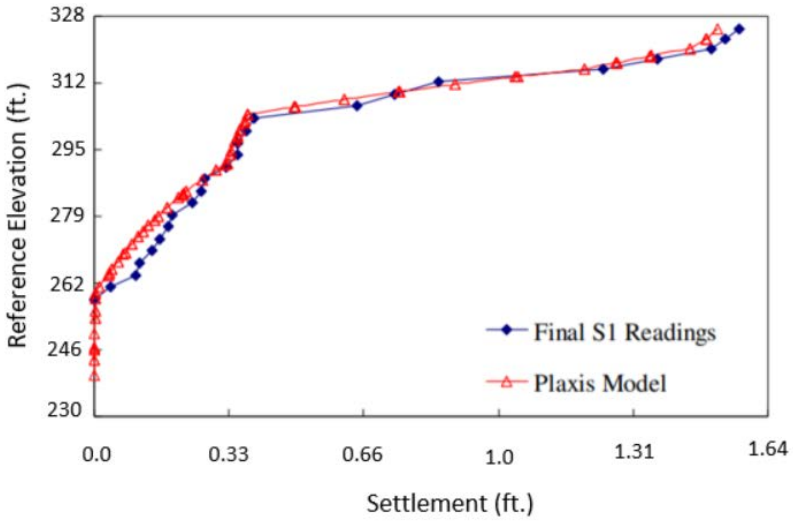

Figure 2-13 Comparison of vertical movement between extensometers and PLAXIS software (Budge et al. 2006)

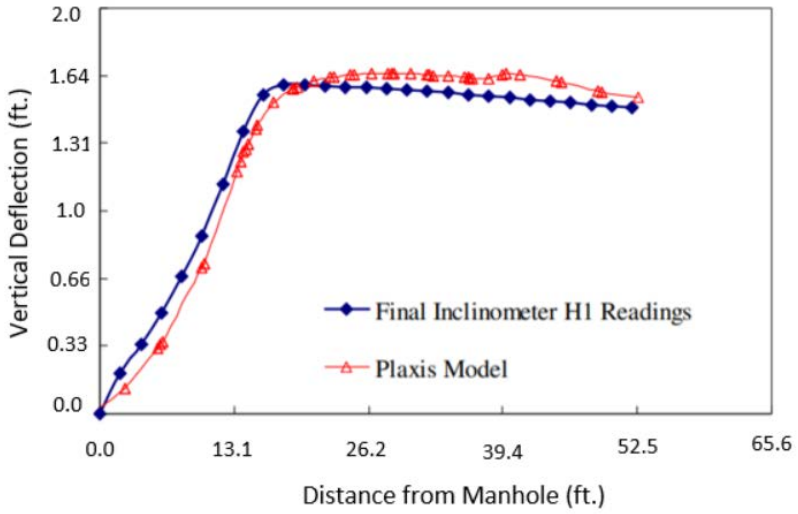

Figure 2-14 Comparison of horizontal movement between inclinometers and PLAXIS software (Budge et al. 2006)

Significant wall movement may be caused by poor quality of backfill soil and poor drainage system. Hossain et al. (2011) investigated a case study of an MSE wall located at State Highway 342 in Lancaster, Texas, which showed lateral movements ranged between 12-18 inches in only 5 years after construction. Several field and laboratory investigations were carried out to detect the cause of the movement. The field investigation included conducting resistivity imaging (RI) scans, and drilling boreholes atop the MSE wall to check for the backfill soil integrity. The RI scans (Figure 2-15) show that water pockets were existed behind the wall facing at multiple locations. The maximum observed lateral movement occurred where the water pockets were detected. The results of the tested soil samples show that it contains high content of clayey sand according to the Unified Soil Classification System. Therefore, it was found that the movement detected on the MSE wall was most likely caused by the poor quality of the backfill soil.

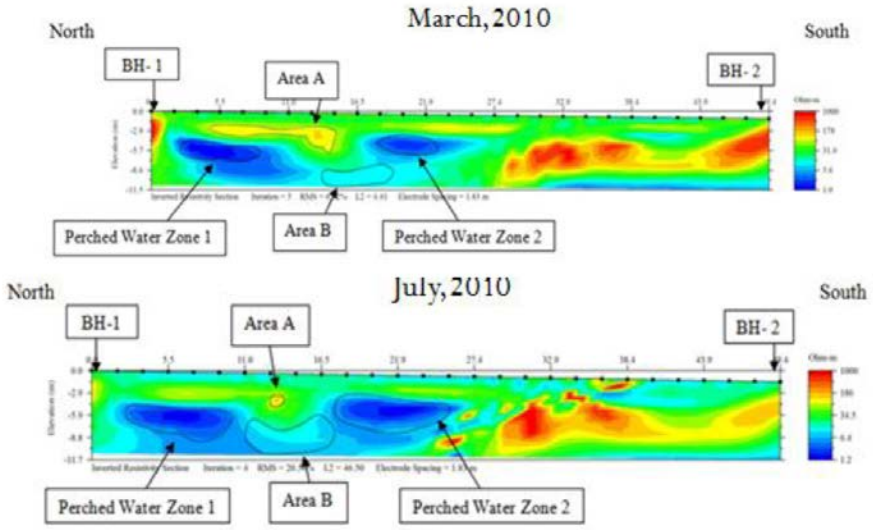

Figure 2-15 Resistivity Imagining (RI) results (Hossain et al. 2011)

A case study (Reddy and Navarrete 2008) addresses testing of small-scale MSE walls reinforced with geosynthetic geogrids. Four small-scale walls were constructed based on a scale of 1:5.5, two were reinforced with High-Density Polyethylene (HDPE) reinforcement, and two were reinforced with Polyethylene Terephthalate (PET) reinforcement. Instrumentation of the walls included the installation of strain and dial gauges to monitor the strains developed in reinforcements and facing lateral movements, respectively, as shown in Figure 2-16. A surcharge load of 3.6 kPa (75 psf) was applied atop the small-scale walls. This applied surcharge load is equivalent to the surcharge load applied on a full-scale MSE wall (20 kPa (415 psf)). These walls were also modeled using FLAC software to compare the results with the experimental data. The lateral displacements conducted from the experimental walls and FLAC software are shown in Figure 2-17 and indicate that there were differences in the results between the

experimental walls and FLAC software. Therefore, a factor “a” was developed and assigned to the modeling results in order to simulate the actual response of the MSE walls (Figure 2-17). The recorded data by strain gauges shows that the strains developed in the reinforcement are less than the serviceability limit states recommended by design methods.

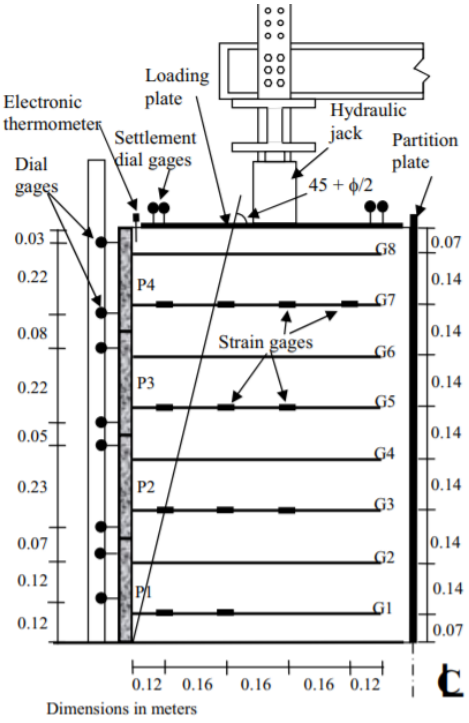

Figure 2-16 Cross-section and instrumentation of the small-scale MSE wall (Reddy and Navarrete 2008)

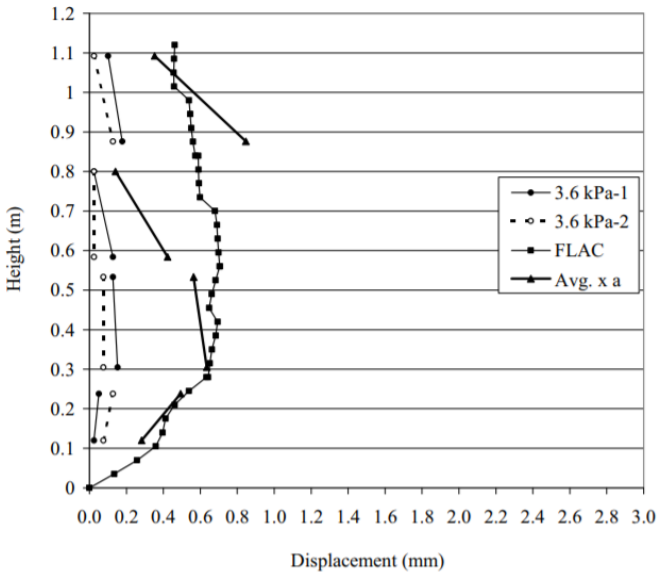

(a) HDPE reinforcement

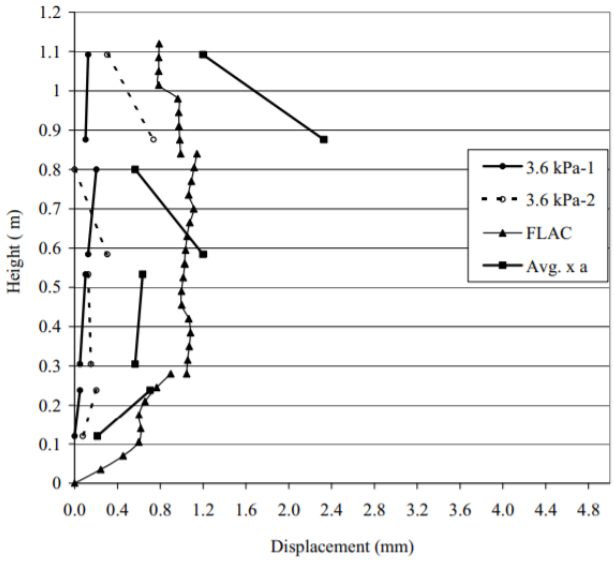

(b) PET reinforcement

Figure 2-17 Lateral movement of small-scale MSE walls using (a) HDPE reinforcement, and (b) PET reinforcement (Reddy and Navarrete 2008)

Extensive investigation (Kibria et al. 2013) was performed on a double-faced MSE (Figure 2-18) located on State Highway 342 in Lancaster, Texas, which exhibited a lateral movement ranges between 12 and 18 inches (300 to 450 mm) after 5 years of construction. The construction of MSE wall was completed in 2004. The filed measurements included the usage of a total station machine, inclinometers, settlement rings, piezometers, and strain gauges. The inclinometers (Figure 2-19) which were installed in December 2009 recorded a significant additional lateral movement of 1.5 inches (38 mm) over the period of December 2009 to August 2011. This movement indicates that the wall exhibits a continuous movement of 3/16 inch/month (4.5 mm/month). Furthermore, a numerical evaluation was carried out using PLAXIS 2D software to investigate the effect of varying the reinforcement length from 0.5H to 0.7H, where the H is the wall height, on the lateral movement. The results conducted by both inclinometers and PLAXIS software are shown in Figure 2-20. Figure 2-21 suggests that the lateral movement could be significantly decreased by increasing the reinforcement length.

(a) MSE wall location

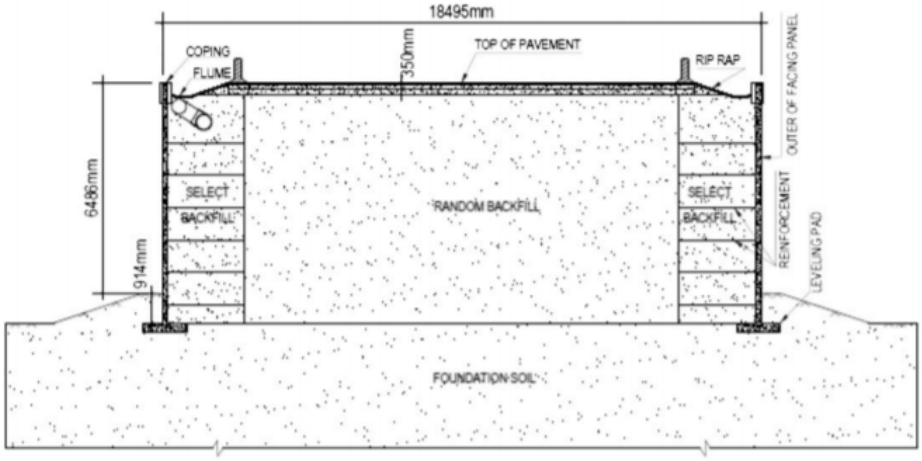

(b) MSE wall cross-section

Figure 2-18 MSE wall details (Kibria et al. 2013)

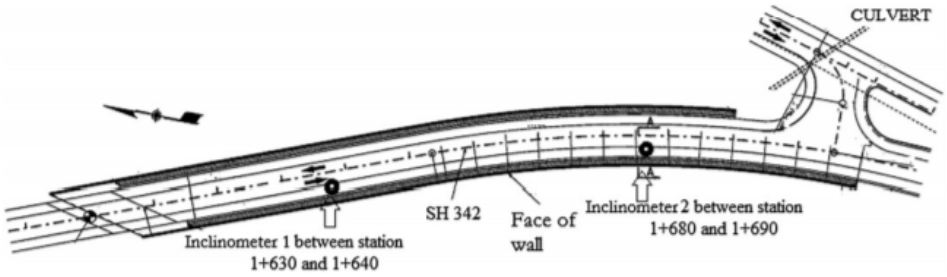

Figure 2-19 Inclinometer locations (Kibria et al. 2013)

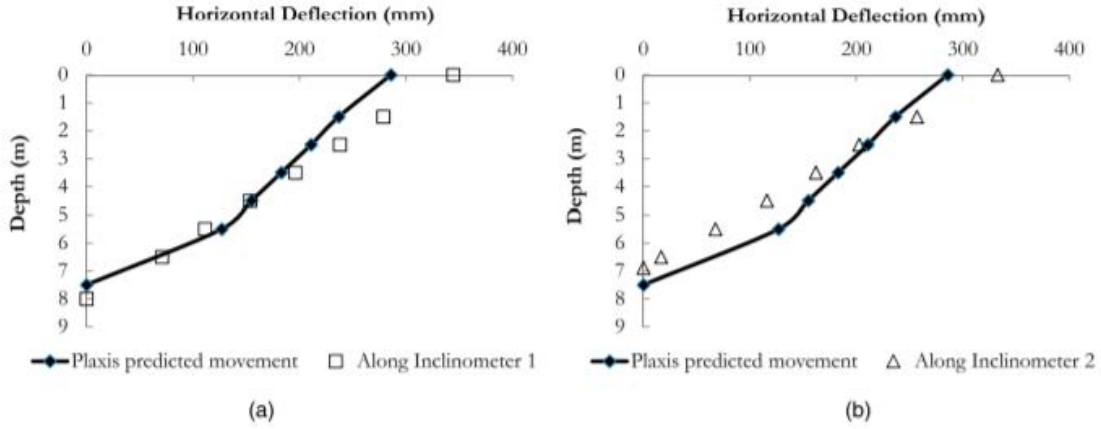

Figure 2-20 Lateral movement of the MSE wall conducted by PLAXIS and inclinometers at (a) Inclinometer 1 location, and (b) Inclinometer 2 location (Kibria et al. 2013)

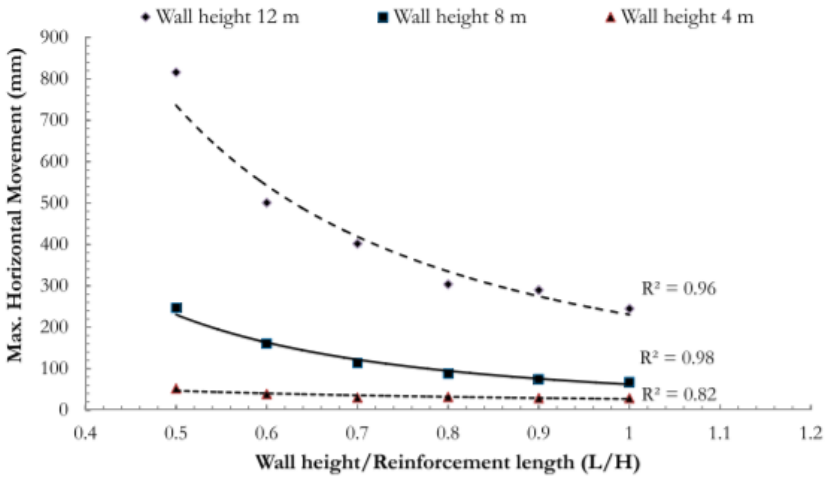

Figure 2-21 MSE wall lateral movement of deferent wall heights and reinforcement lengths by PLAXIS software (Kibria et al. 2013)

A case study (Yoo and Kim 2008) investigated the load application of a 16.4 ft (5 m) high two-tier segmental retaining wall (SRW) reinforced with geosynthetic reinforcement. The surcharge load application was induced by placing concrete cube atop the wall (Figure 2-22). Varying the applied surcharge load through time was achieved by controlling the amount of poured concrete into the cube. This approach was carried out to investigate the accuracy of the designed live load recommended by FHWA. The SRW response was measured using LVTDs and strain gauges installed at the facings and geosynthetic reinforcements, respectively, as shown in Figure 2-23. The conducted results shown in Figure 2-24 show that the deformations and stresses developed are within the serviceability limits; thus, the FHWA designed surcharge load over-predicts the induced surcharge live load.

Figure 2-22 Surcharge load application through the poured concrete (PC) box (Yoo and Kim 2008)

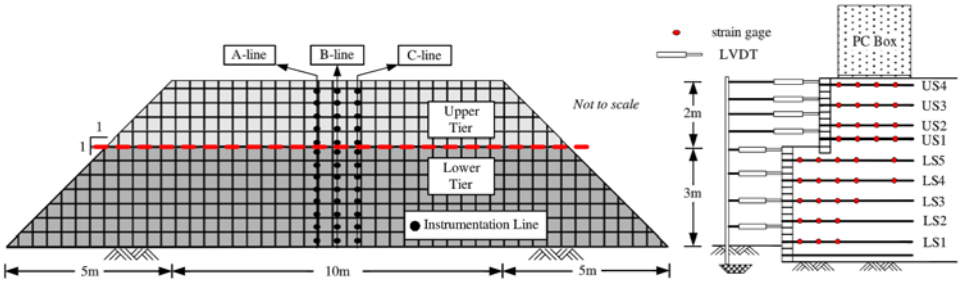

Figure 2-23 SRW instrumentation (Yoo and Kim 2008)

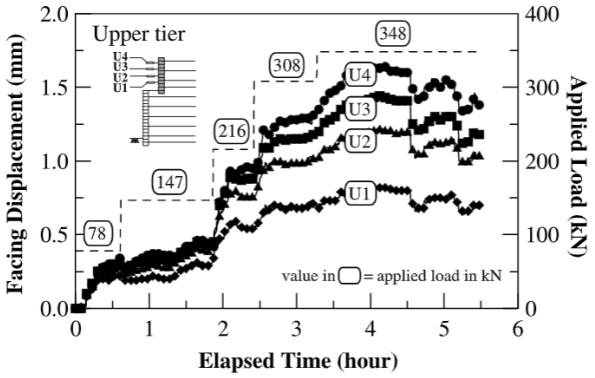

(a) Upper tier displacement

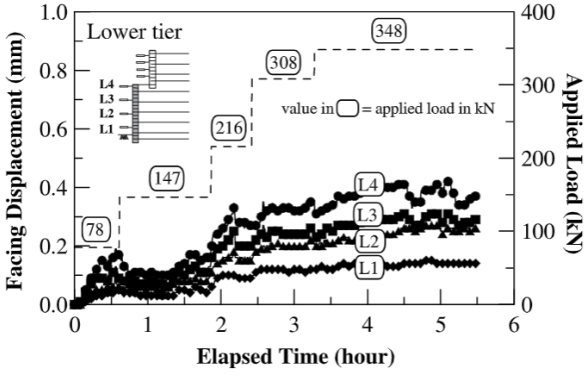

(b) Lower tier displacement

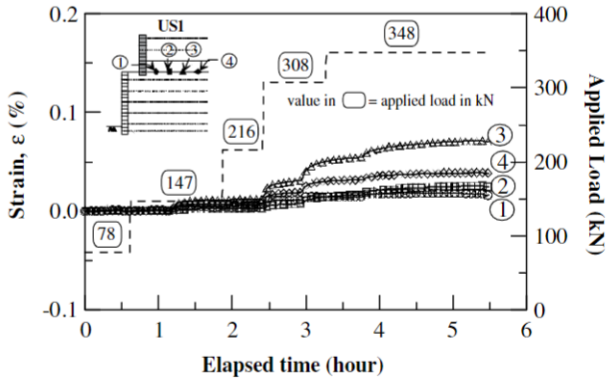

(c) Upper tier reinforcement strains (US1)

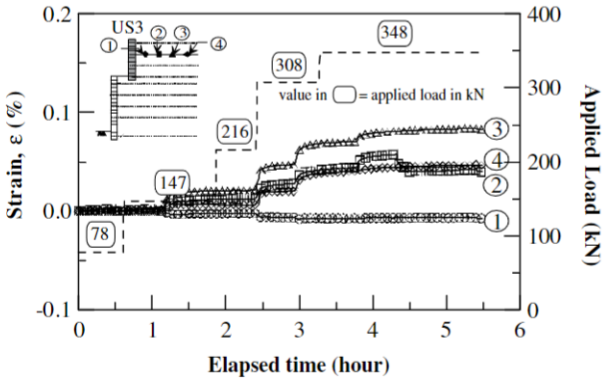

(d) Upper tier reinforcement strains (US3)

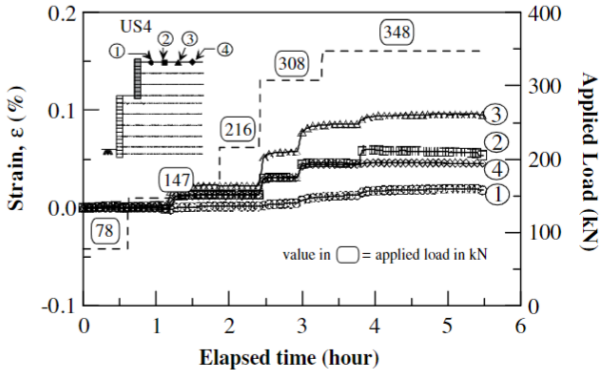

(e) Upper tier reinforcement strains (US4)

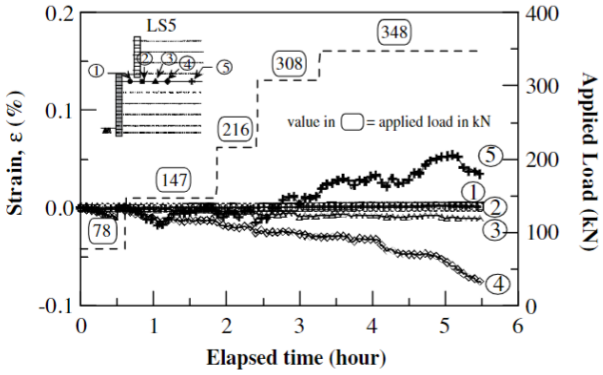

(f) Lower tier reinforcement strains (LS5)

Figure 2-24 SRW instrumentation results (Yoo and Kim 2008)

Abdelouhab et al. (2011) carried out a parametric study on a numerical finite element modeling using FLAC 2D software. Several parameters were investigated to assess the effect of these parameters on the performance of an MSE wall reinforced with geosynthetic reinforcement. The parameters of soil/reinforcement interaction, backfill soil, and geosynthetic reinforcement were studied. The results show that geosynthetic reinforced MSE walls are expected to have higher lateral deformations than the metallic

MSE walls, and the reinforced soil friction angle and cohesion, the interface shear friction, and the geosynthetic stiffness are the most influential parameters.

A numerical model was created using FLAC 2D software (Figure 2-25) by Huang et al. (2009) to simulate two full-scale MSE walls, one is reinforced with extensible material (geosynthetic) and the other one is reinforced with inextensible material (welded wire grid). The reinforced soil was modeled using three different methods, which are Mohr-Coulomb, modified Duncan-Chang hyperbolic model, and Lade's single hardening methods, in order to see which of these soil models predicts better the actual response of an MSE wall. Figure 2-26 shows the lateral movement results using the three different soil models as well as the recorded actual movement. The results show that the different soil models are able to predict the actual reinforced soil behavior.

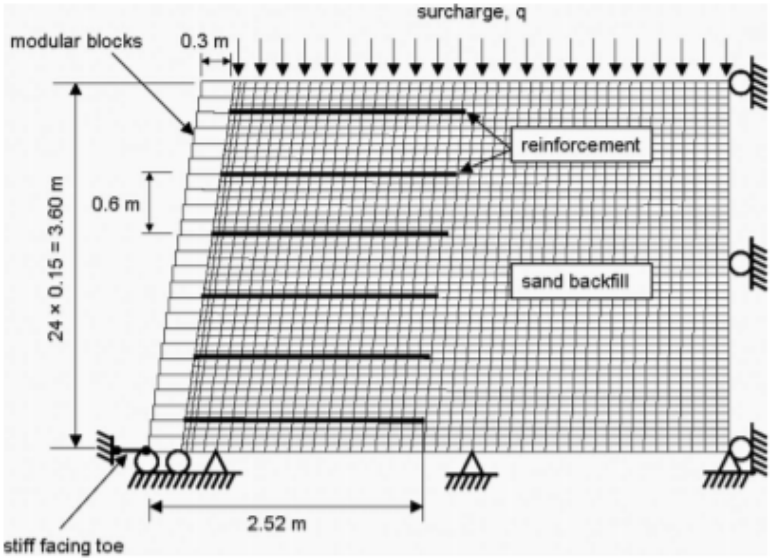

Figure 2-25 2D FLAC numerical model (Huang et al. 2009)

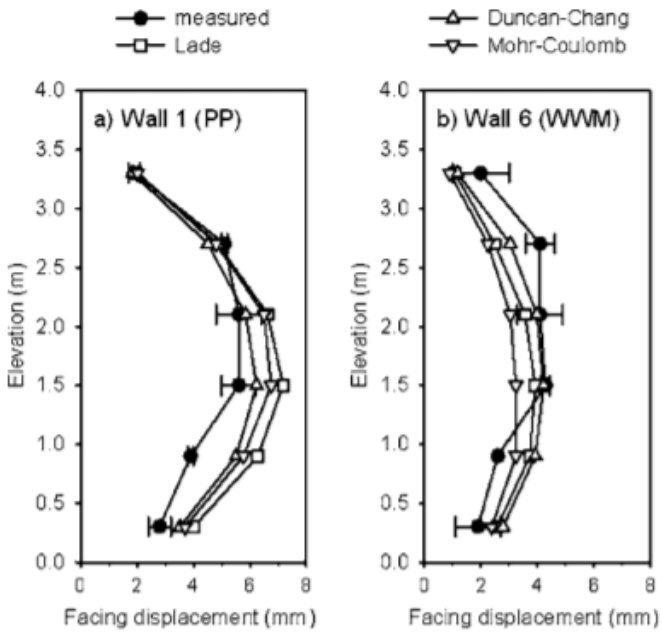

Figure 2-26 Lateral movement comparison (Huang et al. 2009)

A 2D FE modeling was developed using ABAQUS software to simulate the behaviour of geosynthetic reinforced MSE walls, and compare it with the ultimate limit states of the design methods (Ambauen 2014). The numerical wall was verified by comparing its results with the field measurements of a full-scale MSE wall. The results of numerical modeling indicate that the maximum lateral movements of an MSE wall occur at mid-height, as shown in Figure 2-27, and the forces developed in reinforcements are less than the designed values, which means that the design methods overestimate the actual tensile stresses developed in reinforcements.

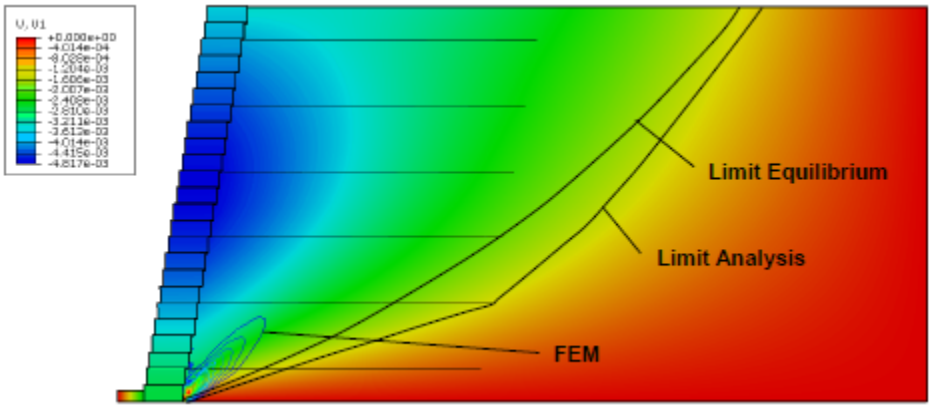

Figure 2-27 Lateral movement in ABAQUS software (Ambauen 2014)

2.5 Internal Stability Checks of MSE Walls

The internal stability of an MSE wall relies on restraining the wall from pullout and rupture of reinforcement. However, there are some uncertainties in the internal stability design of MSE walls. Kim and Salgado (2011) used the first-order reliability method (FORM) to perform reliability analysis on steel strip reinforced MSE walls. The aim was to investigate the integrity of the AASHTO formulas that are used to calculate the reinforcement lengths which are embedded in the active zone of the reinforced soil "L_a". The active reinforcement should be added to the effective reinforcement lengths "L_e" in order to provide the overall reinforcement lengths needed for the pullout resistance. The structural reliability index, β, was considered in the analysis to obtain different ranges of active reinforcement lengths depending on their respective level of safety, as show in Figure 2-28. It was also found that the rupture limit states recommended by ASSHTO are

insensitive to the uncertainties in the internal stability design of steel grid reinforced MSE walls.

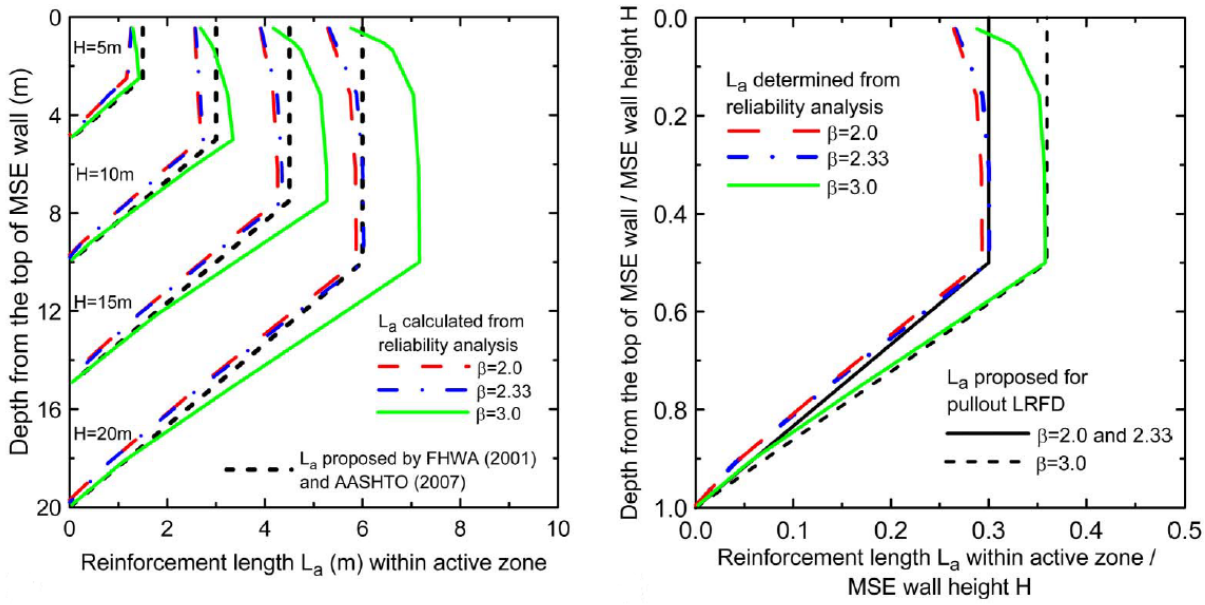

(a) (b)

Figure 2-28 Reinforcement lengths in active zone with respective to (a) depth from the top of MSE wall, and (b) depth from the top of MSE wall/wall height (Kim and Salgado 2011)

Chalermyanont and Benson (2004) performed structural reliability analysis using Monte Carlo simulation to regard the uncertainties in the internal stability design of the tie-back method. The results show that friction angle and unit weight of backfill soil, live surcharge load, reinforcement tensile strength, reinforcement length, and reinforcement spacing are highly affecting the internal probability of failure.

The resistance factors recommended by Load and Resistance Factor Design (LRFD) did not consider the reliability analysis of the steel reinforcement loss due to corrosion in an MSE wall structure. The LRFD design method accounted for the metal loss of reinforcement at 75 or 100 year design life. Fishman et al. (2010) performed a structural reliability analysis on the recommended resistance factors for corrosion and compared it with the observed corrosion rates (Fishman et al. 2010). It was found that the resistance factors derived by the new modifications are lower than the values obtained by the AASHTO factors, which means the current AASHTO resistance factors achieve the targeted probability of failure.

The accuracy of the AASHTO simplified method in designing MSE walls has been investigated using instrumentation of a full-scale MSE wall. This study (Bathurst et al. 2009) has found that the AASHTO simplified method is reasonable in designing MSE walls consist of backfill soils of friction angles less than 45°; however, it under predicts the behavior of an MSE wall when the backfill soil used has a friction angle greater than 45°.

2.6 MSE Wall Types

MSE walls can be categorized based on their facing and reinforcement types as follows:

2.6.1 Facing Types

The facing types can be categorized based on the facing material and shape. Several facing types are used in MSE walls but the most common types are:

- Segmental precast concrete panels; these facing units are made of reinforced concrete and they are comparably larger than the other types, as shown in Figure 2-29(a).
- Modular block wall (MBW); it is relatively small and made of concrete, as shown in Figure 2-29(b).
- Welded wire mesh; this type consists of galvanized steel wire grids as facing units (Figure 2-29(c)).
- Gabions; this type consists of rock filled wire baskets (Figure 2-29(d)), and it can be used in an MSE wall system as facings since it allows the earth reinforcements to be connected to it.
- Geosynthetic reinforcements; they are looped around to form the MSE wall facings similarly to the welded wire mesh facings (Figure 2-29(e)). They can withstand against weather circumstances and fire.
- Cast-in-place (CIP); this type of facings can be used for either geosynthetic or metal reinforced MSE walls. Figure 2-29(f) shows the soil reinforcement connected to the facing wire mesh before pouring concrete.

(a) Segmental precast concrete panels

(b) Modular block wall (MBW)

(c) Welded wire mesh

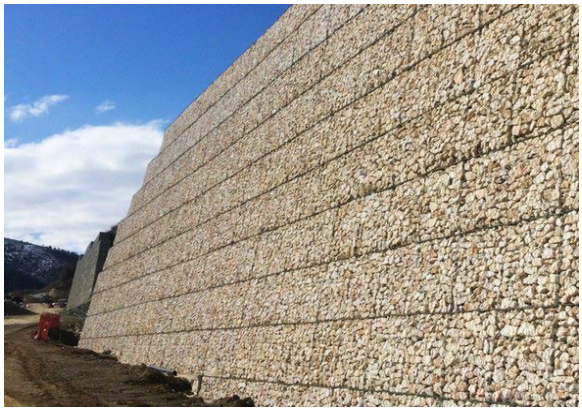

(d) Gabions

(e) Geosynthetic reinforcements

(f) Cast-in-place (CIP)

Figure 2-29 Facing types of MSE walls

2.6.2 Reinforcement Types

The reinforcement types can be categorized based on the material extensibility and element shape as the following:

- Material:
  - Metal; its deformability is much less than that of the backfill soil (inextensible).
  - Polymer; its deformability is close or comparable to that of the backfill soil (extensible).
- Geometry:
  - Steel strips (metal) (Figure 2-30(a)).
  - Steel grids (metal) (Figure 2-30(b)).
  - Geosynthetic sheets (polymer) (Figure 2-30(c)).
  - Geosynthetic geogrids (polymer) (Figure 2-30(d)).

(a) Steel strip

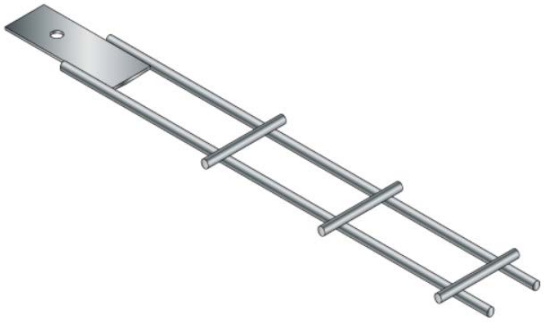

(b) Steel grid

(c) Geosynthetic sheet

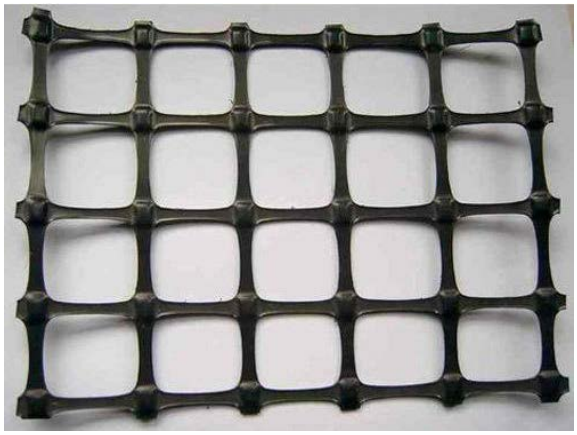

(d) Geosynthetic geogrid

Figure 2-30 Reinforcement types used in MSE walls

Chapter 3
BACKGROUND OF THE INVESTIGATED MSE WALLS

3.1 Description of MSE Walls

The current study was inspired by multiple MSE walls that are currently experiencing unexpected distress such as deformations, settlement, widening of panel joints, and other types of distress associated with MSE walls. The three most critical MSE walls in Fort Worth and Hurst, Texas, were selected for this study. The locations and sections of the monitored MSE walls are as follows:

3.1.1 Wall 264R

Wall 264R is located south of the Bedford Euless Rd and Airport Freeway intersection in Hurst, Texas, as shown in Figure 3-1. The construction of this wall was completed between 1997 and 1998. Wall 264R was built at two different stages. Figure 3-2 shows the two sections of the wall and which can be noted by the change in color between the third and the fourth column panels to the left from the control box.

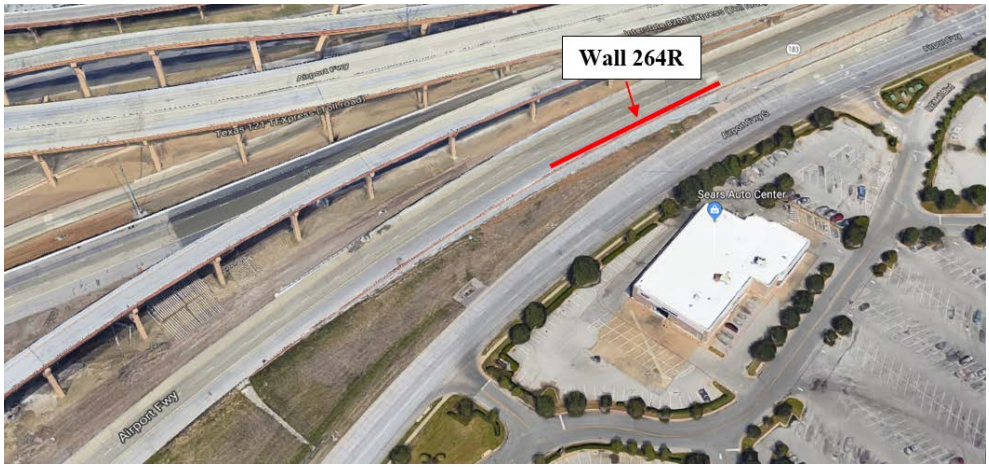

Figure 3-1 Wall 264R location map

Figure 3-2 Old and new sections of Wall 264R

After investigating the entire stretch of the wall, it was decided to monitor the wall portion shown in Figure 3-3, which is from the control box located on the right side of the figure up to 14 wall copings to the left from the control box.

Figure 3-3 Monitored section of Wall 264R

3.1.2 Wall 179L

Wall 179L is located at the intersection of NE Loop 820 and W Pipeline Rd in Hurst, Texas (Figure 3-4). This MSE wall supports the abutment of Exit 22B of the north bound of IH-820.The construction of this wall was completed between 1997 and 1998. The wall section to be monitored shown in Figure 3-5 is from the beginning of the concrete sidewalk up to the “one way” sign.

Figure 3-4 Wall 179L location map

Figure 3-5 Monitored section of Wall 179L

3.1.3 Walls CC1, CC2, and CC3

These are a combination of walls supporting the abutment on the Southwest Blvd Bridge, located at the intersection of Chisholm Trail Pkwy and Southwest Blvd in Fort Worth, Texas (Figure 3-6). The construction of these walls was completed between 2012

and 2013. The wall sections to be monitored of Walls CC1-3 are shown in Figures 3-7(a-c). One column panel to the left and one column panel to the right of the corner between Walls CC1 and CC2, and three column panels to the left and four column panels to the right of the corner between Walls CC2 and CC3 were chosen for the investigation.

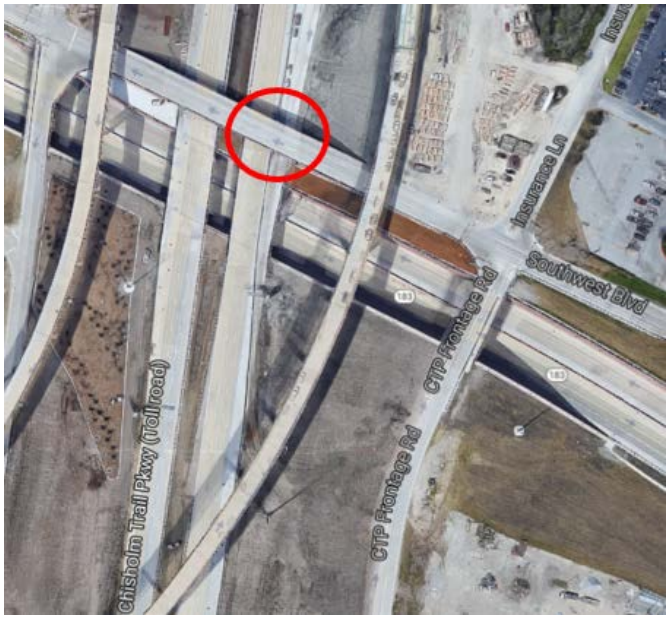

Figure 3-6 Walls CC1, CC2, and CC3 location map

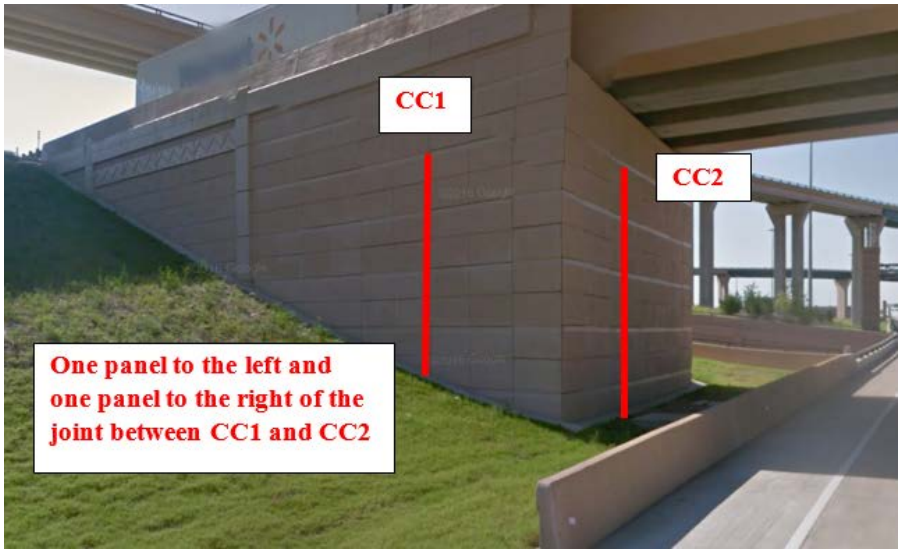

(a) Monitored sections of Walls CC1 and CC2

(b) Monitored section of Wall CC2

(c) Monitored section of Wall CC3

Figure 3-7 Monitored sections of Walls CC1, CC2, and CC3

3.2 Visual Inspection

A visual inspection of the monitored MSE walls was carried out in May 2017. During the field visits at Wall 264R, backfill leakage and wide gaps at panel joints (Figure 3-8(a)), and out of plane movement of panels (Figure 3-8(b)) were observed. The bulging area was observed at the new section of Wall 264R (Figure 3-2). Wall 264R has experienced pressure from the injection of polyurethane foam used to raise a section of concrete pavement on SH183 that was supported by the wall and was undergoing settlement.

(a) Backfill leakage and wide joint opening at Wall 264R

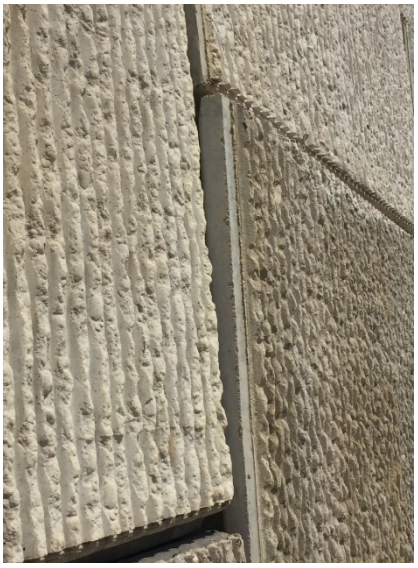

(b) Out-of-plane movement at Wall 264R

Figure 3-8 Wall 264R conditions

Extensive cracks were observed on the copings and the traffic barriers of Wall 179L, as shown in Figures 3-9(a and b). This could be attributed to the differential movement between the wall panels (Figure 3-9(c)). It was also observed that the wall experienced water/backfill leakage at the manhole location shown in Figure 3-10.

(a) Cracks on wall coping at Wall 179L

(b) Cracks on traffic barriers at Wall 179L

(c) Differential movement between panels at Wall 179L

Figure 3-9 Wall 179 conditions

Figure 3-10 Manhole location at Wall 179L

During the inspection that was carried out at Walls CC1-3, differential movement between panels (Figure 3-11(a)), opening of panel joints (Figure 3-11(b)), and leakage of backfill material (Figure 3-11(c)) were observed.

(a) Differential movement between panels at Walls CC1-3

(b) Opening of corner joint at Walls CC1-3

(c) Leakage of backfill soil at Walls CC1-3

Figure 3-11 Walls CC1-3 conditions

Chapter 4
EVALUATION OF MSE WALLS

4.1 Non-Destructive Evaluation

Several non-destructive tests were performed on the critical walls. A 3D robotic laser scanner and crack meters were used to check for the growing movement of the precast panels of the MSE walls. Ground Penetrating Radar (GPR) and Infrared Camera were used to examine the integrity of earth reinforcement and determine if there were any backfill loss behind precast panels, respectively. The Resistivity Imaging (RI) technique was used to investigate the groundwater table and perched water zones in backfill soil.

4.1.1 3D Robotic Laser Scanner

This research aimed to develop a technique to monitor the movement of MSE walls on a timely basis. The Trimble SX10 scanner shown in Figure 4-1(a) is used in this research to monitor the global movement of facing panels. This machine is not only a total station machine, it is also a laser scanner and camera which provides higher efficiency in the field than the other conventional total station types. It proved that it can capture high accuracy 3D data, combine multiple surveys, perform scans at speeds of up to 26,600 Hz at ranges up to 1,970 ft (600 m) and a spot size of 0.55 inch (14 mm) at 328 ft (100 m), and provide versatile post-processing software. The components of the Trimble SX10 laser scanner are shown in Figures 4-1(a through d). The Trimble tablet shown in Figure 4-1(b) provides better efficiency in leveling and setup of the scanner, controls the scanner remotely, and has the video available to see where the scanner is looking at any time.

The Trimble tripod shown in Figure 4-1(c) is used to keep the scanner level and in position throughout the survey process. The 360 prism shown in Figure 4-1(d) is used as a reference location for the instrument calibration.

(a) SX10 scanner

(b) Trimble tablet

(c) Trimble tripod

(d) 360 prism

Figure 4-1 Components of laser scanner

4.1.1.1 SX10 Scanner Setup

The setup of the SX10 requires a fixed control point (instrument station) and two or more back-sights. The back-sights are reference locations placed on rigid objects, and are used to calibrate scanner position with the original setup during the follow up scans. The back-sights are either targets (Figure 4-2) or a 360 prism (Figure 4-1(d)). The targets were attached to rigid surfaces, such as a light pole, using liquid adhesive, as shown in Figure 4-3. The control point locations of the scanner and the back-sight locations of the 360 prism were prepared through drilling small holes in concrete basement, applying liquid adhesive, and inserting MAG nails (Figure 4-4).

Figure 4-2 Target

Figure 4-3 Target used as a back sight placed on a light pole

Figure 4-4 Control point

Figures 4-5 through 4-7 show that Wall 264R has one control point “CP” for the instrument setup location and three back-sight “BS” locations, Wall 179L has two control points and four back-sight locations, and Walls CC1-3 have two control points and three back-sight locations, respectively. Two control points were used for Wall 179L and Walls CC1-3 due to their geometric irregularities.

Figure 4-5 Reference locations of Wall 264R

Figure 4-6 Reference locations of Wall 179L

(a) Reference locations of Wall CC1

(b) Reference locations of Walls CC2 and CC3

Figure 4-7 Reference locations of Walls CC1-3

After installation of the wall targets, back-sights, and instrument control points, the scanner was setup on the control point positions in August 2017. The setup process included leveling the scanner on the control point locations (Figure 4-8), aligning it with the global coordinate system (global N-S direction), shooting the back-sights so that the positioning of the scanner can be calibrated with the original setups during follow up scans, and shooting the wall targets.

Figure 4-8 SX10 robotic laser scanner setup above a control point

4.1.1.2 Installation of Targets

In order to monitor the 3D movement of MSE walls, targets (

Figure 4-2) were installed on the panel corners that exhibit significant movement using adhesive material. For high elevation panels, a bucket truck shown in Figure 4-9 was provided along with lane closures by TxDOT for installing the targets. After that, it was clarified through a numbering system to monitor their movement on a monthly basis. The numbering systems of the walls are shown in Figures 4-10(a through c).

Figure 4-9 Installing targets using a bucket truck

(a) Wall 264R

(b) Wall 179L

(c) Walls CC1-3

Figure 4-10 Target locations at (a) Wall 264R, (b) Wall 179L, and (c) Walls CC1-3

4.1.1.3 Laser Scanning

A laser scanning was conducted on a monthly basis. Following the scans, the data was then transferred to the Trimble Business Center software. Figures 4-11(a-c) show the 3D models generated by Trimble software for the MSE walls.

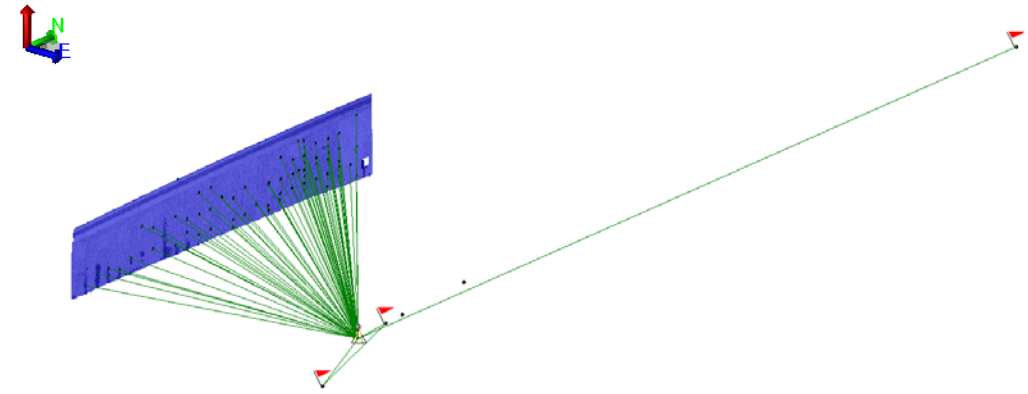

(a) Wall 264R

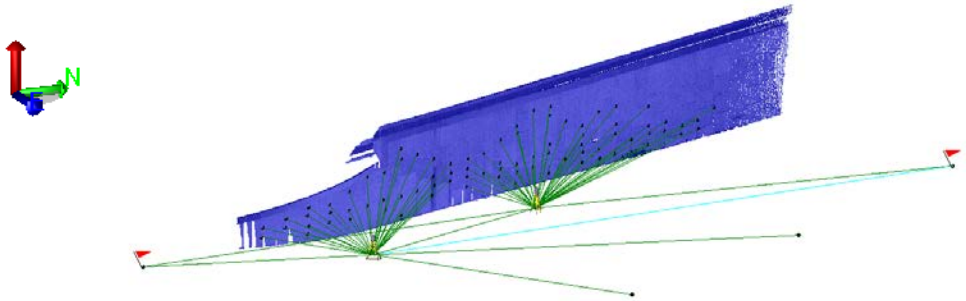

(b) Wall 179L

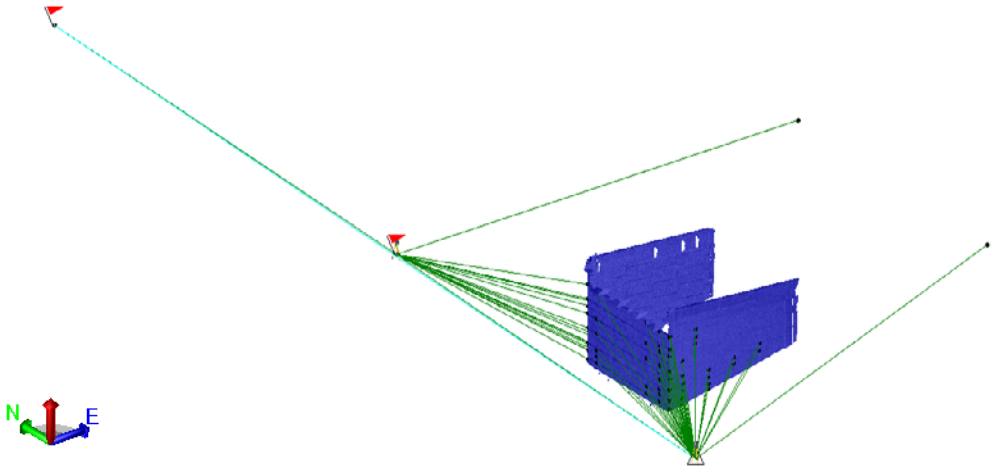

(c) Walls CC1-3

Figure 4-11 3D models generated by Trimble Business Center software of (a) Wall 264R, (b) Wall 179L, and (c) Walls CC1-3

4.1.2 Crack Meters

Crack meters (Figure 4-12) were used to monitor the relative movement between the precast panels of Wall 264R. This wall was selected to be monitored using this method due to its significant movement detected by laser scanning and visual observation. In December 2018, five crack meters were installed on the joints that show the most movement. Figure 4-13 shows the crack meter locations at Wall 264R.

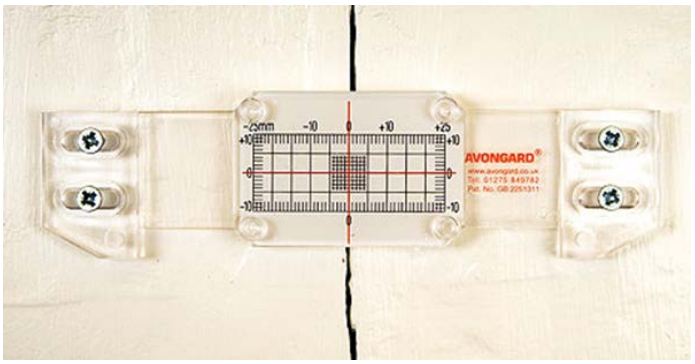

Figure 4-12 Crack meter

Figure 4-13 Crack meter locations at Wall 264R

4.1.3 Ground Penetrating Radar (GPR)

Ground Penetrating Radar (GPR) is a real-time NDT technique that uses high frequency radio waves to investigate features buried underground. It has been used for various applications, such as archaeology, geology, utility detection, and bridge and road condition assessment. This technique relies on an electromagnetic wave which is propagated into the material under investigation. The GPR shown in Figure 4-14 sends radio waves through the material using a transmitter. Those high-frequency waves get reflected when they hit a different material in path. The reflected waves are received by a receiver antenna (Riad 2017). The GPR provides scans with valuable information about the materials and reinforcement depth at any time. The GPR scans are presented in two forms, A-scan or B-scan.

Figure 4-14 GPR machine (Riad 2017)

GPR scans were conducted atop Wall 179L to locate broken earth reinforcement, air voids, and water pockets in the soil inside the MSE wall. To achieve these objectives, the choice of the antenna frequency was very important. Thus, the investigation used two types of antennas to cover different ranges of depth. For penetration depths of 3 to 12 ft and 12 to 18 ft, a 400MHz and a 270 MHz frequency antenna were chosen, respectively. Table 4-1 shows the various available GPR antenna frequencies and the corresponding penetration depths.

Table 4-1 GPR Antenna frequency and corresponding penetration depths

Center Frequency	Depth of Penetration	Typical Applications
2600 MHz*	0-12 in (0.4 m)	Concrete Evaluation
2000 MHz Palm	0-12 in (0.4 m)	Concrete Evaluation
1600 MHz*	0-18 in (0.5 m)	Concrete Evaluation
900 MHz	0-3 ft (0-1 m)	Concrete Evaluation, Void Detection
400 MHz*	0-12 ft (0-4 m)	Utility, Engineering, Environmental, Void Detection
270 MHz*	0-18 ft (0-6 m)	Utility, Engineering, Geotechnical
200 MHz	0-30 ft (0-9 m)	Geotechnical, Engineering, Environmental

For the scan area highlighted in Figure 4-15 (144 ft by 20 ft), a total of 48 horizontal line scans at 3 ft spacing (transverse to the traffic) and 9 vertical line scans at 2 ft spacing (parallel to the traffic) were considered. The scan grid is shown in Figure 4-16. Each one of the line scans was performed using the 400 MHz antenna in normal orientation, the 400 MHz antenna in cross-polarized orientation, the 270 MHz antenna in normal orientation, and the 270 MHz antenna in cross-polarized orientation.

The GPR scan was conducted in a series of line scans that could be combined to construct a map of the soil layers with voids positions, along with the position and depth of reinforcement layers. The scan is very sensitive to rebar and metal objects embedded within the scan area.

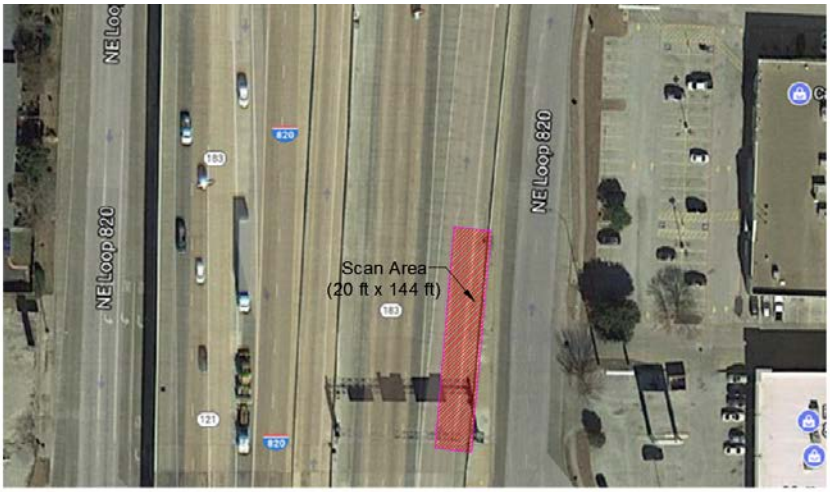

Figure 4-15 Scan area using GPR at Wall 179L

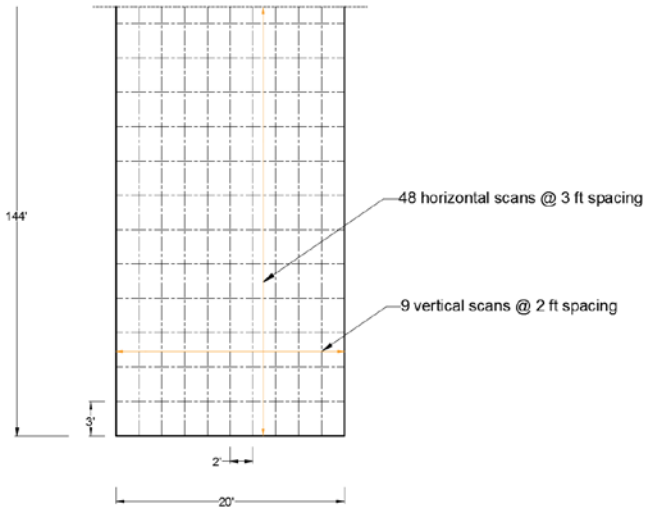

Figure 4-16 Scan grid using GPR at Wall 179L

GPR scans (Figure 4-17) can be collected and presented in one or two dimensions. A GPR B-scan is a 2D image of the subsurface. By moving the antenna atop the MSE wall, a series of A-Scans were generated. The B-scans are then developed by combining the A-scans.

Figure 4-17 GPR scanning with 400 MHz antenna

4.1.4 Infrared Camera

An infrared camera generates an image using infrared radiation. The use of the infrared camera is to convert infrared radiation, which cannot be seen by the human eye, into a visual image. The conducted infrared radiation by the infrared camera provides valuable information regarding heat dissipation throughout the material that is being scanned, and the presence of any delamination.

In this study, a “Flir E50” infrared camera shown in Figure 4-18 was used. This camera produces images of 240×180 pixels, and detects the thermal variations across the area captured by the camera. The aim of this technique was to detect if there are any gaps between concrete panels and backfill soil. Figure 4-19 shows an infrared scan conducted on the precast panels of Wall 264R.

Figure 4-18 Infrared camera

Figure 4-19 Infrared camera scan at Wall 264R

4.1.5 Resistivity Imaging (RI)

Resistivity Imaging (RI) is a geophysical technique for conducting scans of sub-surface structures using electrical resistivity measurements placed at the surface by installing electrodes into boreholes. The application of RI is to investigate the groundwater table and perched water zones. Figures 4-20(a through d) show the RI components.

(a) Electrode

(b) Cable

(c) Multi electrode switch box

(d) RI SuperString

Figure 4-20 RI components

The setup of the RI machine requires placing 28 electrodes with uniform spacing, ranging between 5 to 6 ft. The electrode tips had to be in contact with the top layer of the backfill soil in order to capture 2D subsurface images; therefore, the concrete pavement of the shoulder was drilled at the electrode marked locations shown in Figures 4-21(a through c) atop each MSE wall.

(a) RI scan area at Wall 264R

(b) RI scan area at Wall 179L

(c) RI scan area at Walls CC1-3

Figure 4-21 RI scan areas

The process of the RI scanning included drilling 28 holes (Figure 4-22(a)), inserting and hammering the electrodes through the concrete holes (Figure 4-22(b)), connecting the electrodes with the RI cable (Figure 4-22(c)), connecting the cable with the Multi Electrode Switch Box and RI SuperString (Figure 4-22(d)), conducting the RI scan (Figure 4-22(d)), and patching the 28 holes with a rapid repairing mortar according to DMS-4655 TxDOT specifications (2017) (Figure 4-22(e)).

(a) Drilling 28 holes

(b) Inserting and hammering the electrodes

(c) Connecting the electrodes to RI cable

(d) Connecting the RI cable to Multi Electrode Switch Box and RI SuperString, and conducting RI scan

(e) Patching the holes with rapid concrete mortar

Figure 4-22 RI process

4.2 NDE Results

4.2.1 Laser Scanning Results

Following the laser scan, the data was transferred to the Trimble business software and the target coordinates of the MSE walls were generated. Then, charts were developed for all the targets, as shown in Figures 4-23 through 4-31. The movement is relative to the first scan conducted in August 2017. The last scan conducted was in November 2018 for Walls 179L and CC1-3, and June 2019 for Wall 264R. Three charts were generated for each wall in order to monitor the 3D movement (N-S, E-W, and the vertical directions). A related figure is added under each chart to visualize the 3D

movement. Based on the data analysis, all the targets behind the range of SX10 scanner error (0.06 to 0.12 inches) were considered to be stable.

Figures 4-23 to 4-25 show that Wall 264R exhibits some movement towards the east (max. 0.156 inch) and a considerable downward movement (max. 0.325 inch). Based on Figures 4-26 through 4-28, a few targets on Wall 179L moved in the southern direction (max. 0.228 inch). Wall 179L showed some movement in the eastern direction (max. 0.216 inch) while only a few targets moved downward (max. 0.168 inch). Walls CC1-3 look stable in all the directions, as shown in Figures 4-29 through 4-31.

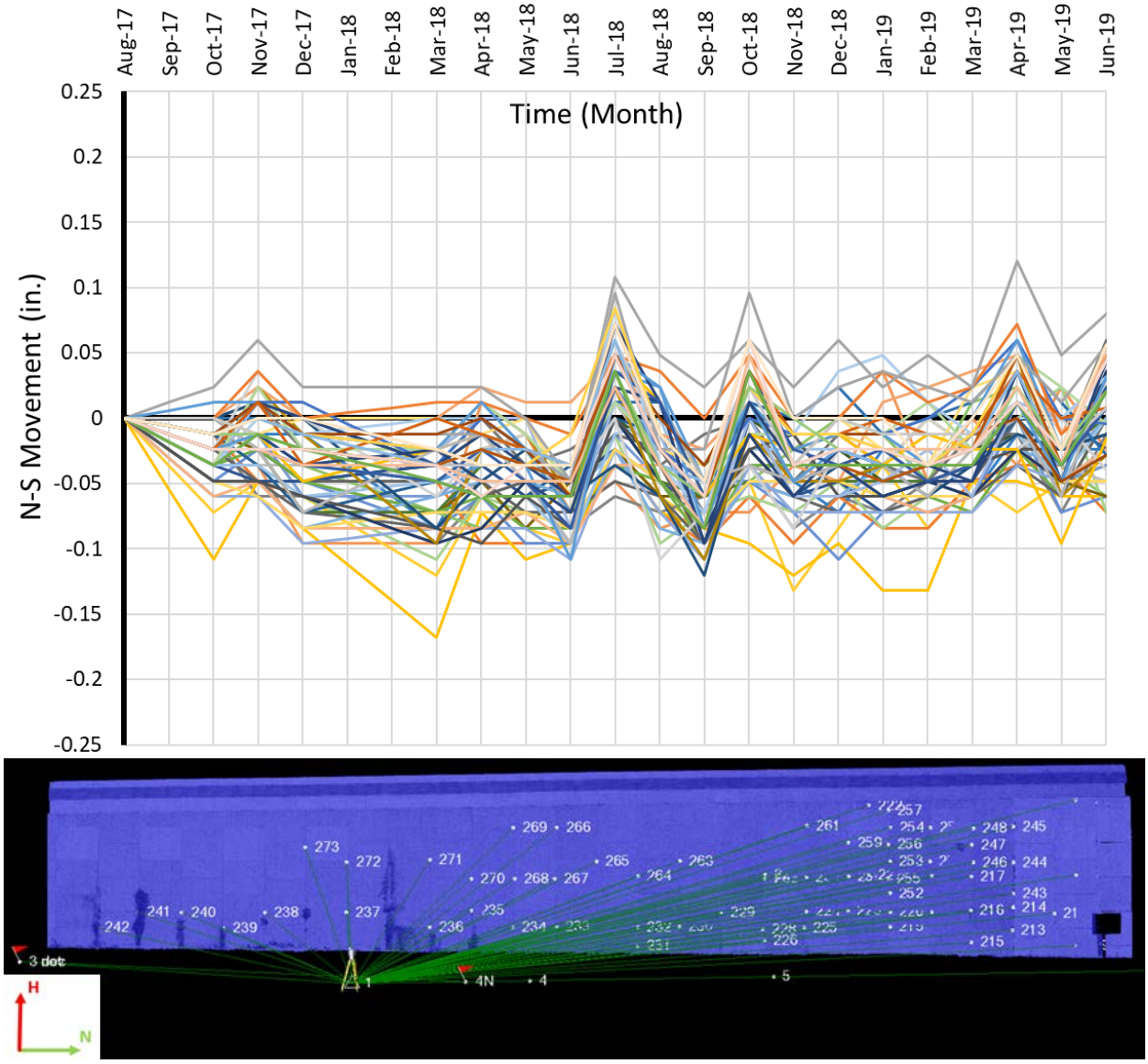

Figure 4-23 Movement in N-S direction of Wall 264R

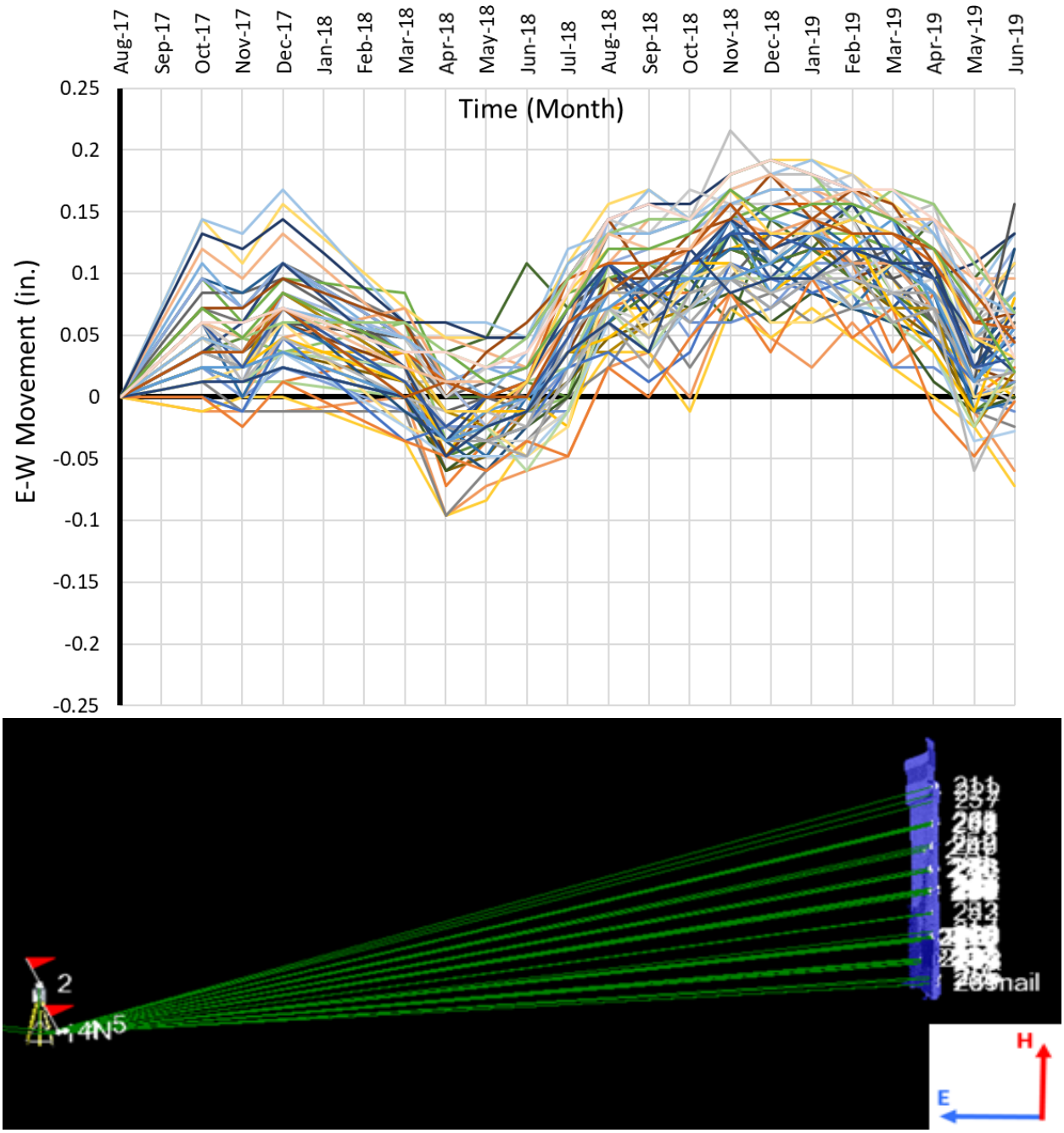

Figure 4-24 Movement in E-W direction of Wall 264R

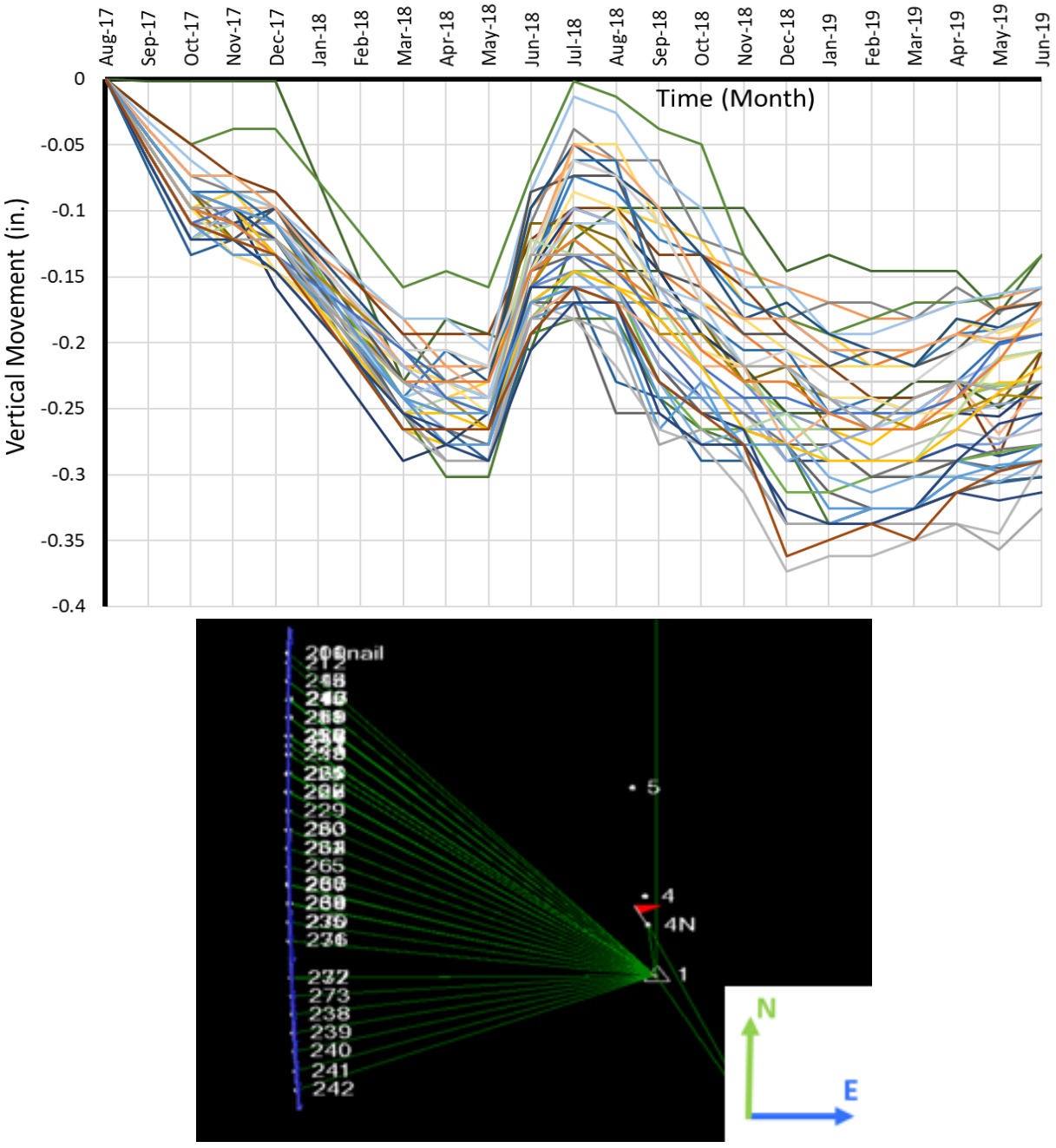

Figure 4-25 Movement in vertical direction of Wall 264R

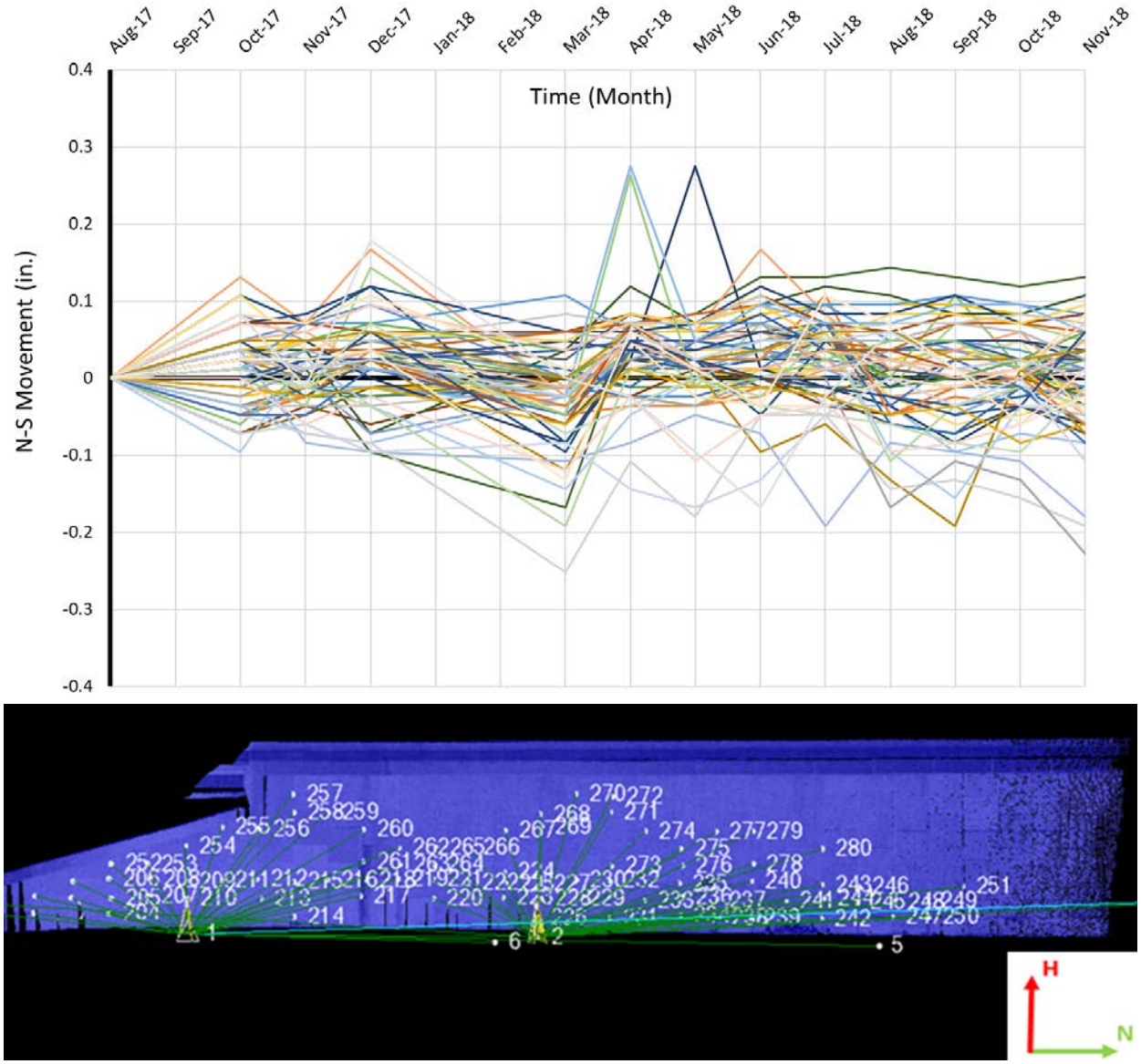

Figure 4-26 Movement in N-S direction of Wall 179L

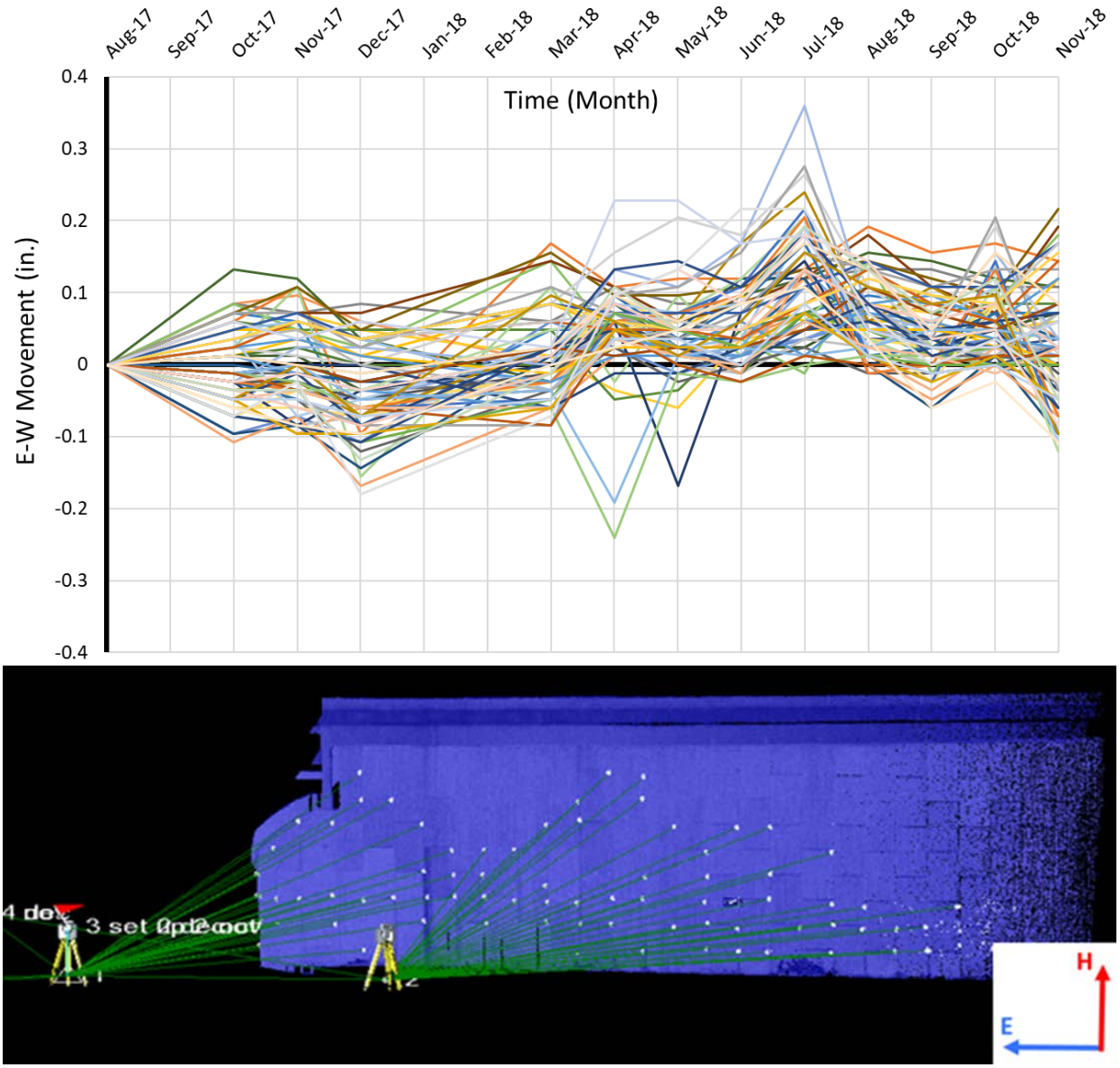

Figure 4-27 Movement in E-W direction of Wall 179L

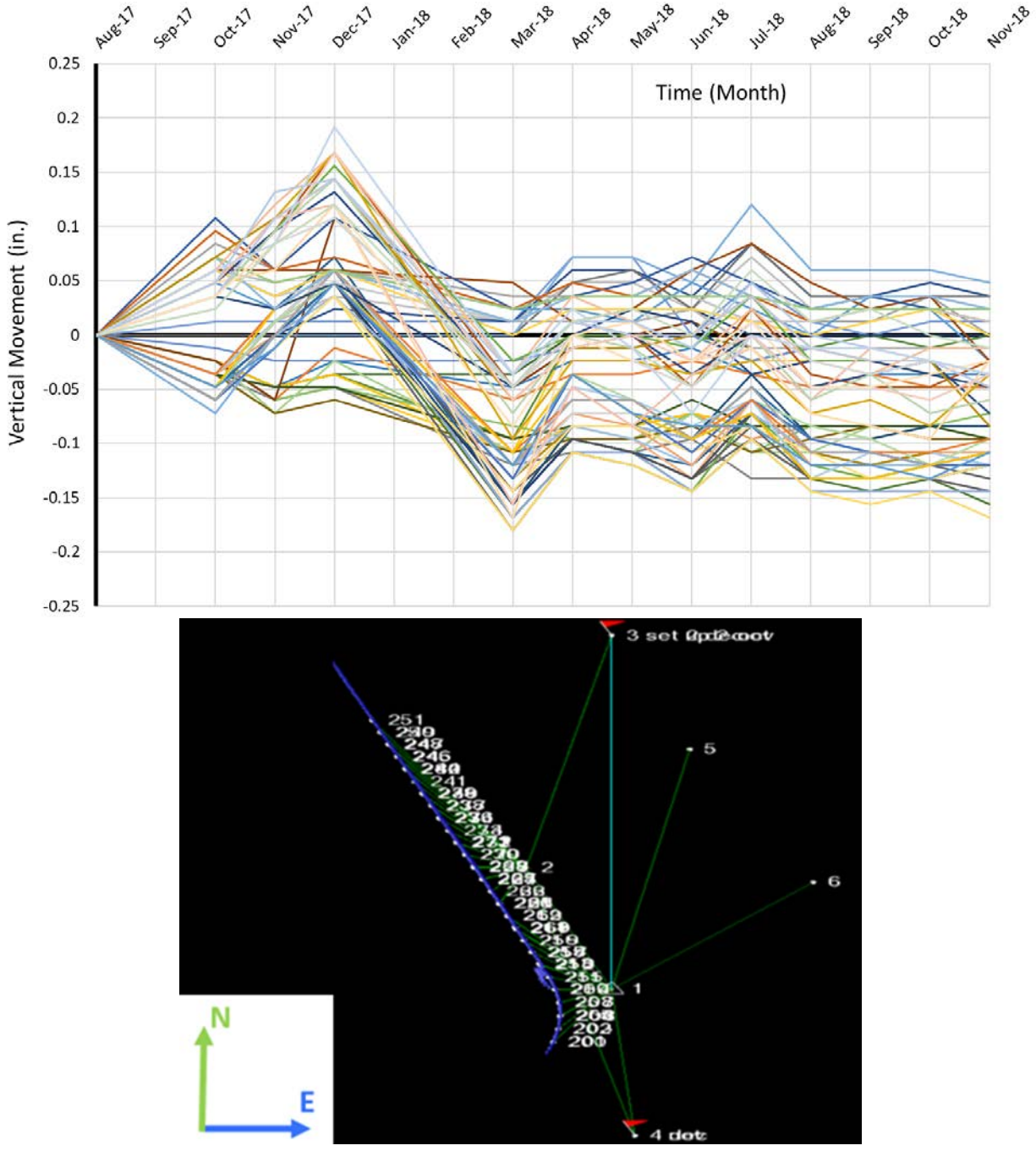

Figure 4-28 Movement in vertical direction of Wall 179L

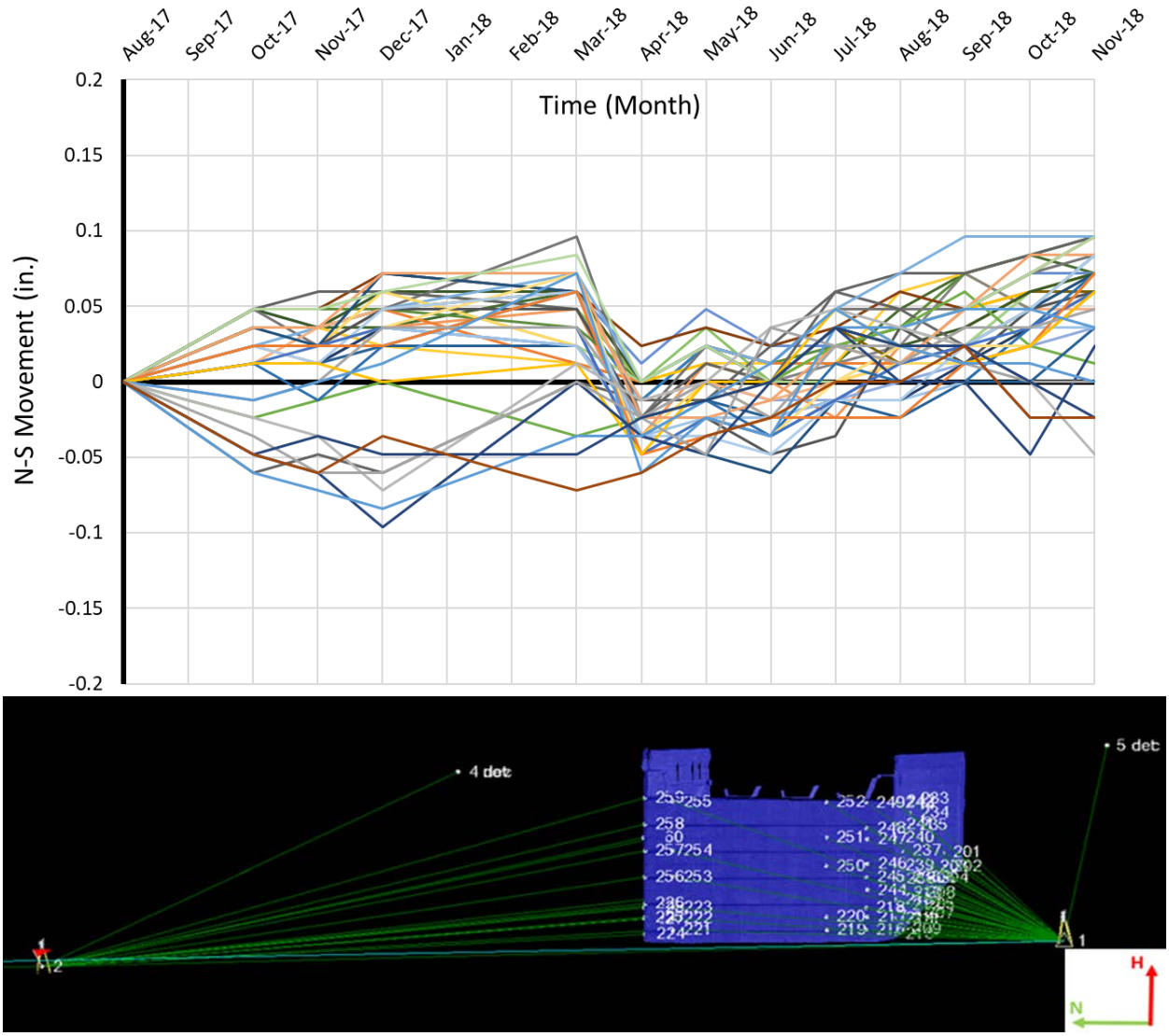

Figure 4-29 Movement in N-S direction of Walls CC1-3

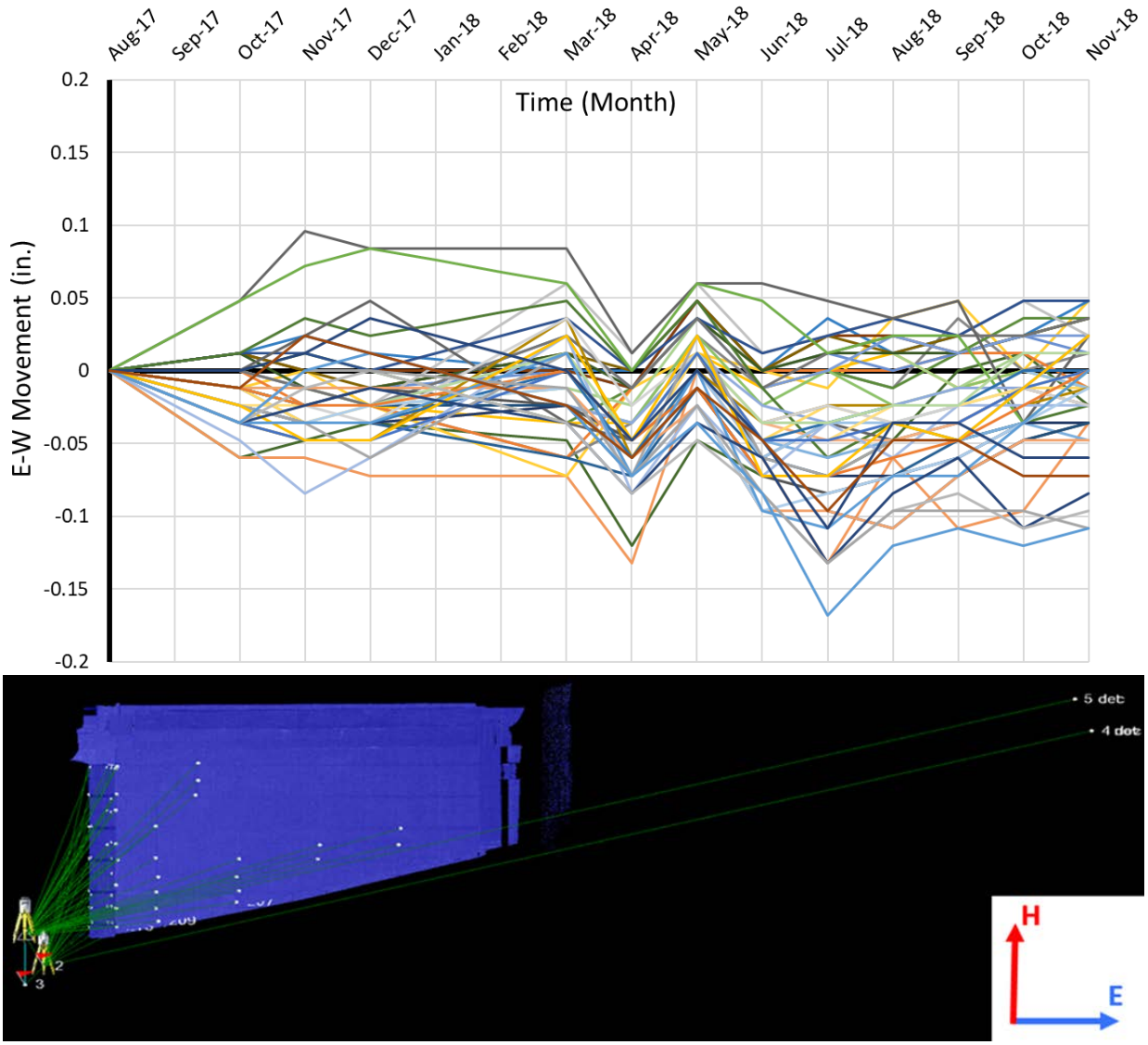

Figure 4-30 Movement in E-W direction of Walls CC1-3

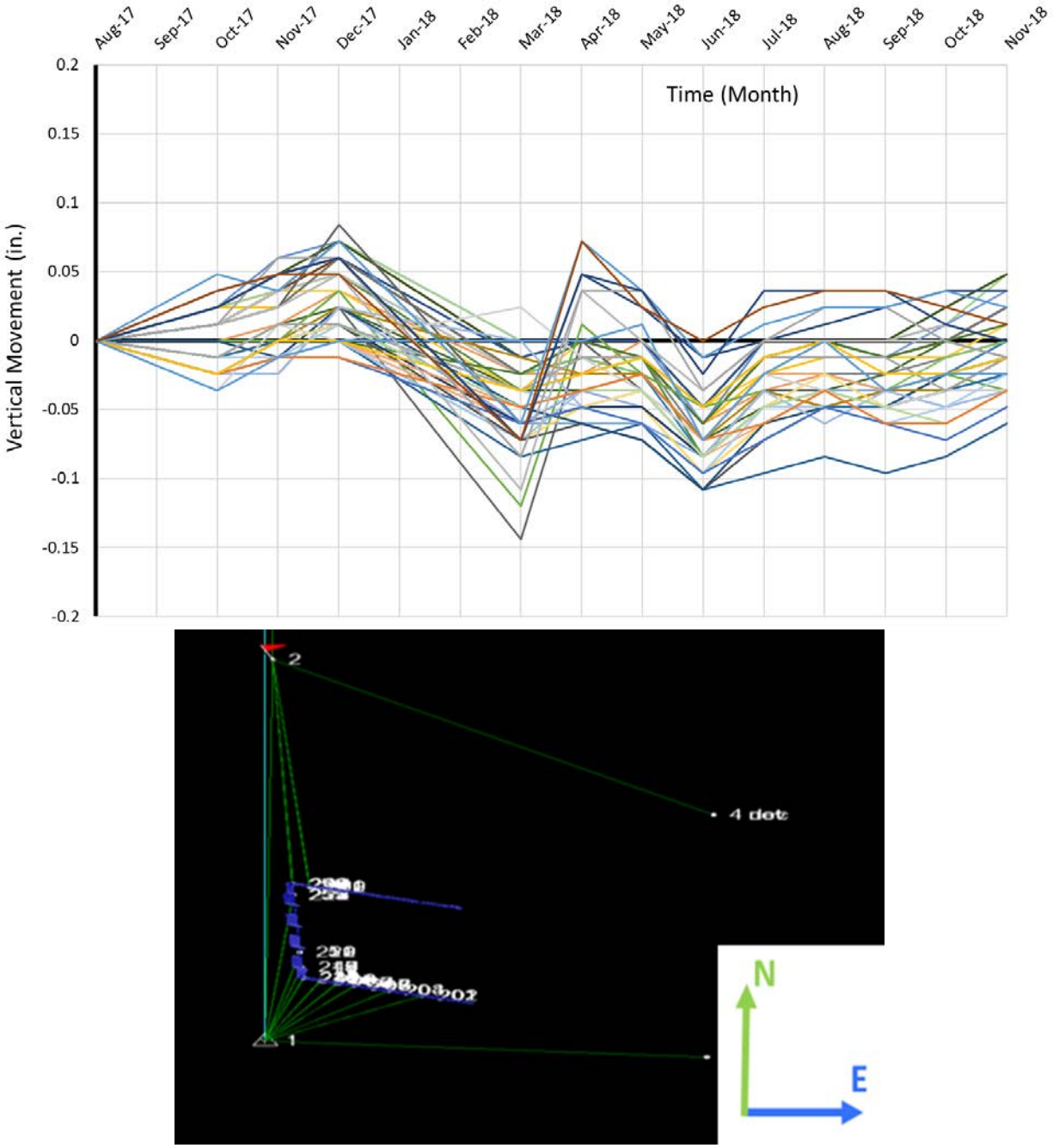

Figure 4-31 Movement in vertical direction of Walls CC1-3

As Walls 264R and 179L which located in Hurst, TX, have shown movement through the conducted monitoring period, it was decided to compare their movement with the closest rainfall station, locates within 1 mile away from the walls, in order to investigate whether the movement is correlated to seasonal variation or not. The rainfall data (Figure 4-32) was collected from the National Centers for Environmental Information (NOAA). The monthly average precipitation was used for the comparison. It can be noted that heavy rain events affect Wall 264R by causing lateral (out-of-plane) movement and settlement as the spikes shown in Figures 4-24 and 4-25 occurred when heavy rains took place. On the other hand, the survey data conducted at Wall 179L seems to have no correlation with precipitation. This could be caused by the manhole that is existed behind the precast panels of Wall 179L, which might leak water into the backfill soil at different times from the rain events.

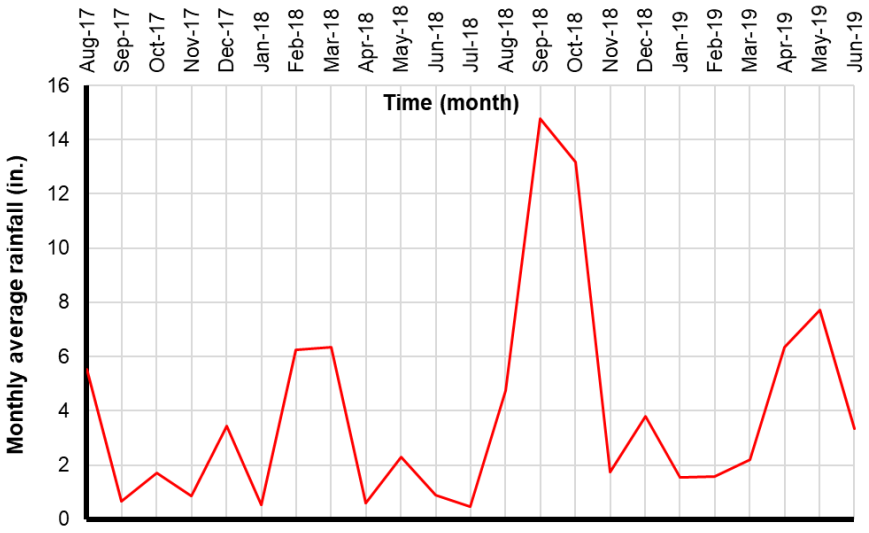

Figure 4-32 Average monthly rainfall recorded by rainfall station

4.2.2 Crack Meter Results

The readings of the crack meters are relative to the installation date, December 2018. The last reading of the crack meters was taken in June 2019.The readings shown in Figures 4-33(a and b) show that the wall is exhibiting settlement, approximately 0.05 inch in a 6 month period, as well as a slight lateral movement towards the north.

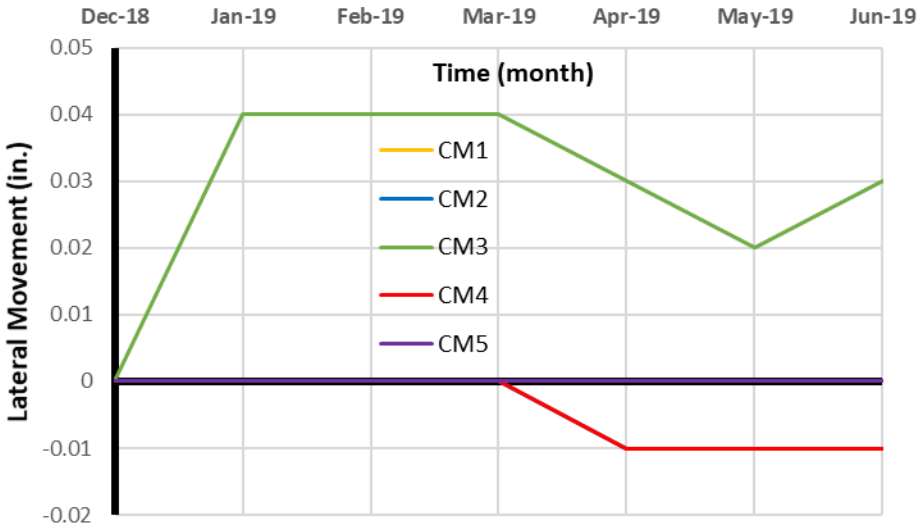

(a) Lateral movement

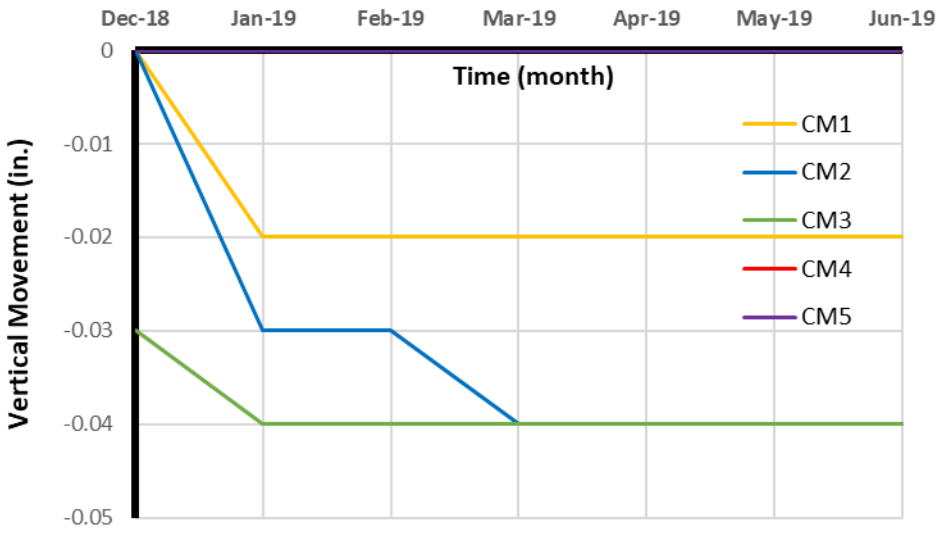

(b) Vertical movement

Figure 4-33 Crack meter readings

4.2.3 GPR Results

Figure 4-34 illustrates a sample of a GPR B vertical scan (parallel to the traffic) showing the rebar positions, the soil layers and the earth reinforcement, and Figure 4-35 shows a sample of a GPR B horizontal scan (transverse to the traffic) using the 400 MHz antenna. The type of scan, along the shoulder or the road section, can be identified in the scan.

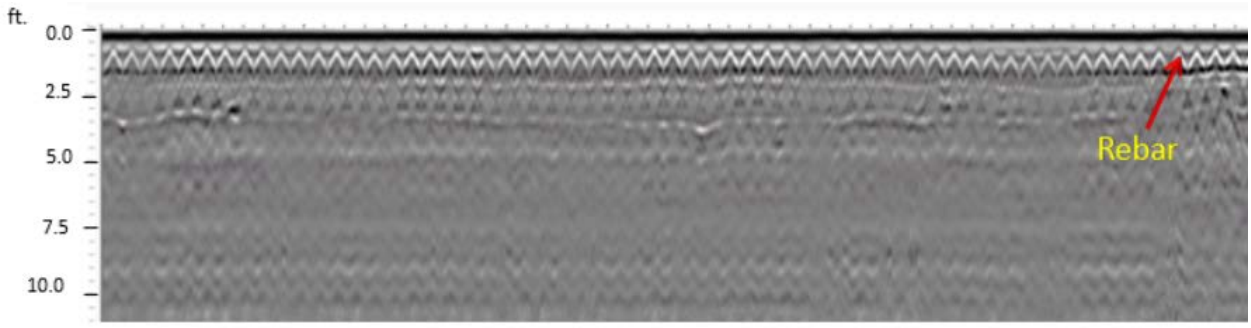

Figure 4-34 GPR B Scan parallel to the traffic

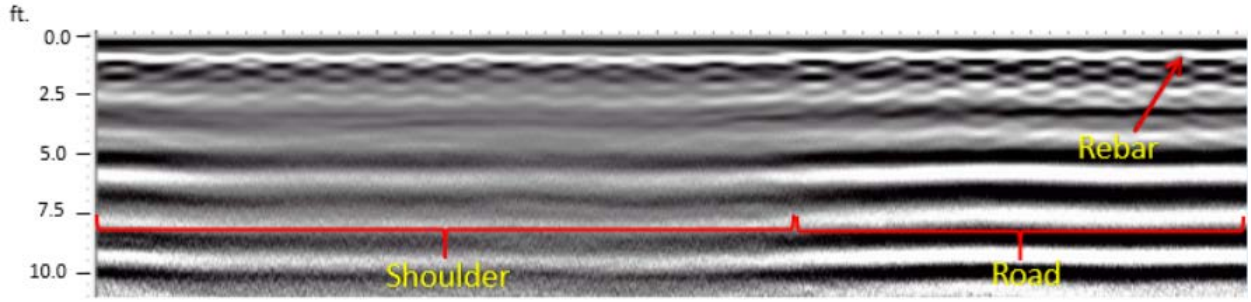

Figure 4-35 GPR B Scan transverse to the traffic

Initial analysis of the scan data showed that the penetration depth and the resolution of the scan were heavily affected by the steel reinforcement in the pavement and the density of the reinforcement layers.

4.2.4 Infrared Camera Results

As the infrared camera is highly affected by the temperature variation, the temperature distribution that is caused by the sunlight varies at the external surfaces of the concrete panels and it is higher than that at the front face of the backfill soil. Thus, the

infrared waves could not pass through the concrete panels and the gaps between the panels and the backfill soil could not be detected. Figures 4-36(a-d) show a sample of infrared camera scans conducted on the concrete panels.

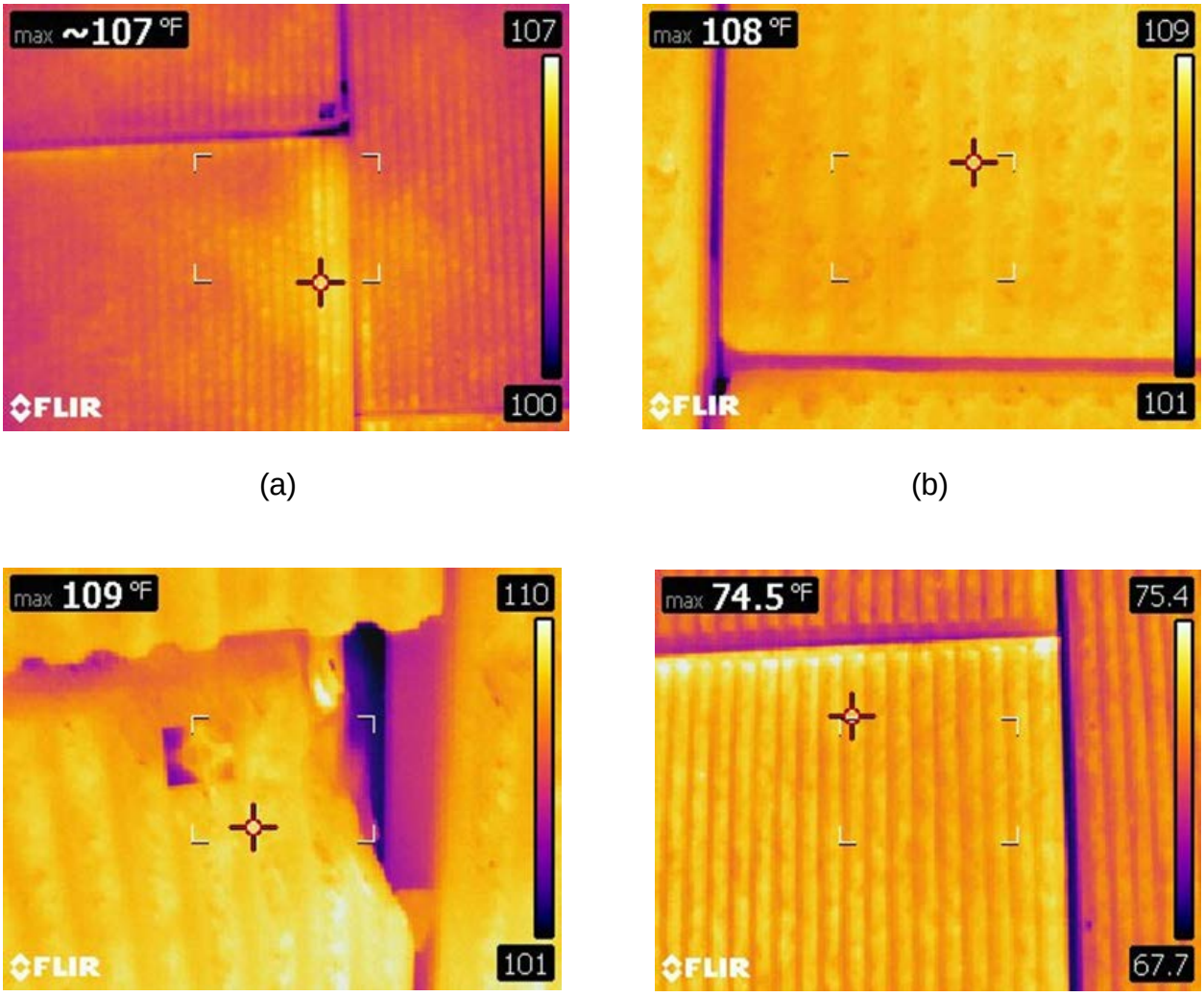

(a) (b)

(c) (d)

Figure 4-36 Infrared camera scans

4.2.5 RI Results

Two RI scans were conducted on each MSE wall, in Mar.-Apr. 2018 and Sep.-Oct. 2018.The related rainfall data is added under each RI scan to visualize their effect on the backfill soil. For Walls CC1-3, another respective rainfall station was picked to obtain the actual precipitation that occurred in that area during the concerned time. The RI scan events are indicated by dashed lines in the rainfall charts.

Based on Figures 4-37 and 4-38, the RI scans are significantly affected by the rainfall amounts. These figures show that the water zones, indicated by the blue zones, increased at Walls 264R and 179L during the second phase because of the heavy rain that occurred before the scans were conducted.

The RI scans also indicate that Walls 264R and 179L have poor drainage systems since they allow water pockets to be formed behind the facing panels during rain events. On the other hand, Figure 4-39 shows that Walls CC1-3 appear to have a good drainage system as the resistivity of both RI scans is very low in both scans. This is because the backfill soil of Walls CC1-3 consists of only aggregate which has high permeability properties.

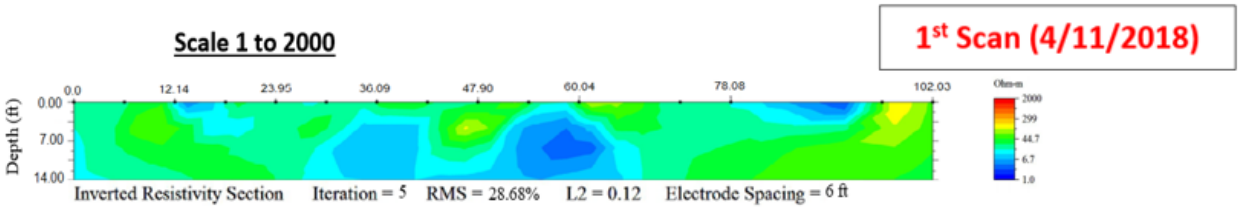

(a) 1st RI scan at Wall 264R

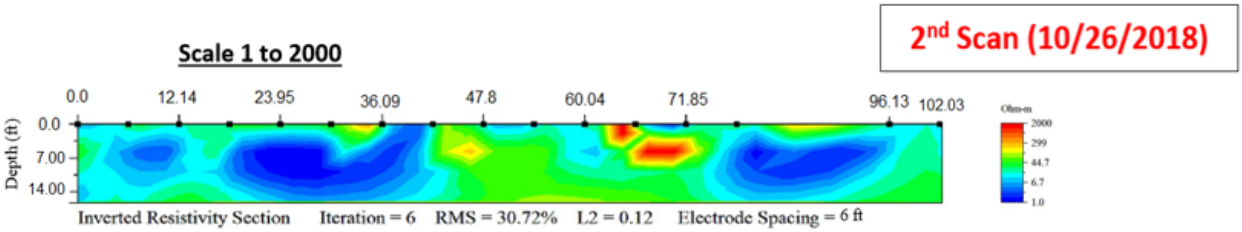

(b) 2nd RI scan at Wall 264R

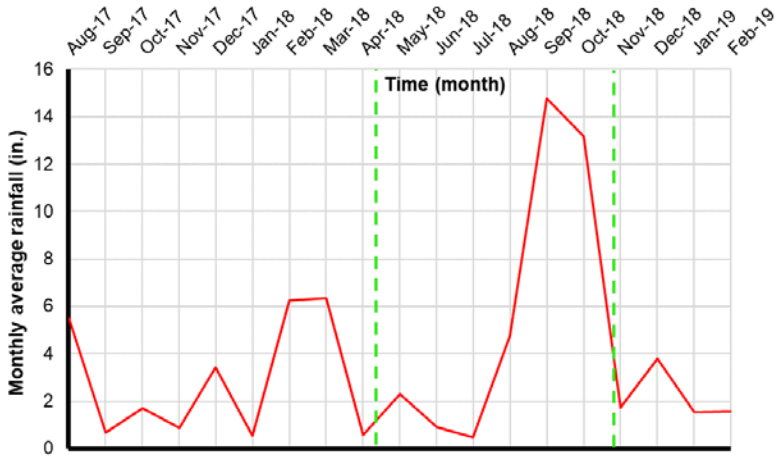

(c) Average monthly rainfall

Figure 4-37 RI scans conducted at Wall 264R along with rainfall and temperature data

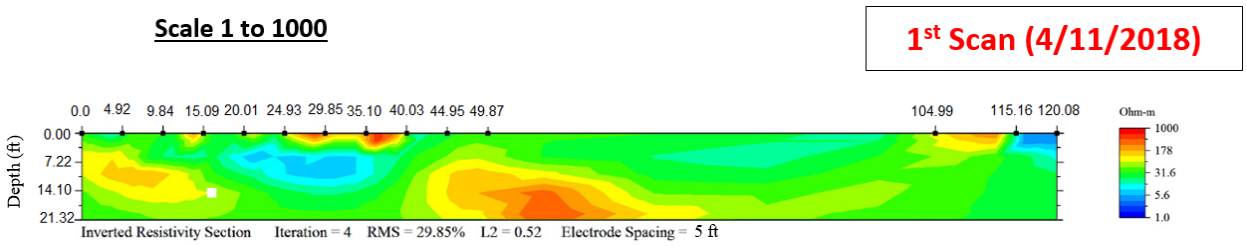

(a) 1st RI scan at Wall 179L

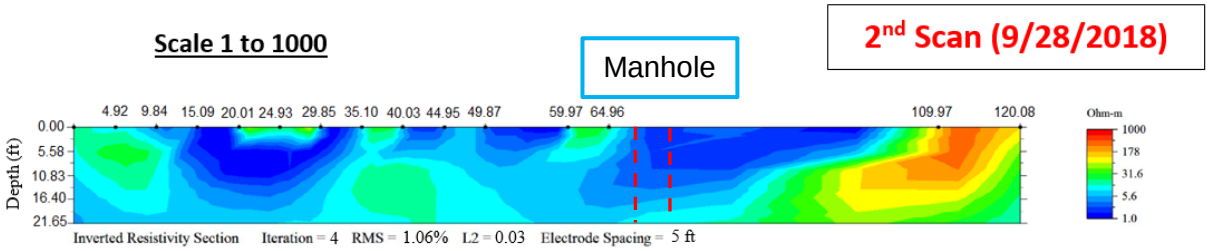

(b) 2nd RI scan at Wall 179L

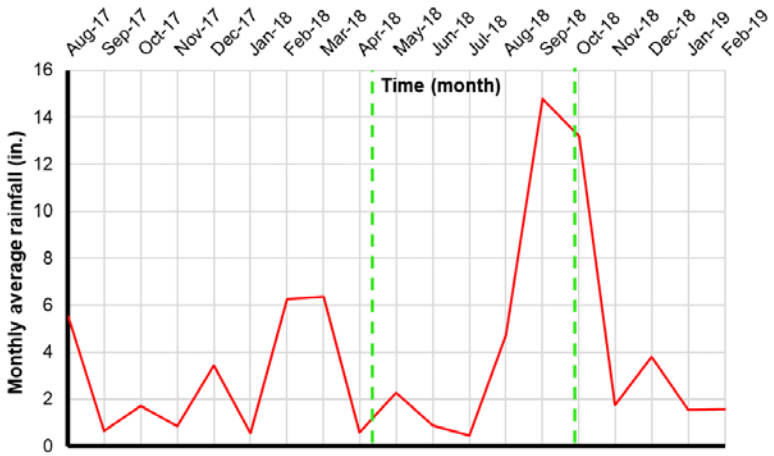

(c) Average monthly rainfall

Figure 4-38 RI scans conducted at Wall 179L along with rainfall and temperature data

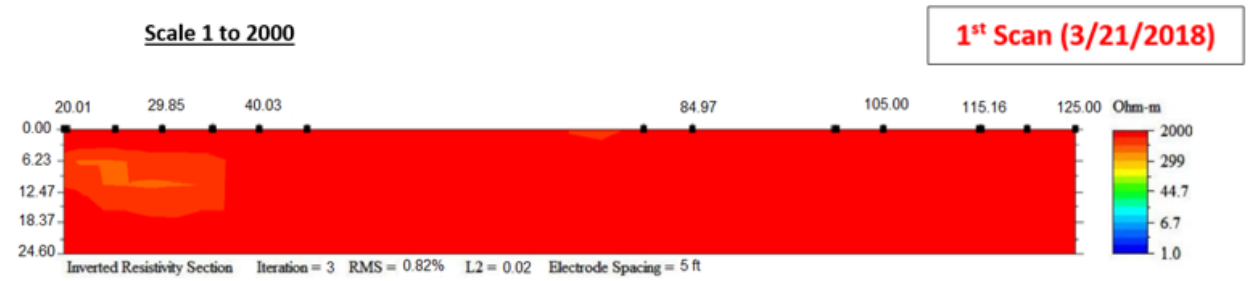

(a) 1st RI scan at Walls CC1-3

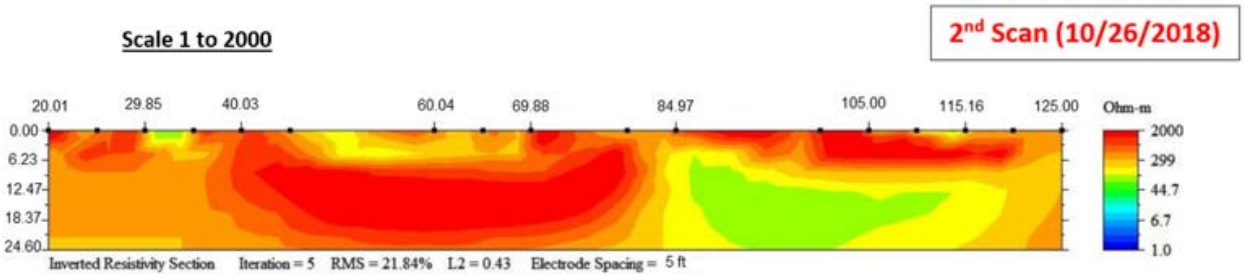

(b) 2nd RI scan at Walls CC1-3

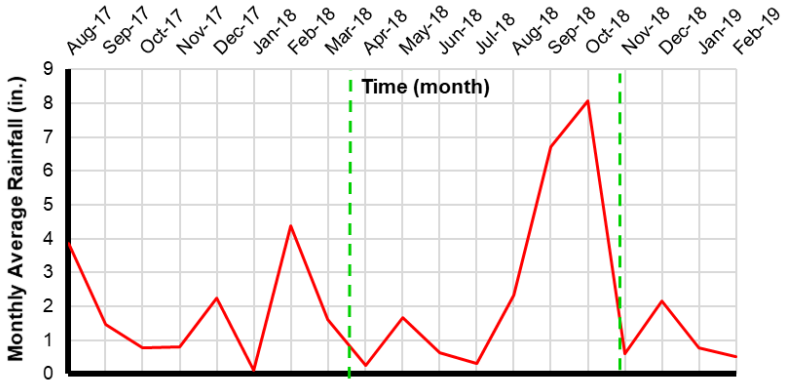

(c) Average monthly rainfall

Figure 4-39 RI scans conducted at Walls CC1-3 along with rainfall and temperature data

4.3 Backfill Soil Testing

The movement could be due to undesirable conditions of backfill soil; therefore, soil samples of the backfill soil were collected, tested, and compared with the standard specifications of TxDOT. Furthermore, the soil samples were needed in this research in order to obtain the needed soil properties for modeling soil material in ABAQUS software. Five boreholes were conducted in March 2018, two at Wall 264R, two at Wall 179L, and one at Walls CC1-3, as shown in Figures 4-40(a through c).

(a) Borehole locations at Wall 264R

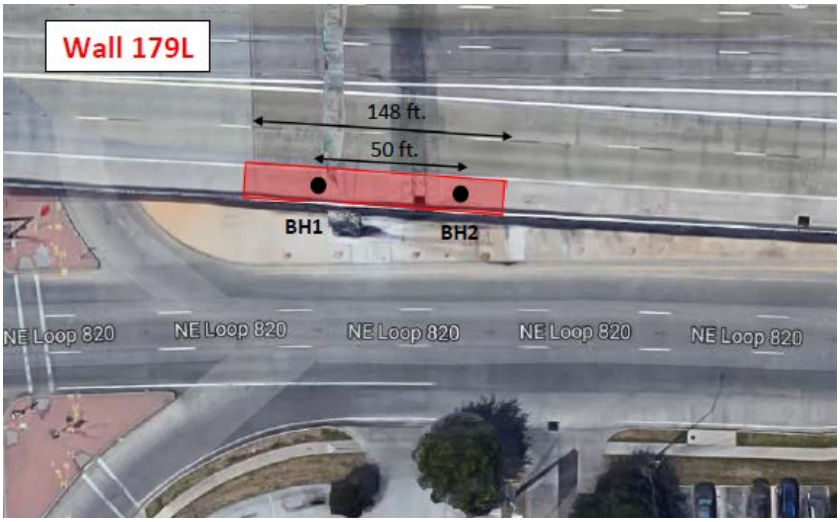

(b) Borehole locations at Wall 179L

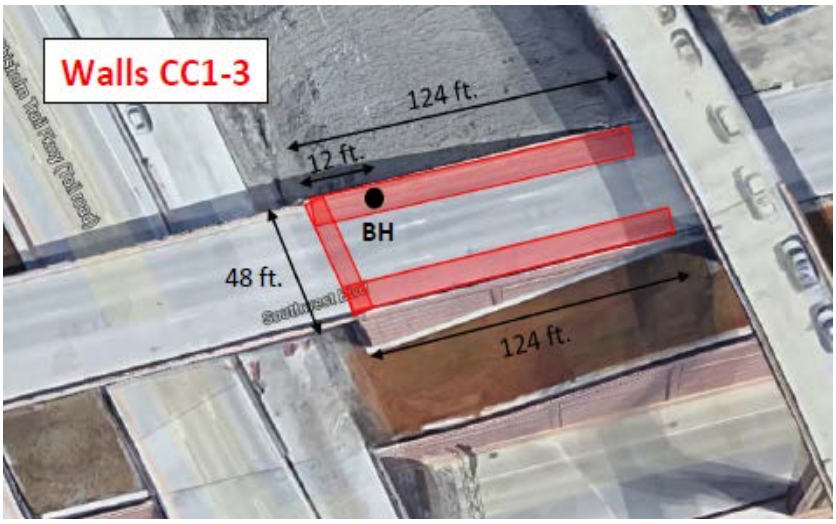

(c) Borehole location at Walls CC1-3

Figure 4-40 Borehole locations

Soil samples were collected at multiple depths throughout the boreholes. This process included drilling around 20 ft throughout the depth of the backfill soil, collecting disturbed and undisturbed samples using Split Spoon Sampler and Shelby tubes,

respectively, filling the boreholes with bentonite clay material, and patching them according to DMS-4655 TxDOT specifications (2017). Figures 4-41(a to d) show the soil test boring process.

(a) Setup

(b) Drilling

(c) Soil samples

(d) Patched borehole

Figure 4-41 Soil test boring process

The type of soil obtained from the boreholes played a role in deciding what tests to be performed. The backfill soil type of Walls 264R and 179L is silty sand, as shown in Figure 4-42. Therefore, Sieve Analysis, Proctor Compaction and Triaxial tests were chosen for testing the soil samples of Walls 264R and 179L. On the other hand, only Sieve Analysis and Angle of Repose tests were chosen for testing the backfill soil of Walls CC1-3. This is because the soil material of Walls CC1-3 is aggregate (Figure 4-42); hence, soil specimens could not be formed for the Proctor Compaction and Triaxial tests since they are cohesionless. The soil samples have to have some amounts of cohesion in order to form soil specimens using molds.

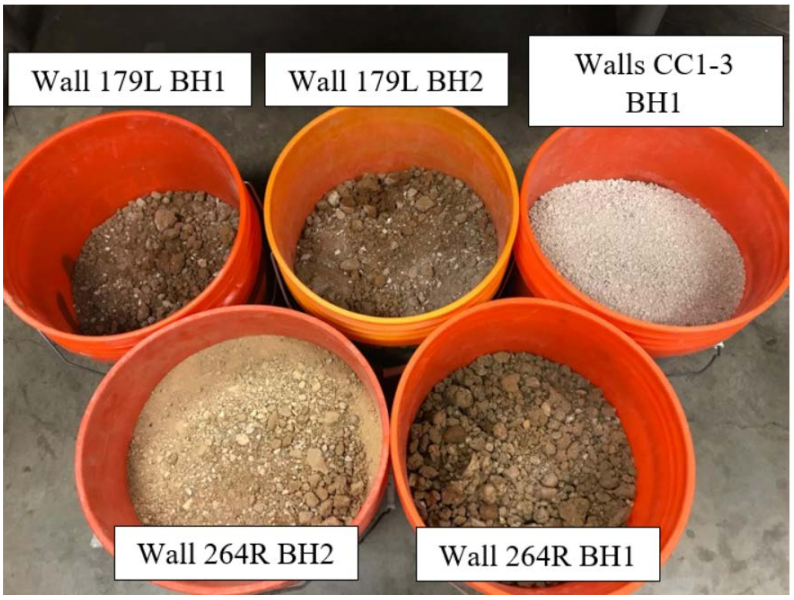

Figure 4-42 Backfill soils obtained from different boreholes

4.3.1 Sieve Analysis Test

The Sieve Analysis method is used to assess the distribution of particle size of a soil sample. The soil sample passes through a stack of progressively smaller mesh sizes. The stack is then broken down to each size and weighed to give an accurate breakdown of the composition of the sample. The backfill soils of Walls 264R, 179L and CC1-3 were tested using this method, as shown in Figures 4-43(a through d).

(a) Prepared soil sample

(b) Arranged sieves

(c) Applying vibration using sieve shaker

(b) Weighing the sieves

Figure 4-43 Sieve analysis test

The backfill soils of the MSE walls were compared with their respective specification books, as follows:

- Walls 264R and 179L follow the 1993 TxDOT Specification Book (Table 4-2).
- Walls CC1-3 follow the 2004 TxDOT Specification Book (Table 4-3).

All the MSE walls have the same soil type, which is Type B; however, the nature of the backfill soil of Walls CC1-3 is different than that of Walls 264R and 179L. This is because the backfill soil of Walls CC1-3 is aggregate, while the backfills of Walls 264R and 179L are silty sand.

Table 4-2 MSE wall backfill material specification according to 1993 TxDOT Spec Book

	Sieve Size	**Percent Passing**
Type A	3 inches	100
	No. 40	0-60
	No. 200	0-15
Type B	6 inches	100
	3 inches	75-100
	No. 200	0-15

Table 4-3 MSE wall backfill material specification according to 2004 TxDOT Spec Book

	Sieve Size	**Percent Retained**
Type A	3 inches	0
	½ inch	50-100
	No. 4	See Note
	No. 40	85-100
Type B	3 inches	0
	No. 4	See Note
	No. 40	40-100
	No. 200	85-100
Type C	3 inches	0
	No. 4	See Note
	No. 200	70-100
Type D	3 inches	0
	3/8 inch	85-100

Two samples were taken from each borehole. For each sample, a sieve analysis test was performed and compared to either the 1993 TxDOT Specification Book (Table 4-2) or the 2004 TxDOT Specification Book (Table 4-3), then the average of the fine

content percentage that passes through the No. 200 sieve of the two samples were calculated and compared with the TxDOT specifications.

4.3.2 Proctor Compaction Test

The Proctor Compaction test is a laboratory test used to determine the optimal moisture content. This is where a given soil type will become most dense and achieve its maximum dry density. The backfill soils of Walls 264R and 179L were tested using this method (Figures 4-44(a-d)), and the evaluated maximum dry density was compared with the TxDOT specifications.

(a) Proctor compaction tools

(b) Preparing soil samples in molds

(c) Weighing soil samples before baking (d) Weighing soil samples after baking

Figure 4-44 Proctor compaction test

4.3.3 Triaxial Test

The Triaxial test is a common test used to measure the mechanical properties of soil, such as cohesive strength (C), friction angle (Ø), and Young's modulus (E). There are several methods to perform the Triaxial test, but the method that was used in this research is the Consolidated Undrained (CU) test. Using this method, the sample is not allowed to drain because the sample is considered to be saturated, as shown in Figure 4-45.

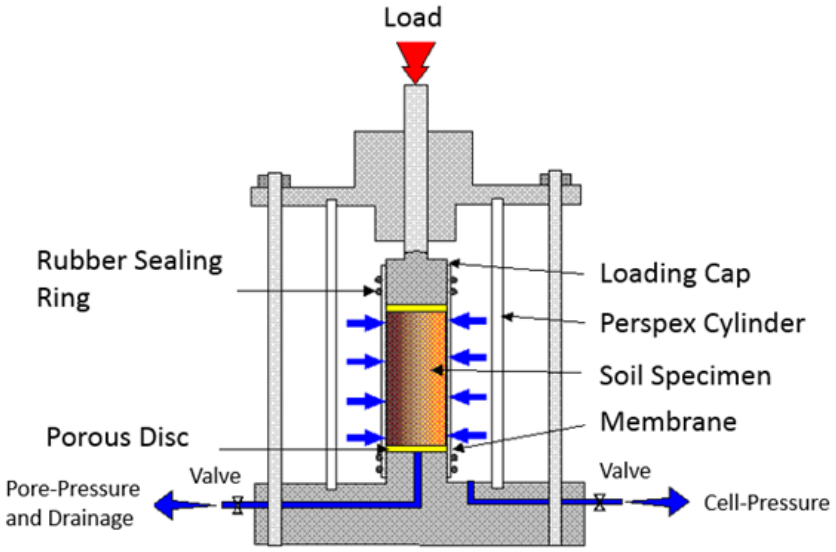

Figure 4-45 Consolidated Undrained (CU) machine

The optimum moisture content "ω_{opt}" conducted from the Proctor Compaction test was used in preparing the soil samples for this test. Two samples were made from each borehole of Walls 264R and 179L. The soil sample was compacted in three layers, kept in a moisture room for at least 16 hours to let the water content distribute uniformly throughout the specimen, wrapped using latex membrane, and inserted in a cell to perform the CU test (Figures 4-46(a-d)).

(a) Preparing soil sample

(b) Compacting soil sample

(c) Setup

(d) Performing Triaxial test

Figure 4-46 Consolidated Undrained (CU) test process

Eight tests were completed using the CU test, two for each borehole of Walls 264R and 179L. This is because in order to obtain soil parameters from a stress-strain plot, at least two Mohr-Coulomb curves are needed. According to TxDOT specifications, the backfill soil should be cohesionless with a minimum friction angle (Ø) of 34^{o}.

4.3.4 Angle of Repose Test

The angle of repose is a macroscopic test used to characterize the behavior of granular materials. This angle of repose has been found to be equal to the angle of internal friction "Ø" of a granular material. It can be measured in a laboratory using the funnel test. This test is used by the American Society of Testing and Materials (ASTM) (Method No. C1444-00; ASTM, 2001).

The funnel test was performed on the backfill soil of Walls CC1-3. Using this method, granular material is placed in a funnel and then it is slowly deposited on a horizontal surface. A cone shape is formed after pouring the granular material through the funnel (Figure 4-47). The bottom of the funnel should be held close to the tip of the cone and gently raised as the size of the cone increases; this is recommended to eliminate the damping effect of falling particles. The angle of repose can be calculated by dividing the height of the cone by half of the average width of the base of the cone, as shown in Figures 4-48(a to c). The angle of repose is measured by taking the inverse tangent of that ratio.

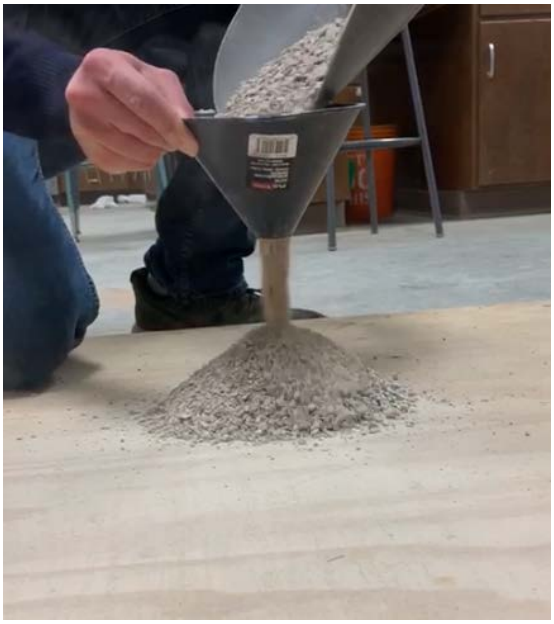

Figure 4-47 Angle of repose test

(a) Measuring 1st diameter of cone

(b) Measuring 2nd diameter of cone

(c) Measuring height of cone

Figure 4-48 Measuring angle of repose

The angle of repose provides a good estimation of the friction angle of soil; however, for an MSE wall situation, the friction angle value of backfill soil in field is higher than the angle of repose. This is because the backfill soil is compacted to some degree in the field. Compaction provides higher shear strength for a soil layer than when it is in its loose state. Therefore, the friction angles of backfill soils in field are slightly higher than the measured angle of reposes. The following equation proposed by Ghazavi et al. (2008) estimates the correlation between the angle of repose (θ) and the field angle of friction (Ø):

$$\theta = 0.36\text{Ø} + 21.2 \quad (4.1)$$

4.4 Soil Testing Results

4.4.1 Sieve Analysis Results

Table 4-4 shows the sieve analysis test results. Based on the results, the backfill soils of Walls 179L and CC1-3 fall within the acceptable range of the TxDOT specifications as the percent of the fine contents does not exceed 15%, while the backfill soil of Wall 264R fails as it has excessive fine content; the percentage of the fine content that passed through sieve No. 200 exceeded 15%.

Table 4-4 Sieve analysis results

Wall	Borehole Number	Sample Number	Sieve Size	Percent Passing	Percent Passing
Wall 264R	BH1	1	6 inches 3 inches No. 200	100 100 19.94 > 15	$P_{200\ avg}$ = 20.6%>15%
		2	6 inches 3 inches No. 200	100 100 21.27 > 15	
Wall 264R	BH2	1	6 inches 3 inches No. 200	100 100 18 > 15	$P_{200\ avg}$ = 17.9%>15%
		2	6 inches 3 inches No. 200	100 100 17.7 > 15	
Wall 179L	BH1	1	6 inches 3 inches No. 200	100 100 13.28	$P_{200\ avg}$ = 14.2%<15%
		2	6 inches 3 inches No. 200	100 100 15.11	

Wall 179L	BH2	1 2	6 inches 3 inches No. 200 6 inches 3 inches No. 200	100 100 13.04 100 100 12.96	$P_{200\ avg}$ = 13%<15%
Walls CC1-3	BH1	1 2	3 inches No. 4 No. 40 No. 200 3 inches No. 4 No. 40 No. 200	100 100 93 2.78 100 100 92.06 2.68	$P_{200\ avg}$ = 2.7%<15%

4.4.2 Proctor Compaction Results

The evaluated maximum dry density was compared with the recommended dry density value by TxDOT. Figures 4-49(a-d) show the proctor compaction test results, and it shows that the backfill soils of Walls 264R and 179L have failed to achieve the optimum dry density value “125 pcf” as all the values are less than this limit.

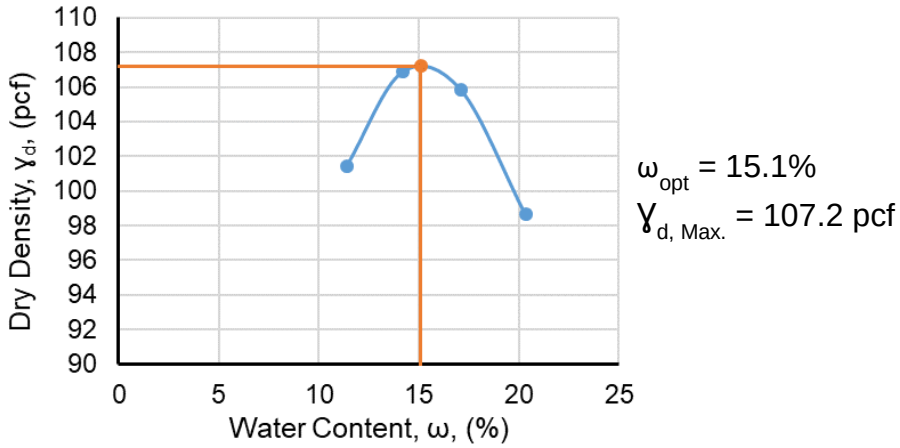

(a) Proctor compaction test results of BH1 of Wall 264R

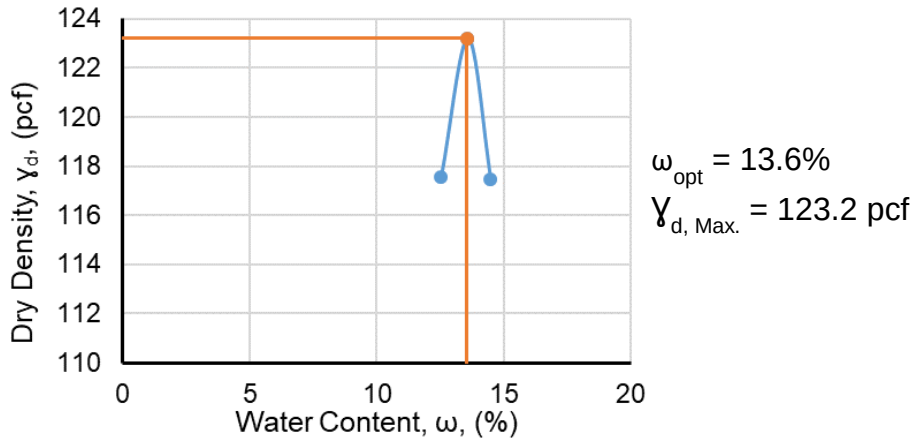

(b) Proctor compaction test results of BH2 of Wall 264R

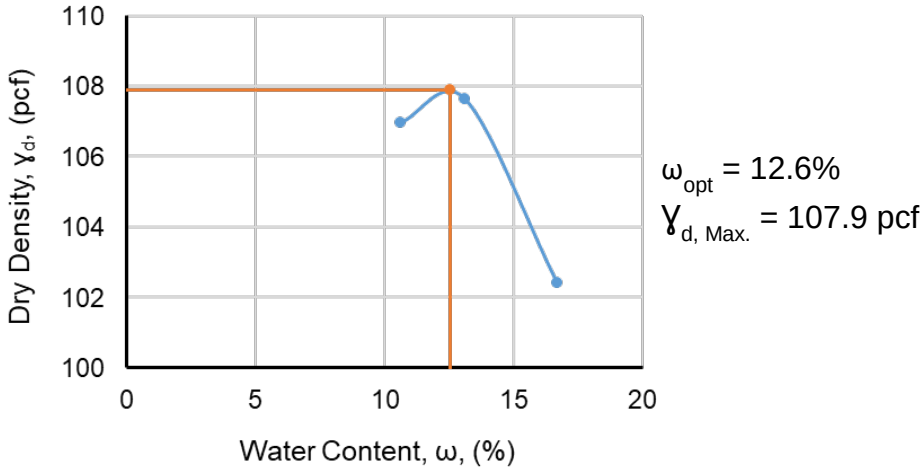

(c) Proctor compaction test results of BH1 of Wall 179L

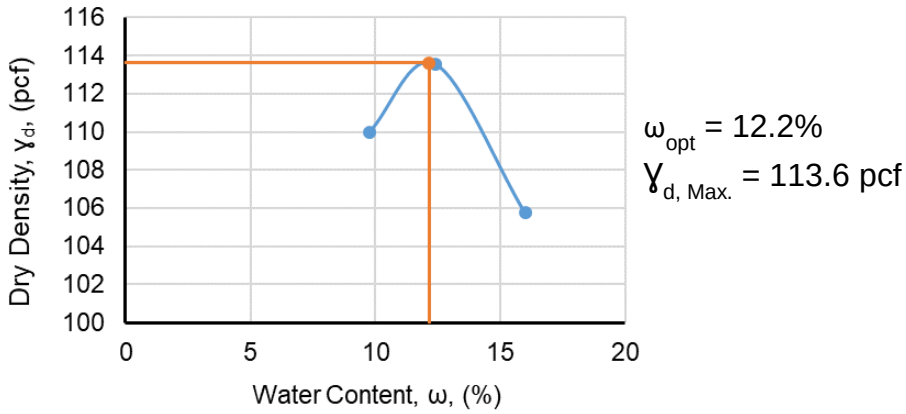

(d) Proctor compaction test results of BH2 Wall 179L

Figure 4-49 Results of proctor compaction tests

4.4.3 Triaxial Test Results

Based on the Triaxial test results shown in Figures 4-50(a-d), the friction angle of BH1 of Wall 264R does not satisfy the minimum recommended value by TxDOT, as the value is 24.5º which is less than 34º. This could be attributed to the type of the selected backfill soil; the wall section at the location of BH1 was built after the completion of the section of where BH2 is located (Figure 4-51). It seems that the backfill soil selected for the old section, BH2 location, satisfies the TxDOT specifications, while the backfill soil selected for the new section does not. On the other hand, Wall 179L have met the minimum friction angle at both borehole locations. Figures 4-50(a-d) also show that the cohesion values of the two MSE walls are very small which can be ignored.

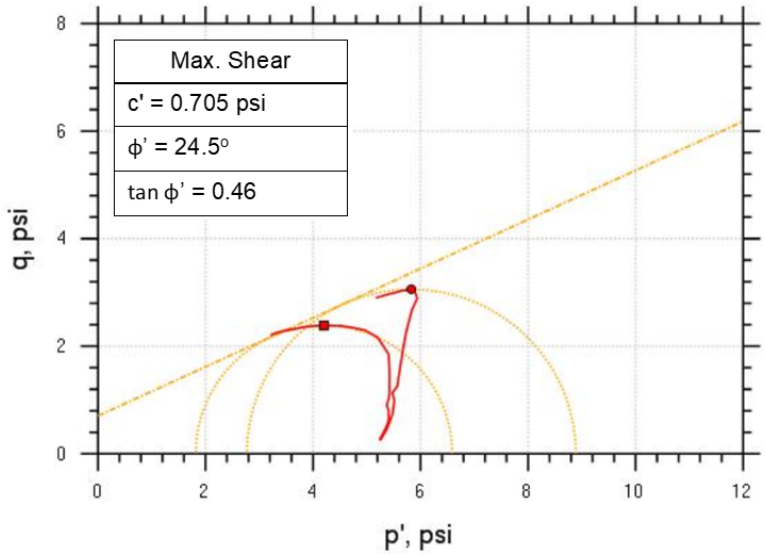

(a) CU test results of BH1 of Wall 264R

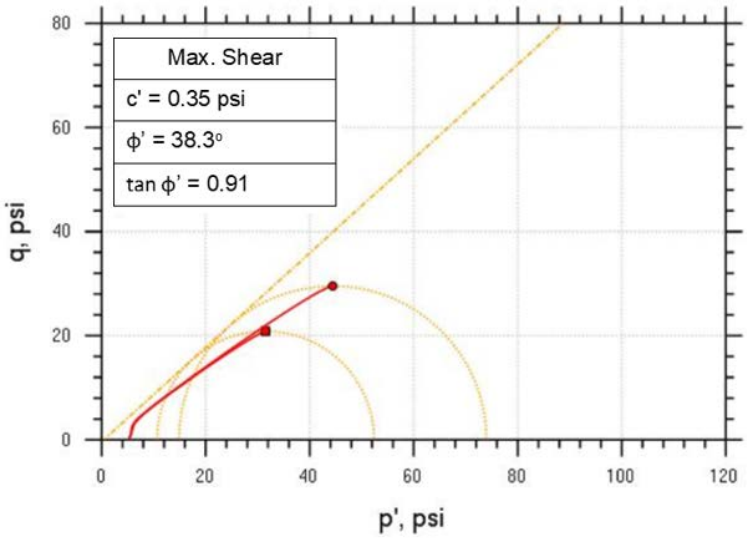

(b) CU test results of BH2 of Wall 264R

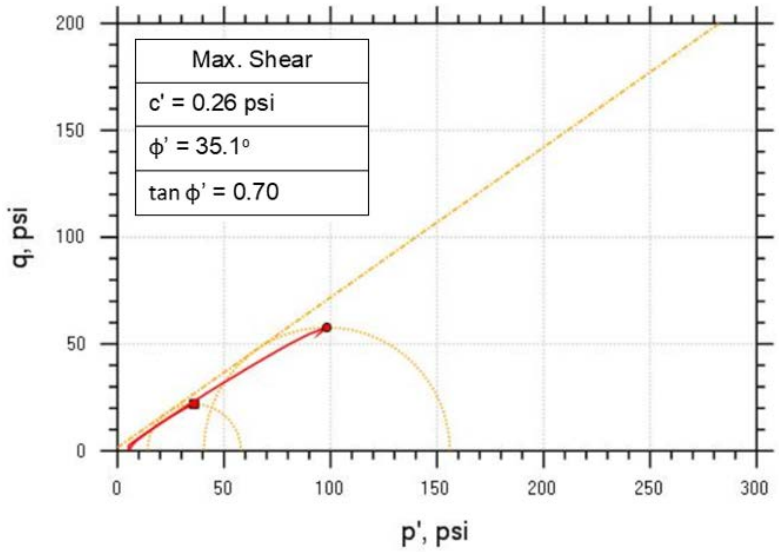

(c) CU test results of BH1 of Wall 179L

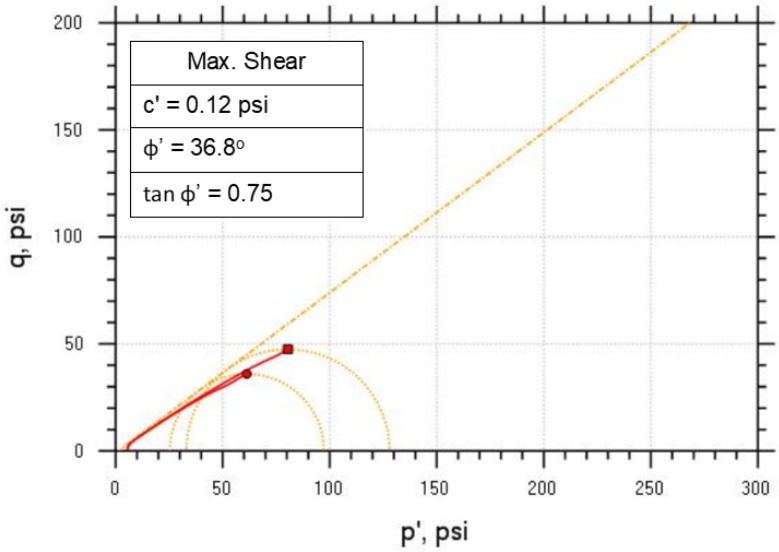

(d) CU test results of BH2 of Wall 179L

Figure 4-50 Consolidated Undrained (CU) test results

Figure 4-51 Old and new sections of Wall 264R

4.4.4 Angle of Repose Results

This test was performed on the backfill soil of Walls CC1-3. Five soil samples were taken out to be tested using this method. Table 4-5 shows that all the soil samples of Walls CC1-3 have met the minimum recommended friction angle by TxDOT, 34º, as all the conducted friction angles values surpassed this limit.

Table 4-5 Angle of repose test results

Sample Number	**Cone Dimensions (in.)**	**Average Diameter (in.)**	**Angle of Repose** $\emptyset = \tan^{-1}(\frac{h}{\frac{davg}{2}})$
1	d_1 = 7.5 d_2 = 7 h = 2.5	d_{avg} = 7.25	Ø = 34.6º
2	d_1 = 8.25 d_2 = 8.5 h = 3.125	d_{avg} = 8.375	Ø = 36.73º

3	d_1 = 9.25 d_2 = 9.875 h = 3.375	d_{avg} = 9.562	Ø = 35.22^o
4	d_1 = 9.125 d_2 = 9.25 h = 3.125	d_{avg} = 9.188	Ø = 34.23^o
5	d_1 = 7.625 d_2 = 7.75 h = 2.625	d_{avg} = 7.688	Ø = 34.33^o

Chapter 5
FINITE ELEMENT MODELING

5.1 Introduction

A Finite Element Modeling (FEM) of the west side of Wall CC1 was created in ABAQUS CAE (ABAQUS 2016) software to simulate the geometric and material properties of the MSE wall as closely as possible. The objective of the numerical modeling was to develop a modeling framework to simulate the behavior of the actual MSE walls, and conduct a parametric study to investigate the effect of the MSE wall parameters that may potentially lead to a failure of an MSE wall. This is helpful in investigating the effect of internal failures, such as pullout or rupture of reinforcement, on the behavior of MSE walls. Reinforcement failure cannot be conducted by visual inspection or experimental field testing since it is inaccessible as it is embedded deeply in the reinforced soil.

The numerical evaluation involved several aspects of theoretical and practical interest. Important issues including material models, element types, material interactions, mesh, convergence, boundary conditions, model calibration, surcharge load application, and parametric study, are discussed below.

5.2 Material Properties

5.2.1 Concrete

In the last decade, several constitutive models were developed to simulate the behavior of concrete, including cracking and crushing. There are two models available in

ABAQUS to predict the concrete behavior: the brittle cracking model and the concrete damage plasticity model (Simulia 2011). The brittle cracking model is usually used when the concrete material is expected to be dominated by tensile cracking; it models the concrete material as linear elastic for the case of compression, which does not resemble reality (Martin 2010). On the other hand, the concrete damage plasticity model assumes that the main two failure mechanisms of concrete are cracking and crushing. The propagation of cracks is modeled using this method by using continuum damage mechanics and stiffness degradation (Obaidat 2011).

In this research, the concrete material was modeled in ABAQUS using the concrete damaged plasticity approach. ABAQUS uses the damaged plasticity model proposed by Lubliner et al. (1989). The compressive and tensile behavior of concrete used are illustrated in Figures 5-1(a and b). Figure 5-1(a) shows the behavior under uniaxial tension. The stress-strain response follows a linear elastic relationship until the value of the failure stress is reached. The failure stress corresponds to the onset of micro-cracking in the concrete material. Beyond the failure stress, the formation of micro-cracks is represented microscopically with a softening stress-strain response, which induces strain localization in the concrete structure (Simulia 2011).

Figure 5-1(b) shows the behavior under uniaxial compression. The response is linear until the value of initial yield is reached. In the plastic regime, the response is typically characterized by stress hardening followed by strain softening beyond the ultimate stress (Simulia 2011). This method was validated using multiple experimental

reinforced concrete beams. Therefore, the proposed method is valuable for ABAQUS software in assessing existing reinforced concrete structures in the absence of more detailed test results.

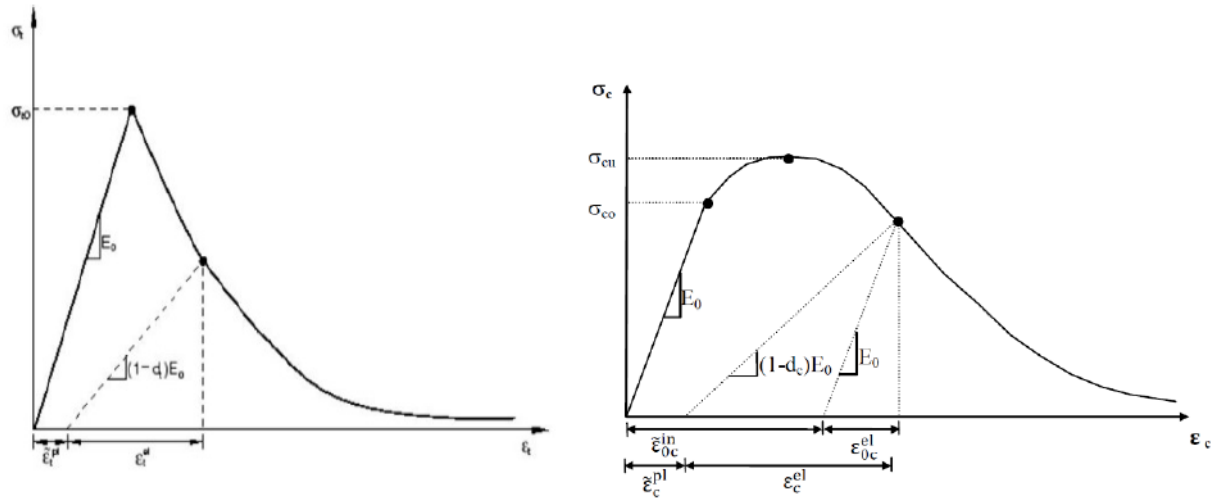

(a) Uniaxial tension (b) Uniaxial compression

Figure 5-1 Response of concrete to uniaxial loading (Simulia 2011)

The concrete damage plasticity model requires the values of Poisson's ratio, elastic modulus, description of compressive and tensile behavior, and the plastic damage parameters. The five plastic damage parameters are dilation angle, flow potential eccentricity, ratio of initial equi-biaxial compressive yield stress to initial uniaxial compressive yield stress, ratio of the second stress invariant on the tensile meridian to that on the compressive meridian, and viscosity parameter that defines viscoplastic regularization. The values of the last four parameters were recommended by the ABAQUS documentation (Simulia 2011) for defining concrete material and were set to

0.1, 1.16, 0.667, and 0.01, respectively. The dilation angle and Poisson's ratio were chosen as 35° and 0.15, respectively.

5.2.2 Soil

The soil part is massive in an MSE structure. It commonly behaves as an elastic–plastic material. There are a large number of available soil constitutive models that can be used to predict the soil behavior, including Winkler Model, Mohr–Coulomb Model, (Modified) Cam–Clay model, Duncan–Chang Model, and Elastic Continuum Model (Abdel-Mohti and Khodair 2014). In this research, the soil material was modeled using the Mohr–Coulomb method. This method is elastic–perfectly plastic and takes into account the effect of stress on soil strength. The failure criteria is defined by the friction angles and soil cohesion. It assumes that the failure is controlled by the maximum shear stress, which also depends on the normal stress as per the following formula:

$$\tau = c - \sigma.\tan\phi \quad (5.1)$$

where τ is the shear stress, σ is the normal stress, c is the cohesion of the material, and ϕ is the material angle of friction. This can be represented by plotting Mohr's circle for states of stress at failure in terms of the maximum and minimum principal stresses (Figure 5-2). The backfill soil was modeled with a cohesion (c) and friction angle (ϕ) values of 0 and 34^o, respectively.

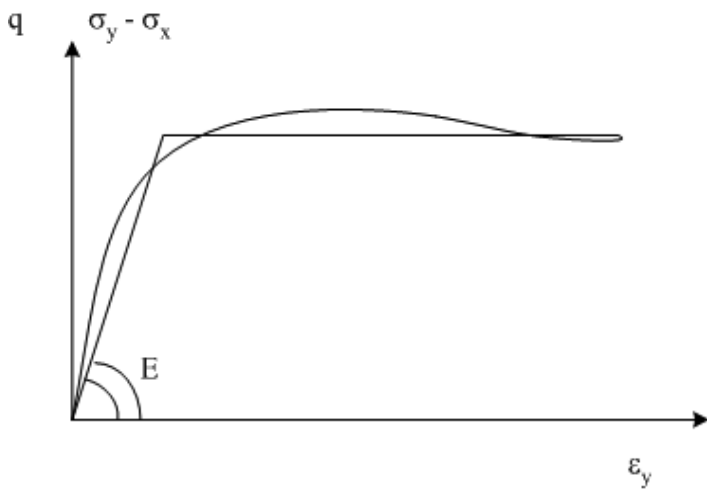

Figure 5-2 Mohr-Coulomb method

5.2.3 Steel

Steel is initially linear-elastic for stress less than the initial yield stress. At ultimate tensile strain, tensile strength is reduced (Figure 5-3). The constitutive model used in ABAQUS to simulate the steel reinforcement was the classical metal linear elastic-plastic model (Obaidat 2011). The steel grid was modeled based on the layout drawings of Wall CC-1 for steel grids (grade 65).

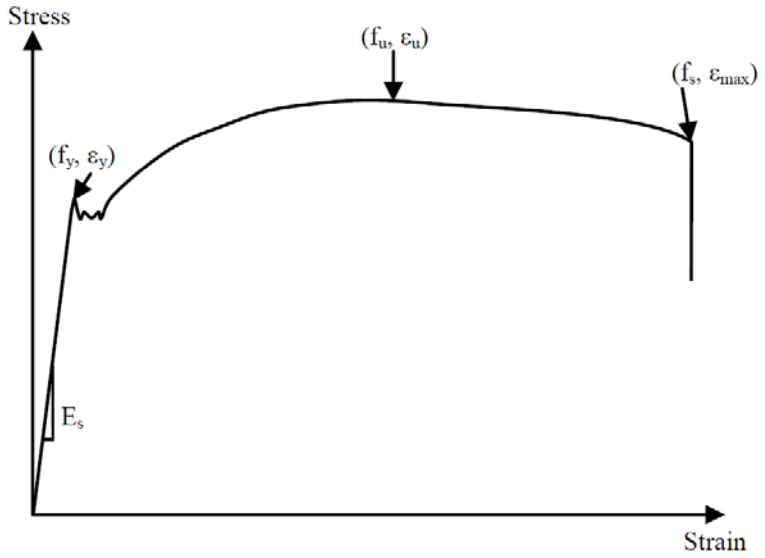

Figure 5-3 Stress-strain curve for typical steel (Obaidat 2011)

5.2.4 HDPE Geosynthetic

High-Density Polyethylene (HDPE) reinforcement is a polymeric material that is used extensively as earth reinforcement. The geosynthetic material type that was used in this research is the HDPE UX 1600MSE provided by Tensar International Corporation. According to the manufacturer, the HDPE material behavior was evaluated by performing a tensile strength test, ASTM D 6637. The stress-strain response follows a linear elastic-plastic relationship; the material keeps stretching to accommodate the tensile load applied. Figure 5-4 shows the tensile response of the HDPE UX 1600MSE material provided by Tensar, and the constitutive model used to simulate the HDPE material in ABAQUS.

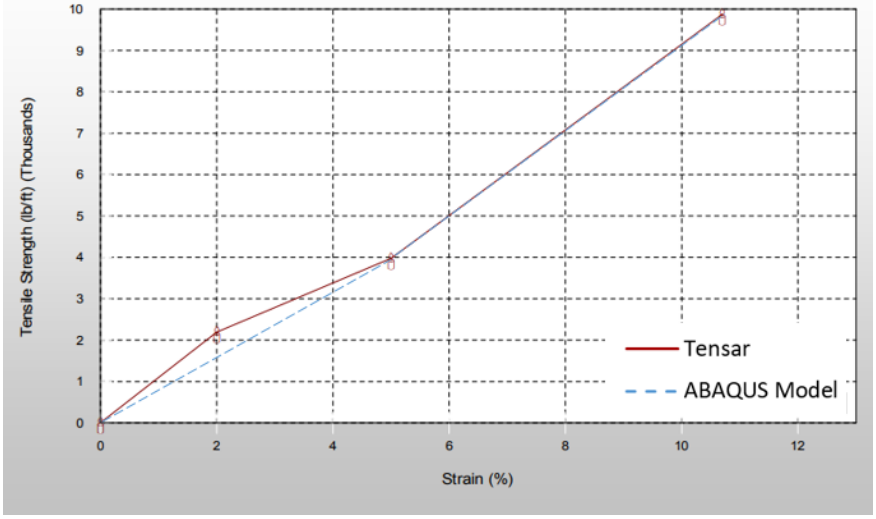

Figure 5-4 Tensile behavior of HDPE UX 1600MSE

5.3 Element Types

The defined geometry was discretized into elements. ABAQUS has an array of element types for modeling the MSE wall. The concrete and soil were modeled using C3D8R (solid, eight-node) elements. The reinforcement was modeled using T2D2 (truss, 2-node) element. Figure 5-5 shows the element families that are most commonly used in ABAQUS (Almomani 2018).

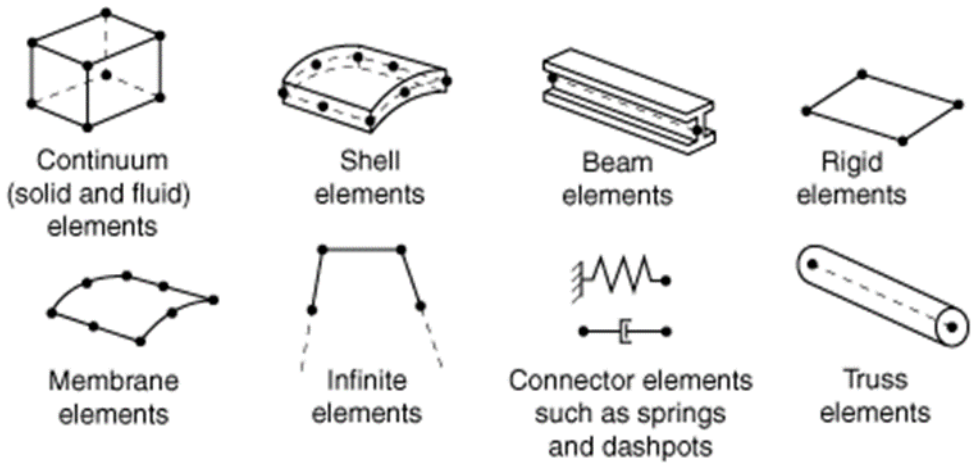

Figure 5-5 ABAQUS element families (Almomani 2018)

5.4 Material Interactions

The interfaces between different parts or materials in the FE model were developed individually for each type of interface. Since all of the interfaces were individually defined, the general contact interaction properties were set as panel-panel and panel-soil interfaces. Panel-panel was defined for the interactions between precast panels themselves, precast panels and copings, copings and approach slab, and copings and traffic barriers. Panel-soil was defined for the interactions between the precast panels and soil, and the approach slab and soil. These interaction properties contain both normal and tangential definitions. For mechanical behavior in the normal direction, “hard contact” was set for the pressure overclosure and the default constraint enforcement method was used (Ambauen 2014). Separation was allowed after initial contact. For the tangential mechanical behavior, a penalty friction formulation was used with isotropic directionality.

This was chosen based on the results from concrete-concrete interface shear testing (Hatami and Bathurst 2005). The interface shear resistance is modelled in ABAQUS as a friction coefficient using the basic Coulomb friction model expressed as:

$$\tau = \mu_S . \sigma \quad (5.2)$$

where μ_S is the coefficient of static friction. The coefficient of static friction used for panel-panel interface is 0.7 (Xu et al. 2019). For panel-soil friction, the coefficient of static friction is calculated as tan (δ), where δ is the friction angle between soil and concrete (estimated as "0.67ϕ" according to AASHTO LRFD Bridge Specifications). In the FE model, this value was set to 0.417 as the friction angle of soil (ϕ) was taken as 34^o. For both interaction properties, the specified maximum elastic slip as a fraction of the characteristic surface dimension was set to 0.005. Separation of the included surfaces was allowed after contact so that the soil elements would not be in tension by the outward movement of the facing panels, which would lead to convergence issues.

5.5 Reinforcement Constraints

Based on previous work involving physical modeling of the interface between earth reinforcement and the embedment soil, it is apparent that the interaction is dependent on the soil particle size relative to the reinforcement apertures (Lee 2000). It was found that pullout resistance approaches the full shearing soil resistance if the soil particles are small enough to be compacted into the reinforcement apertures. This interlocking behavior was simulated in our FE model using "embedded region" constraint in ABAQUS. This

simulation assumes that there would be no relative slipping between the reinforcement and soil, and this is acceptable in modeling because of the large aperture of the reinforcement relative to the soil particle size. Hence, pullout would manifest as shear in the soil zone which is adjacent to the reinforcements (Yoo and Kim 2008).

The steel grid and HDPE geogrid earth reinforcement were modeled explicitly as beam elements and embedded into the backfill soil section. The reinforcement of the precast panels, copings and traffic barrier were modeled explicitly as beam elements and embedded into the concrete sections. The earth reinforcement was inserted 2 inches inside the precast panels and constrained to the panels using embedded region constraint. This technique simulated a tie connection between the tips of the earth reinforcement and the precast panels.

5.6 Boundary Conditions

The boundary conditions of the FE model of the west side of Wall CC1 shown in Figure 5-6 are achieved by supporting the back side of the wall with a pinned connection while allowing it to move vertically, supporting the sides of the wall with a ruler connection that restrains the wall to move in a direction perpendicular to the wall sides, and supporting the bottom with a pinned connection in all directions.

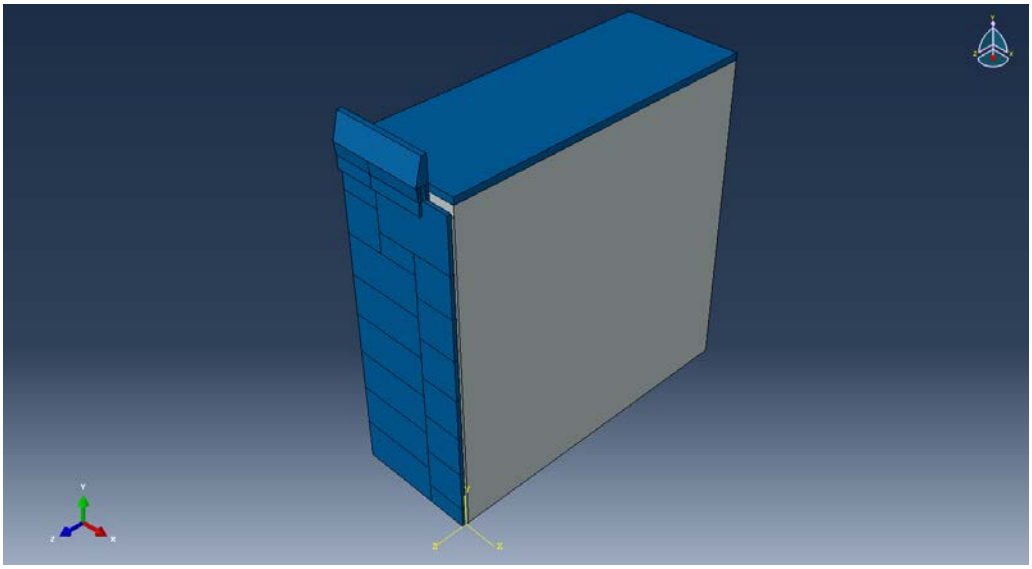

Figure 5-6 ABAQUS model geometry for the west side of Wall CC1

5.7 Surcharge Application

In the FE modelling, the surcharge load was assumed to be a uniform pressure applied to the entire top surface of the approach slab. The surcharge was applied in a separate step, where the load was increased incrementally up to a maximum pressure of 250 psf according to AASHTO LRFD (2014). This surcharge load is equivalent to γ times h_{eq}, where γ is the backfill unit weight and h_{eq} is an equivalent surcharge soil layer (equals to 2 ft).

5.8 Model Calibration

A preliminary 2D MSE wall model shown in Figure 5-7 was developed in ABAQUS to calibrate two small-scale (1:5.5) experimental MSE walls from literature (Reddy and Navarrete 2008), as shown in Figure 5-8. The aim of the calibration was to accurately

reflect the present condition of MSE walls and validate the model parameters and properties of the 3D model developed for the west side of Wall CC1.

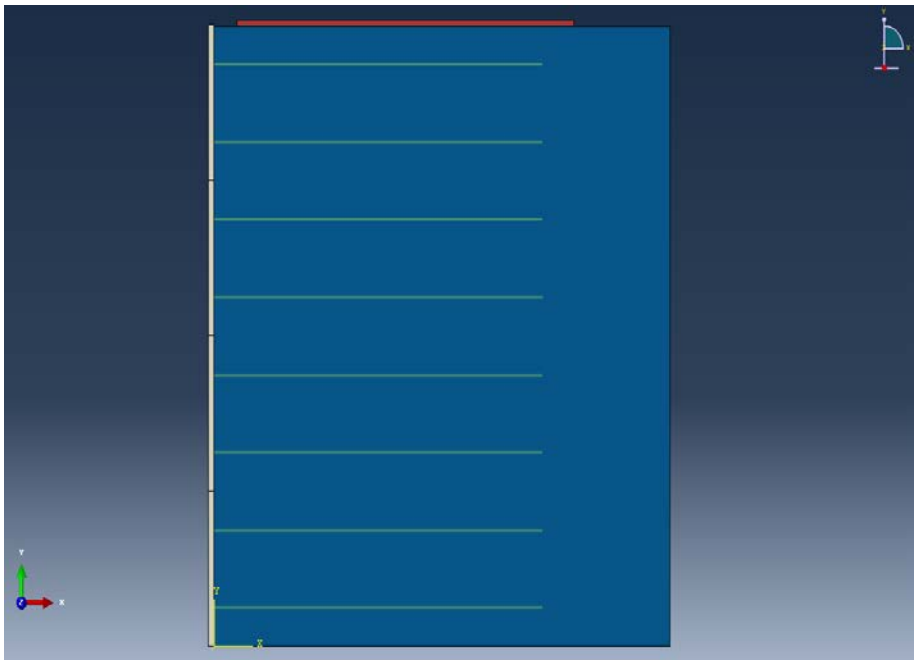

Figure 5-7 Numerical small-scale MSE wall in ABAQUS software

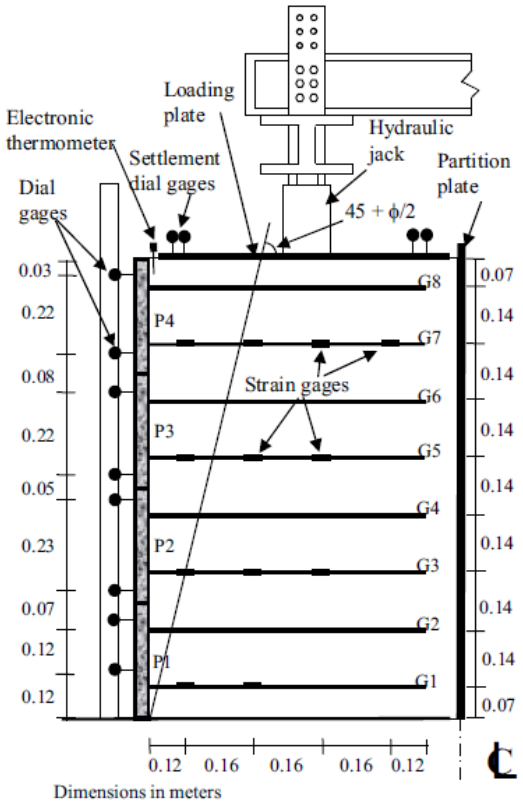

Figure 5-8 Small-scale MSE wall cross-section (Reddy and Navarrete 2008)

The two experimental walls used high density polyethylene (HDPE) reinforcement as earth reinforcement. The material properties of the experimental walls are shown in Table 5-1. In ABAQUS, shell element type was chosen for the precast panels and backfill soil, while wire elements were chosen for the HDPE reinforcement.

Table 5-1 Material properties of the small-scale MSE walls (Reddy and Navarrete 2008)

Property	Value	Unit
	Soil	
Density	105	Pcf
Modulus of Elasticity (E)	191.45	Psi
Poisson's Ratio (ν)	0.3	-
Angle of Friction (Ø)	36	-
Cohesion (C)	0.029	Psi
	Facing Panels	
Density	149.83	Pcf
Modulus of Elasticity (E)	3450.19	Ksi
Poisson's Ratio (ν)	0.15	-
	HDPE Straps	
Modulus of Elasticity (E)	105.73	Ksi
Poisson's Ratio (ν)	0.3	-

The field measurements of the strain gauges (locations are shown in Figure 5-8) were taken once a load of 30 lb was applied atop the experimental walls using loading plates. This load is equal to a total surcharge of 17 psf and it is equivalent to 1:5.5 of the loading used in full-scale MSE walls, which is 92 psf. This load was applied for 48 hours. The load was then increased to obtain a surcharge of 76 psf, which is 1:5.5 of the design surcharge of 418 psf. The next surcharge level was 134 psf (equivalent to 835 psf of a full-scale surcharge load) and was kept for 72 hours. In this research, a comparison between the panel lateral movements of the ABAQUS modeling and the two small-scale walls was carried out, as shown in Figure 5-9.

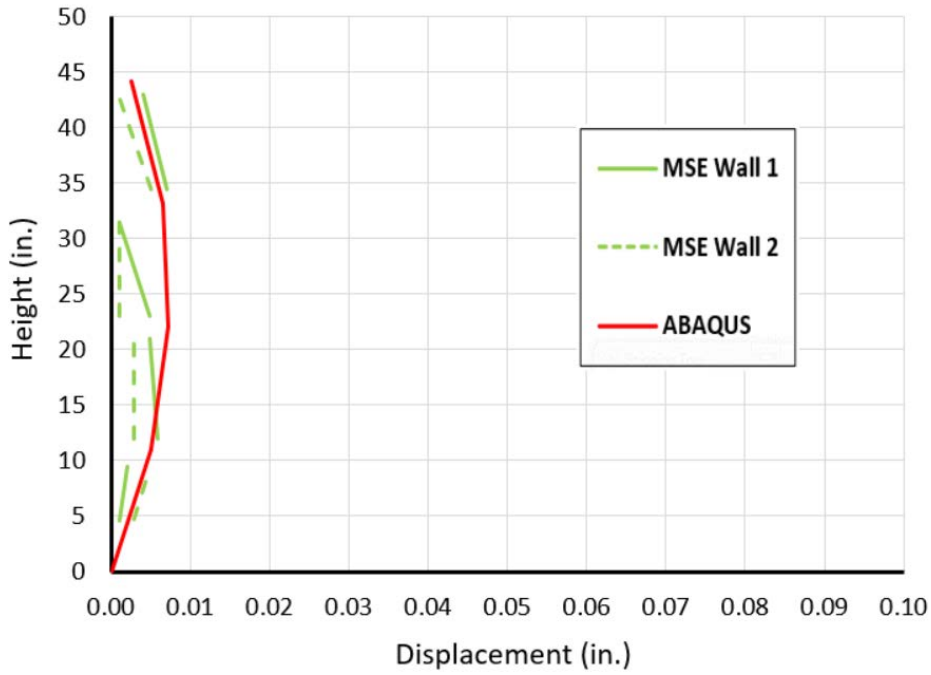

Figure 5-9 MSE Lateral displacement comparison between small-scale MSE walls and ABAQUS modeling

Another comparison was conducted on the strain gauge readings, as shown in Figure 5-10. The term “H-5-3 (1)” means strain value at reinforcement layer 5, position number 3 (the third strain gauge away from the panel) and (1) means the result obtained from MSE Wall 1). AB stands for ABAQUS output values. The strain values of the experimental walls range between 0 and 0.001, while the strain values obtained from FE modeling range between 0 and 0.0014. However, both the experimental walls and ABAQUS modeling show similar strain patterns with the increase of surcharge live load. Furthermore, in both experimental walls, the largest strains appeared at layer 5 and the lowest appeared at layer 1, the same as what was observed from the FE modeling results.

Therefore, the calibrated ABAQUS numerical model is capable of representing the behavior of MSE walls.

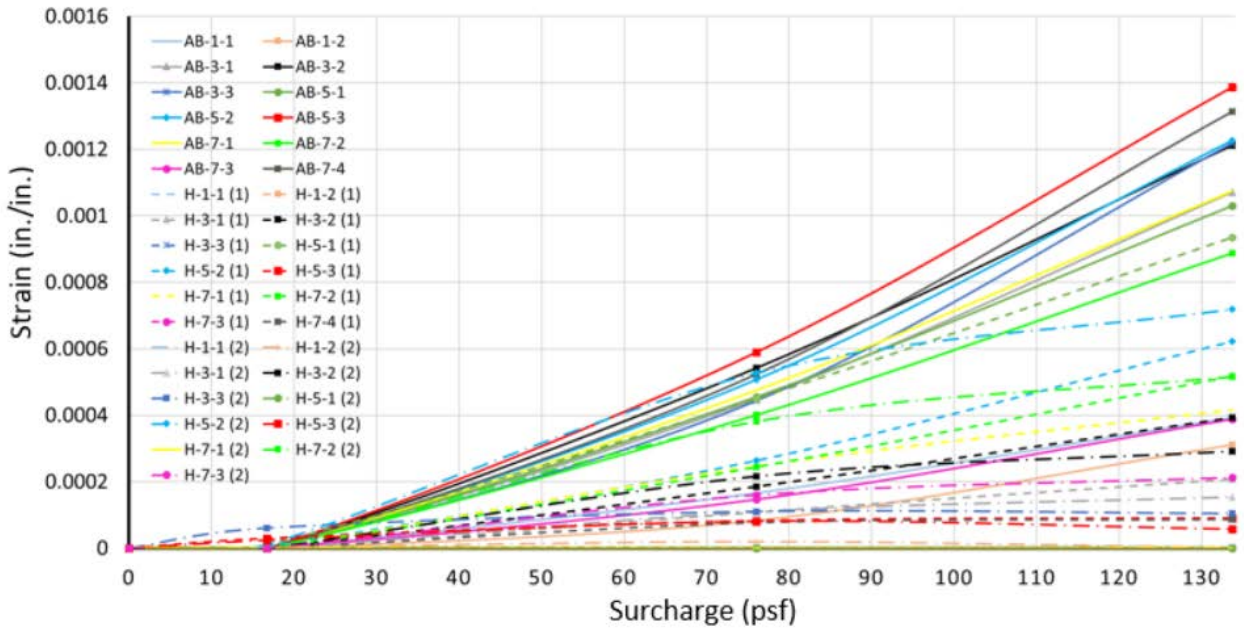

Figure 5-10 Comparison of strain readings between small-scale MSE walls and ABAQUS modeling

5.9 Validation Procedure

After verification from above, the west side model of Wall CC1 (Figures 5-6 and 5-12) was finalized. This numerical modeling was developed with the goal of detecting the cause of Wall CC1 movement. The geometry of the wall was taken based on the TxDOT drawings (Figure 5-11). The first two panel columns shown in Figure 5-11 were chosen for the numerical study. The precast panel and the steel grid details were taken based on the shop and layout drawings of Wall CC1. Welded wire grid (W11xW11) grade 65 is used

as earth reinforcement, and precast panels (Class H) with a compressive strength of 4 ksi is used for the precast panels. The width and height of the numerical wall were taken as 15.375 ft and 40.22 ft, respectively based on the drawings.

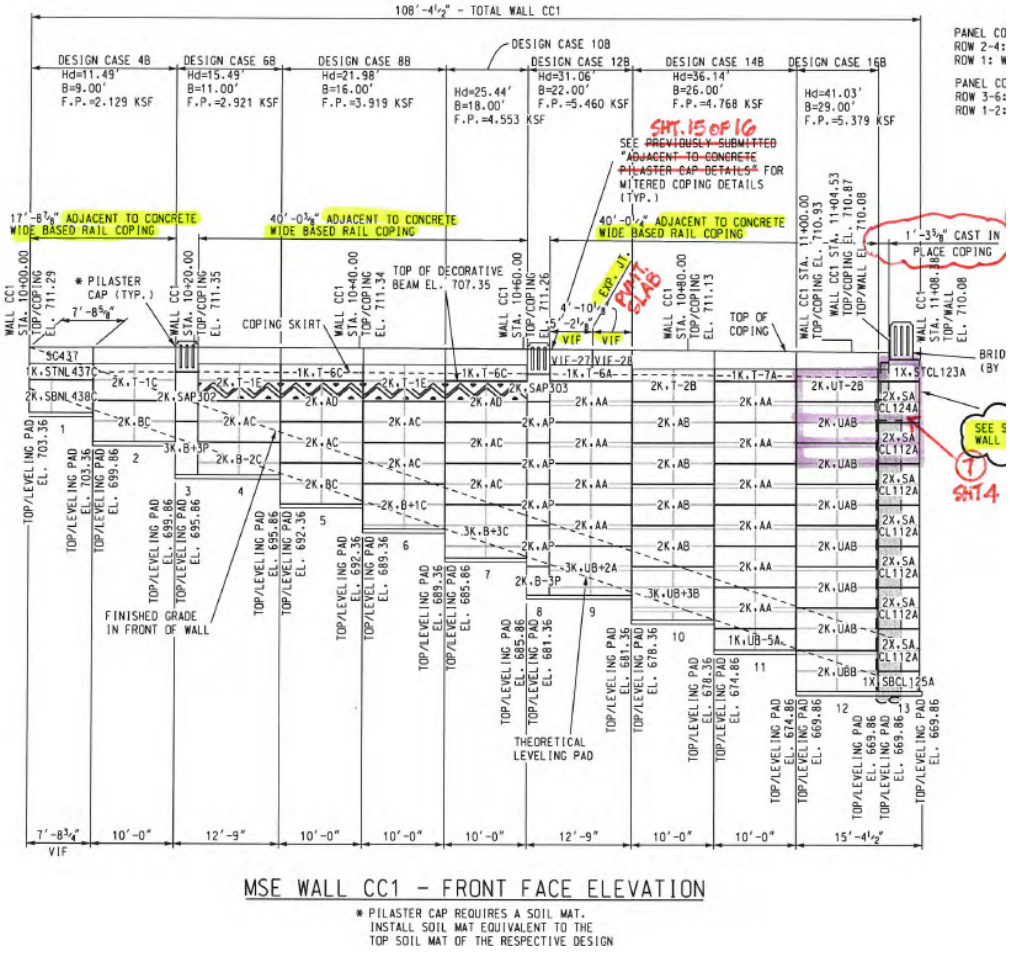

Figure 5-11 Wall CC1 layout

Figure 5-12 Walls CC1 and CC2

5.10 Typical Finite Element Model

Based on the previous assumptions, a 3D ABAQUS FEM of a typical MSE wall was created, as shown in Figure 5-13. The aim of this model is to simulate a standard MSE wall so that a parametric study can be carried out considering multiple parameters that may have a significant effect on the wall performance. The geometry, boundary conditions, material properties, loads, analysis methods and contact were involved in defining the ABAQUS modeling, based on the above sections.

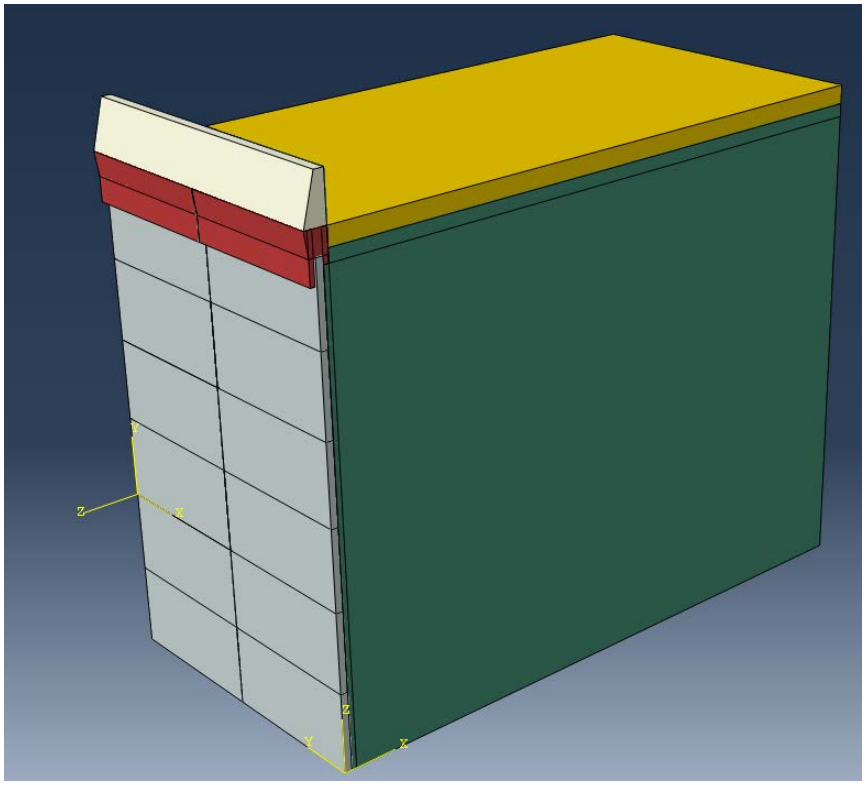

Figure 5-13 Typical MSE wall model geometry in ABAQUS software

5.10.1 Mesh Selection

The defined geometry was discretized into elements. ABAQUS has an array of element types for modeling the MSE wall. As previously assumed for the FE model of Wall CC1, the concrete and soil in the typical model were modeled using C3D8R (solid, eight-node) elements, and the reinforcement was modeled using T2D2 (truss, 2-node) element.

Another major issue that needs to be addressed for any finite element model is the mesh size and the element selection to ensure a balance between convergence,

accuracy of model, and run-time (Timilsina 2018). Several basic models were run to ascertain the optimum mesh size for the model. Initially, different mesh sizes were picked for each component. For the backfill soil, mesh sizes of 80 in., 60 in., 40 in., 30 in., 24 in., 20 in., and 18 in. were used to determine the optimum soil mesh size. The out-of-plane movement of precast panels was chosen for the investigation, as shown in Figures 5-14(a-e). The 20 in. mesh size shown in Figure 5-14(a) has no significant change in the accuracy than the smaller mesh size (18 in.). It was hence decided to use a mesh size of 20 in. for soil to save computer run-time. Similarly, a mesh sensitivity analysis was carried out for the other structural components of the wall model. Hence, 20 in. mesh size was selected for the approach slab, 4 in. for precast panels, 4 in. for copings, and 10 in. for traffic barriers (Figures 5-14(a-e)).

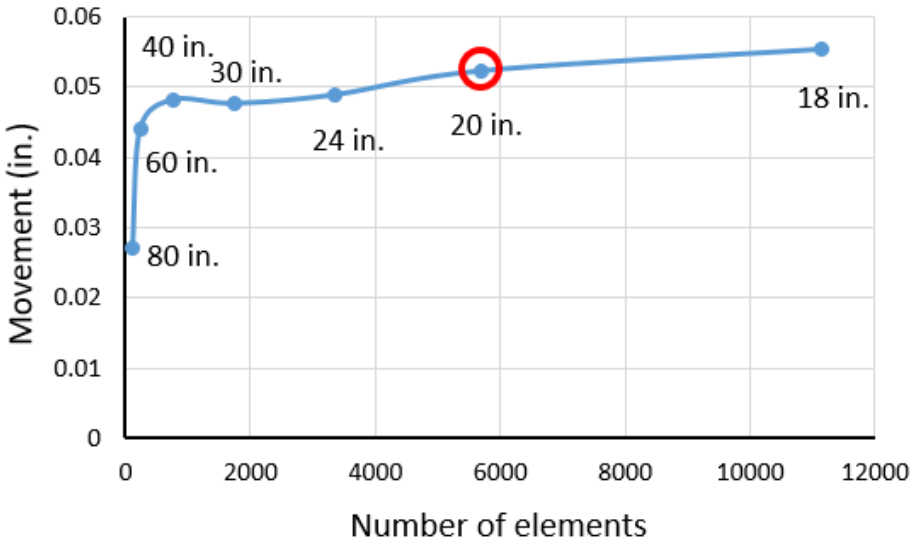

(a) Backfill soil

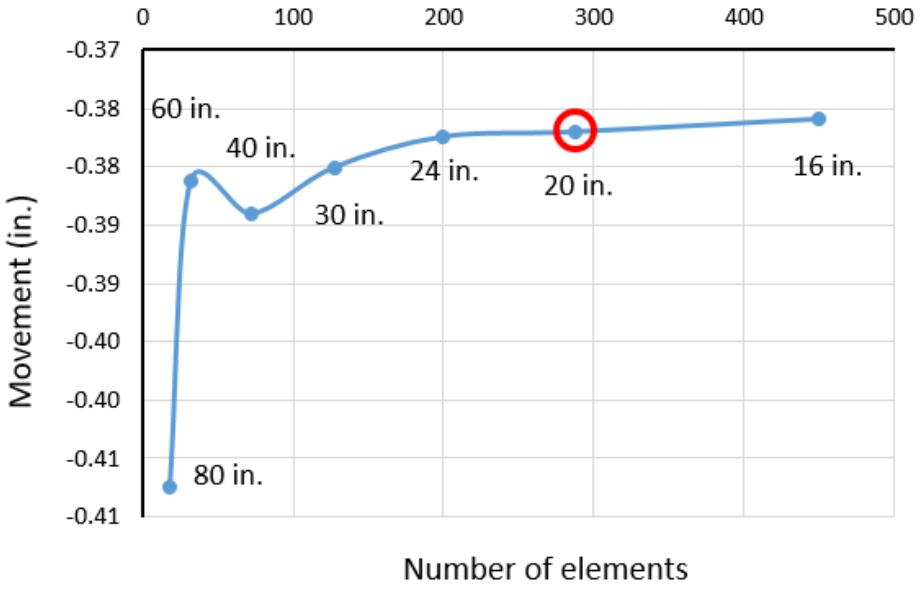

(b) Approach slab

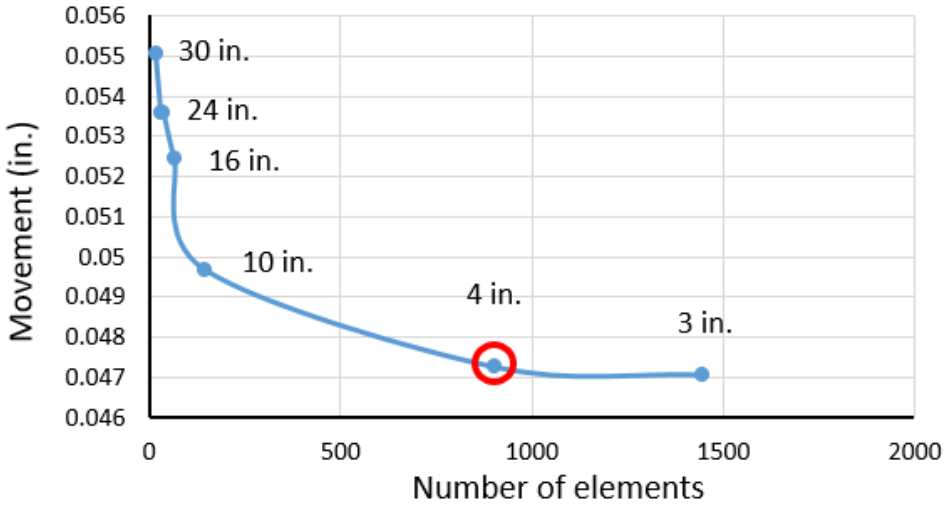

(c) Precast panel

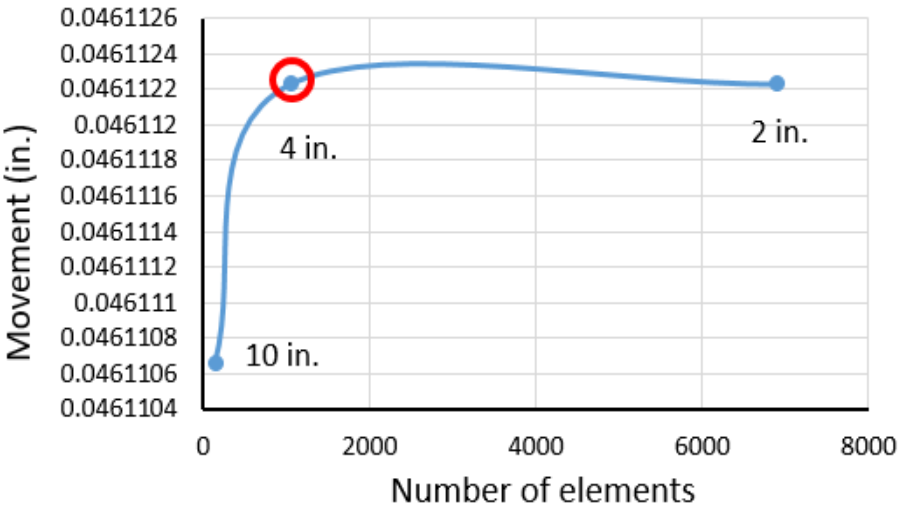

(d) Coping

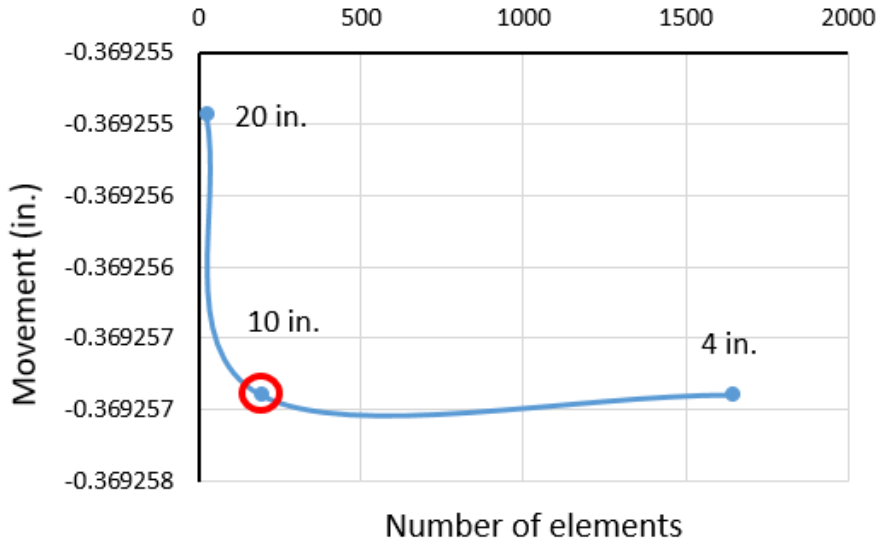

(e) Traffic barrier

Figure 5-14 Mesh sensitivity analyses

5.10.2 Geostatic Pressure Application

A geostatic pressure was applied on the backfill soil of the FE modeling. The geostatic pressure is caused by the self-weight of soil mass and tends to increase the out-of-plane movement of wall panels; thus, it tends to increase the tensile stresses in earth reinforcement. At any depth, two stresses are developed by the geostatic pressure, the vertical geostatic stress (σ_V) which is caused by the weight of upper soil layers, and the horizontal geostatic stress (σ_H), which is caused by the lateral confinement of soil particles and the vertical stresses. These two components can be estimated using a coefficient of lateral earth pressure (K_o) as per the following equations:

$$\sigma_V = \gamma . z \tag{5.3}$$

$$\sigma_H = K_o . \sigma_V \tag{5.4}$$

$$K_o = \frac{\nu}{1-\nu} = 1 - \sin(\emptyset) \tag{5.5}$$

where:

σ_V = vertical pressure at depth z (psf)
γ = unit weight of soil (pcf)
z = depth from ground surface (ft.)
σ_H = horizontal pressure at depth z (psf)
K_o = lateral earth pressure coefficient at rest
ν = Poisson's ratio of soil
$\emptyset$ = soil friction angle

These parameters were assigned in ABAQUS software using a predefined field "geostatic stress" as shown in Figure 5-15 (the values were inserted in SI units). The height of the numerical MSE wall is 30 ft, the unit weight is 125 pcf, and the Poisson's ratio of soil is 0.3. Thus, from Equations 4.3 through 4.5, σ_V and σ_H are equal to 3750 psf and 1605 psf, respectively. Figures 5-16(a and b) show the vertical and horizontal stresses developed by the geostatic pressure in the numerical modeling, respectively.

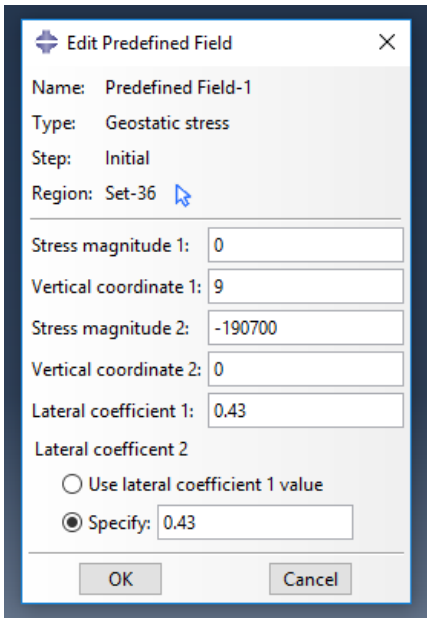

Figure 5-15 Geostatic stress predefined field in ABAQUS software

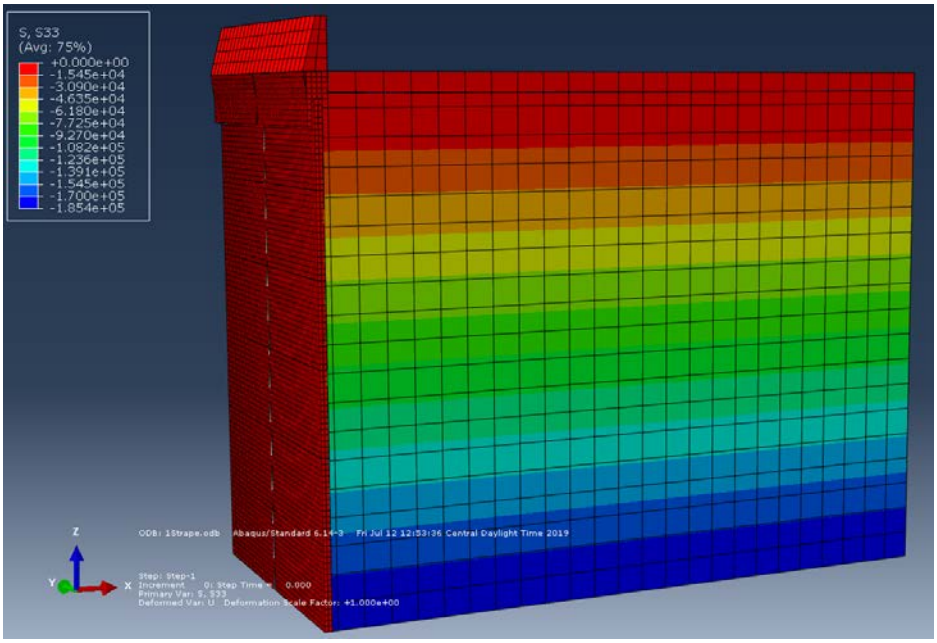

(a) Vertical geostatic stress "σ_V"

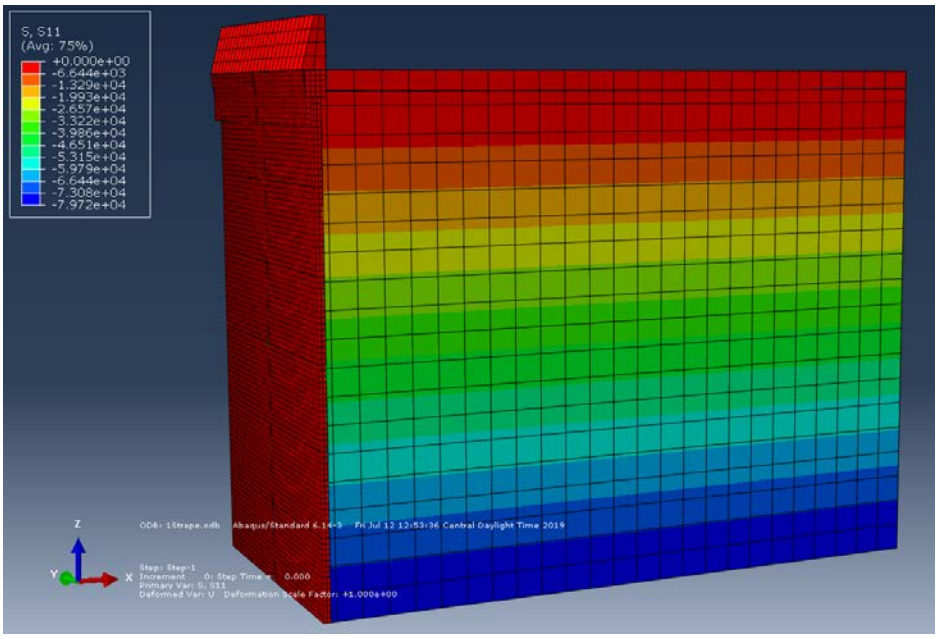

(b) Horizontal geostatic stress "σ_H"

Figure 5-16 Geostatic soil stresses in ABAQUS software

5.10.3 Parametric Study

A parametric study on the 3D typical MSE wall using ABAQUS software was carried out to investigate the effect of the main parameters that may potentially lead to a failure of an MSE wall. The parametric study was initiated using the Design of Experiments (DOE) using Minitab software. Six main parameters were chosen that consisted of two cases each for this study, resulting in 64 different models. These parameters are:

- Pore water pressure.
  - The effect of water pockets at the mid-third height of the numerical wall was investigated, as shown in Figure 5-17. The mid-third height was picked since pore pressure exists usually behind the precast panels as water pockets by referring to the resistivity imaging scans. Furthermore, the pore pressure was initially investigated by applying it at top-third, mid-third, and lower-third heights of the numerical wall. However, it was found that the wall performance is affected the most when the pore pressure exists at mid-third height. Therefore, the pore pressure was modeled by assigning a triangular pressure by increasing the pressure from zero at the top of the fourth panel to 624 psf at the bottom of the third panel (Figure 5-17). The pore pressure was calculated as the unit weight of water times the concerned height.

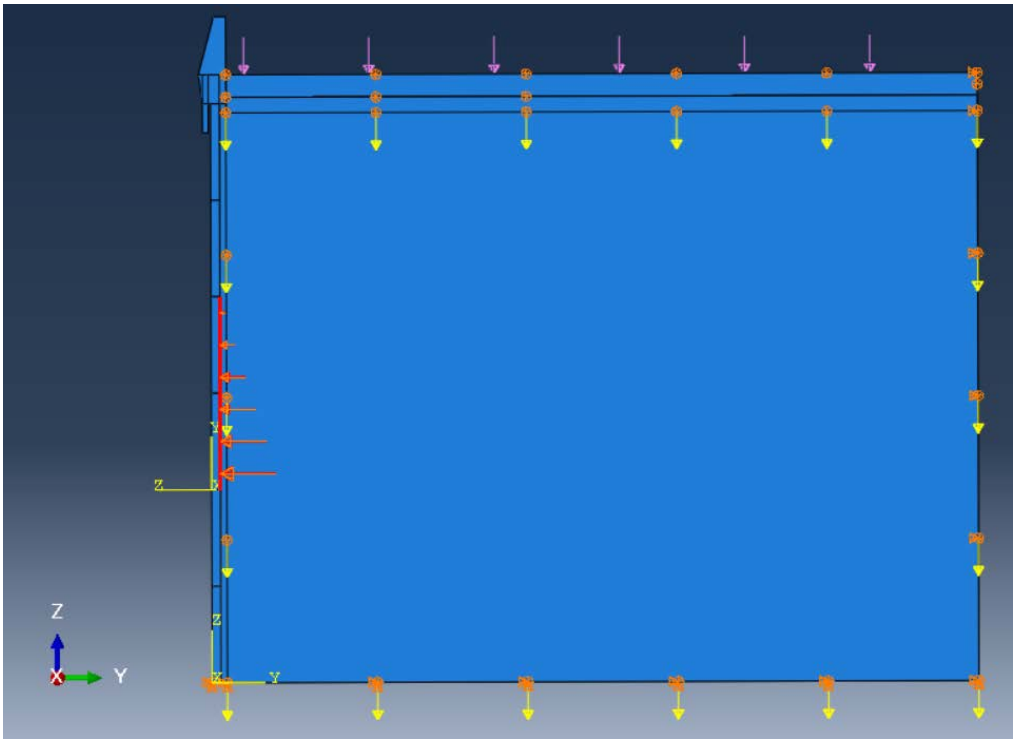

Figure 5-17 Hydrostatic pressure applied at mid-third Height of numerical MSE wall

- Reinforcement type.
  - As the MSE wall performance depends on the reinforcement extensibility, metal (inextensible) or geosynthetic (extensible) reinforcement, a parameter was investigated regarding this aspect using the most common reinforcement type used in MSE walls of each category. These types are: 1) Steel grid grade 65 (inextensible), and 2) Tensar HDPE UX 1600 MSE (extensible). The modeled reinforcements are show in Figures 5-18 (a through d).

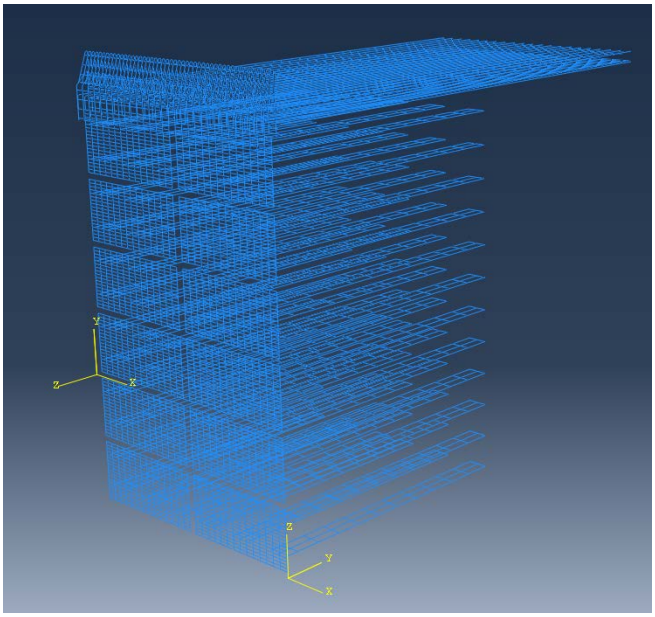

(a) Reinforcement model with steel grids

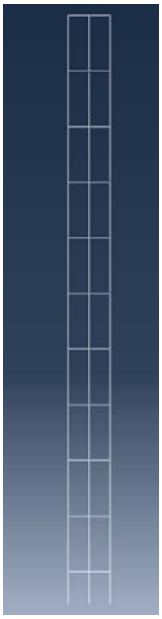

(b) Steel grid

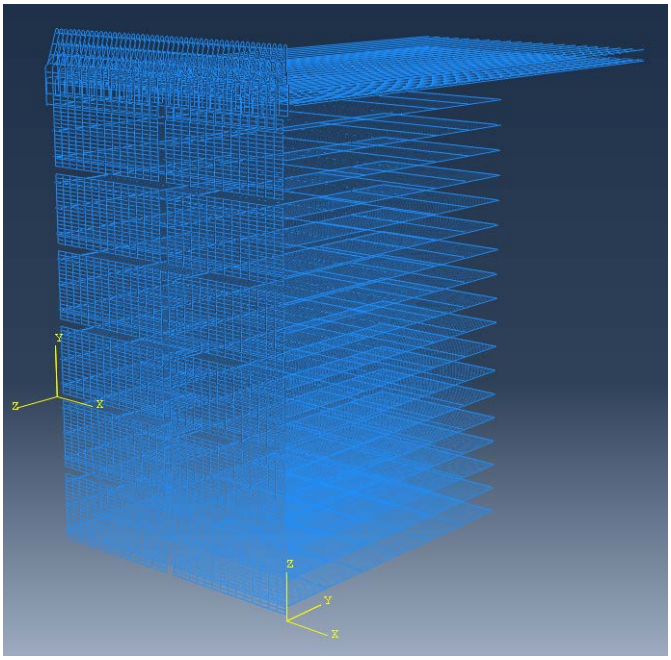

(c) Reinforcement model with HDPE geogrids

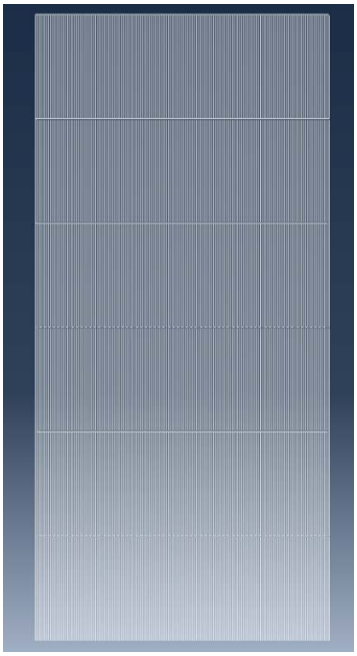

(d) HDPE geogrid

Figure 5-18 Reinforcement models in ABAQUS

- Reinforcement length.
  - The effect of reinforcement lengths of 0.7H and 1.0H (where H is the wall height) was studied in this research since the minimum recommended reinforcement length is 0.7H as specified by the FHWA (2009).

- Breakage/slippage of reinforcement.
  - The reinforcements are inaccessible since they are embedded in the backfill soil; therefore, it is challenging to check for the reinforcement integrity. Nevertheless, since a corroded or pulled out reinforcement might significantly affect the stability of MSE walls, a parameter of reinforcement breakage/slippage was investigated in this research through eliminating 1/18 of the overall earth reinforcement. The middle reinforcements that are attached to the fourth row-panels (Figure 5-19) were selected for the elimination as the maximum movement recorded by the wall was observed when those chosen reinforcements were eliminated.

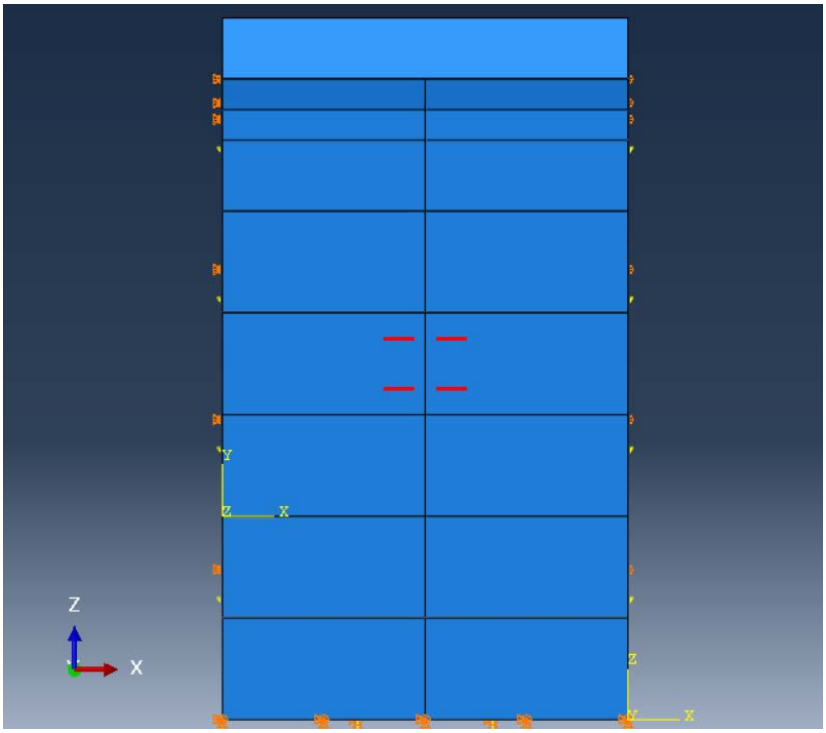

Figure 5-19 Reinforcement breakage/slippage of numerical MSE wall

- PCP compressive strength.
  - ➢ The effect of PCP compressive strength of 4 ksi and 5 ksi was studied.

- Backfill soil properties.
  - ➢ The backfill soil of an MSE wall should be cohesionless as recommended by the FHWA (2009). However, the selected backfills might have fine contents which exceed the specified limits. Thus, a parameter of backfill soil with cohesion, 418 psf (20 kPa), and without cohesion was studied.

Table 5-2 shows the 64 different models picked for the parametric study by varying the six parameter properties among these models. This was done to develop correlations

between the wall parameters and investigate which combinations have the most effect on the MSE wall performance. The parameter properties were designated with the following acronyms:

NP = No pore pressure applied.
P = Pore pressure is applied.
S = Reinforcement type is Steel grid (grade 65).
HDPE = Reinforcement type is HDPE UX 1600MSE.
0.7H = Reinforcement length is set to 0.7H (H is the wall height).
1.0H = Reinforcement length is set to 1.0H (H is the wall height).
NB = No breakage/slippage in reinforcement.
B = Breakage/slippage of reinforcement is considered (1/18 of overall reinforcement).
4 = PCP has a compressive strength of 4 ksi.
5 = PCP has a compressive strength of 5 ksi.
CL = Cohesionless backfill soil.
C = Cohesive backfill soil (418 psf).

Table 5-2 Parametric study models

Model Num.	Pore Pressure	Reinf. Type	Reinf. Length	Reinf. Breaking/ Slippage	PCP Comp. Strength (ksi)	Cohesion (psf)
1	NP	S	0.7H	NB	4	0
2	P	S	0.7H	NB	4	0
3	NP	S	1.0H	NB	4	0
4	P	S	1.0H	NB	4	0
5	NP	S	0.7H	B	4	0
6	P	S	0.7H	B	4	0
7	NP	S	1.0H	B	4	0

8	P	S	1.0H	B	4	0
9	NP	S	0.7H	NB	5	0
10	P	S	0.7H	NB	5	0
11	NP	S	1.0H	NB	5	0
12	P	S	1.0H	NB	5	0
13	NP	S	0.7H	B	5	0
14	P	S	0.7H	B	5	0
15	NP	S	1.0H	B	5	0
16	P	S	1.0H	B	5	0
17	NP	S	0.7H	NB	4	C
18	P	S	0.7H	NB	4	C
19	NP	S	1.0H	NB	4	C
20	P	S	1.0H	NB	4	C
21	NP	S	0.7H	B	4	C
22	P	S	0.7H	B	4	C
23	NP	S	1.0H	B	4	C
24	P	S	1.0H	B	4	C
25	NP	S	0.7H	NB	5	C
26	P	S	0.7H	NB	5	C
27	NP	S	1.0H	NB	5	C
28	P	S	1.0H	NB	5	C
29	NP	S	0.7H	B	5	C
30	P	S	0.7H	B	5	C
31	NP	S	1.0H	B	5	C
32	P	S	1.0H	B	5	C
33	NP	HDPE	0.7H	NB	4	0
34	P	HDPE	0.7H	NB	4	0
35	NP	HDPE	1.0H	NB	4	0
36	P	HDPE	1.0H	NB	4	0
37	NP	HDPE	0.7H	B	4	0
38	P	HDPE	0.7H	B	4	0
39	NP	HDPE	1.0H	B	4	0
40	P	HDPE	1.0H	B	4	0
41	NP	HDPE	0.7H	NB	5	0
42	P	HDPE	0.7H	NB	5	0
43	NP	HDPE	1.0H	NB	5	0
44	P	HDPE	1.0H	NB	5	0
45	NP	HDPE	0.7H	B	5	0

46	P	HDPE	0.7H	B	5	0
47	NP	HDPE	1.0H	B	5	0
48	P	HDPE	1.0H	B	5	0
49	NP	HDPE	0.7H	NB	4	C
50	P	HDPE	0.7H	NB	4	C
51	NP	HDPE	1.0H	NB	4	C
52	P	HDPE	1.0H	NB	4	C
53	NP	HDPE	0.7H	B	4	C
54	P	HDPE	0.7H	B	4	C
55	NP	HDPE	1.0H	B	4	C
56	P	HDPE	1.0H	B	4	C
57	NP	HDPE	0.7H	NB	5	C
58	P	HDPE	0.7H	NB	5	C
59	NP	HDPE	1.0H	NB	5	C
60	P	HDPE	1.0H	NB	5	C
61	NP	HDPE	0.7H	B	5	C
62	P	HDPE	0.7H	B	5	C
63	NP	HDPE	1.0H	B	5	C
64	P	HDPE	1.0H	B	5	C

The items that were selected for comparison purposes are maximum out-of-plane movement of the precast panels, and maximum stresses developed in the earth reinforcement and their respective locations.

5.11 Modeling Results

The 64 numerical models shown in Table 5-2 were generated in ABAQUS and successfully completed. The parameter properties are designated in the graph legends with the acronyms used in Table 5-2.

Figures 5-20 to 5-21 show a comparison of the out-of-plane movement of the 64 Models, and Figures 5-22 to 5-23 show a comparison of the maximum recorded tensile stress in earth reinforcement of the 64 Models. The first 32 models shown in Table 5-2 were reinforced with steel grid reinforcement, while the other 32 models were reinforced with geosynthetic reinforcement. The plotted lines in Figures 5-20 to 5-23 show a comparison between the different models that consisted of different reinforcement lengths, different cohesion properties of the backfill soil, different compressive strengths of the precast panels, and different reinforcement situations in case if there is a breakage/slippage or not. The y-axes of these figures represent the status of the pore water pressure applied; the bottom of the y-axes represent the models when the pore pressure is not applied, and the top of the y-axes represent the models when a 624 psf pore pressure is applied linearly to the mid-third high panels, as shown in Figure 5-17. The x-axes of Figures 5-20 to 5-21 represent the maximum conducted out-of-plane movement of the precast panels (negative movement indicates out-of-plane movement). The x-axes of Figures 5-22 to 5-23 represent the maximum recorded tensile stress in earth reinforcement.

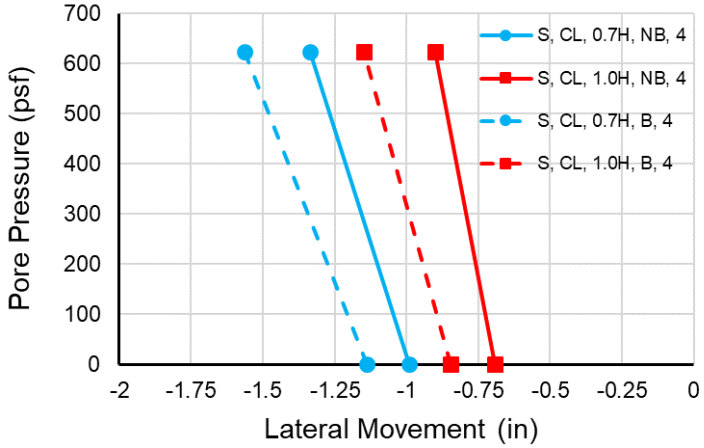

(a) Lateral movement of MSE walls reinforced with steel grids, and consisted of cohesionless backfill soil and 4 ksi precast panels

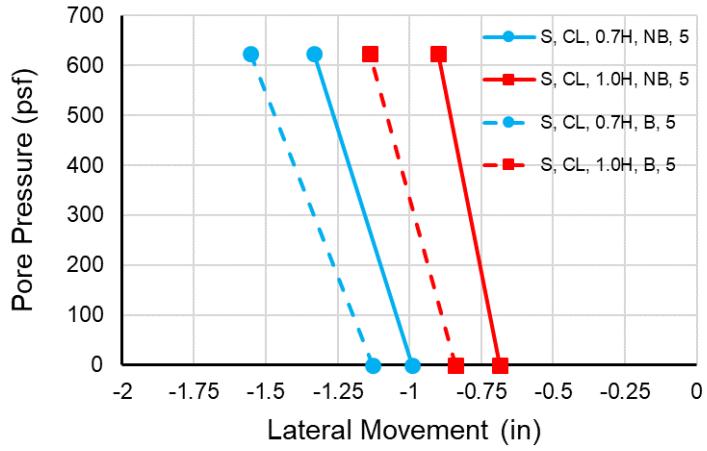

(b) Lateral movement of MSE walls reinforced with steel grids, and consisted of cohesionless backfill soil and 5 ksi precast panels

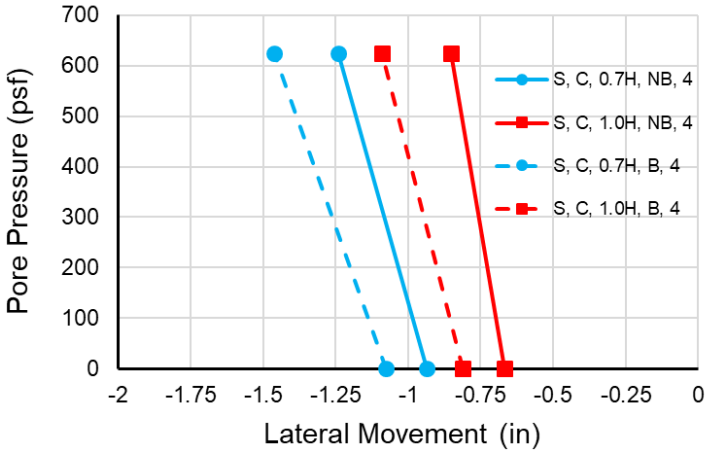

(c) Lateral movement of MSE walls reinforced with steel grids, and consisted of cohesive backfill soil and 4 ksi precast panels

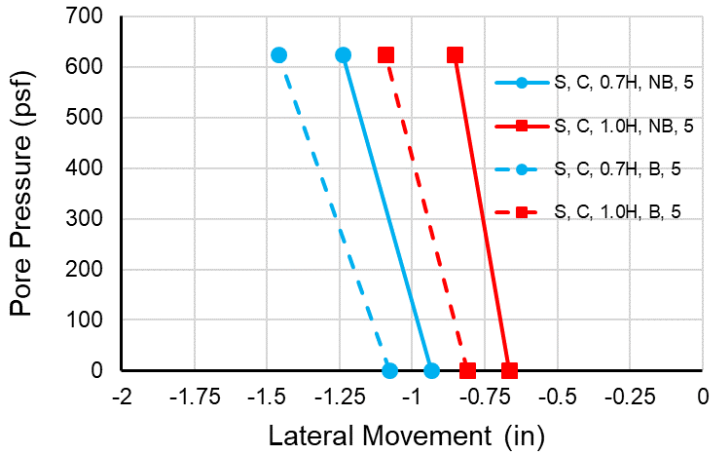

(d) Lateral movement of MSE walls reinforced with steel grids, and consisted of cohesive backfill soil and 5 ksi precast panels

Figure 5-20 Lateral movement of MSE walls reinforced with steel grids

Figures 5-20(a-d) show the lateral movement of modeled steel grid reinforced MSE walls, and it shows that the lateral movement increases when the pore pressure is applied, if breakage/slippage of reinforcement has occurred, and the reinforcement length is taken as 0.7H. However, by comparing Figure 5-20(a) with Figure 5-20(b), it can be noted that varying the compressive strength of the precast panels from 4 ksi to 5 ksi does not affect the lateral movement of the MSE walls, as the respective models show the same movements. Furthermore, from the comparison between Figure 5-20(a) and Figure 5-20(c), and Figure 5-20(b) and Figure 5-20(d), it can be noted that the MSE walls exhibit less lateral movement by approximately 0.05-0.1 inches when its backfill soils have an amount of cohesion of 418 psf. Figures 5-21(a-d) show the lateral movement of HDPE geogrid reinforced MSE walls.

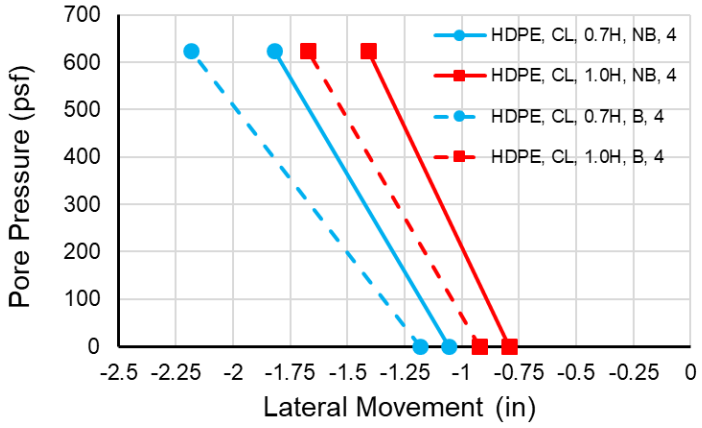

(a) Lateral movement of MSE walls reinforced with HDPE geogrids, and consisted of cohesionless backfill soil and 4 ksi precast panels

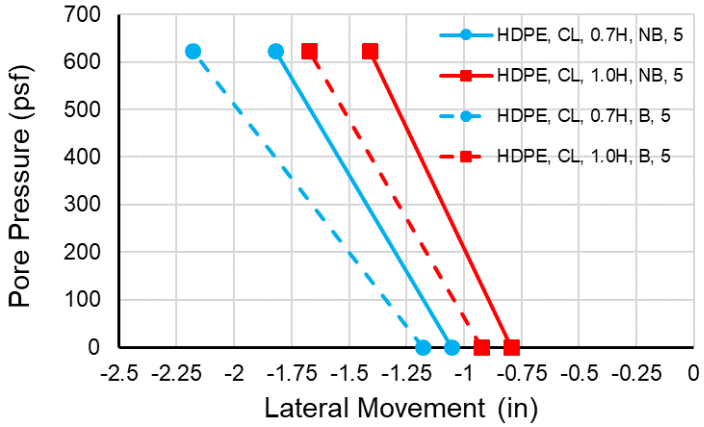

(b) Lateral movement of MSE walls reinforced with HDPE geogrids, and consisted of cohesionless backfill soil and 5 ksi precast panels

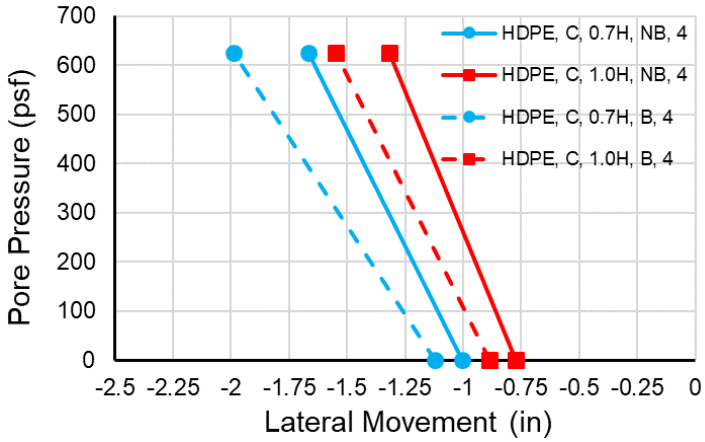

(c) Lateral movement of MSE walls reinforced with HDPE geogrids, and consisted of cohesive backfill soil and 4 ksi precast panels

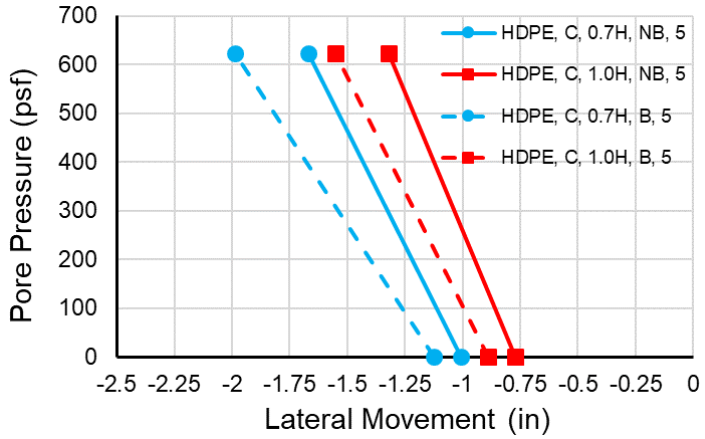

(d) Lateral movement of MSE walls reinforced with HDPE geogrids, and consisted of cohesive backfill soil and 5 ksi precast panels

Figure 5-21 Lateral movement of MSE walls reinforced with HDPE geogrids

Figures 5-21(a-d) show that the lateral movement increases for the case of HDPE reinforced MSE walls when the pore pressure is applied, if breakage/slippage of reinforcement has occurred, and the reinforcement length is taken as 0.7H, same as what

was noted from the steel grid reinforced MSE models. However, the HDPE geogrid reinforced MSE walls showed higher overall lateral movements than the steel grid reinforced MSE walls.

It can be also noted from Figures 5-21(a-d) that varying the compressive strength of the precast panels from 4 ksi to 5 ksi does not affect the lateral movement. Furthermore, from the comparison between Figure 5-21(a) and Figure 5-21(c), and Figure 5-21(b) and Figure 5-21(d), it can be noted that the MSE walls exhibit less lateral movement by approximately 0.05-0.1 inches when its backfill soils have an amount of cohesion of 418 psf.

Figures 5-22(a and b) and Figures 5-23(a and b) show the ultimate stress developed in reinforcement of MSE walls reinforced with steel grids and HDPE geogrids, respectively, for the modeled walls which consisted of 4 ksi compressive strength precast panels. These figures show that the reinforcement length does not affect the developed stresses in reinforcement regardless to the reinforcement type. Also, Figures 5-22(a and b) show that the breakage/slippage of reinforcement increases significantly the ultimate tensile stresses in the steel grids in the presence of pore pressure. On the other hand, the ultimate tensile stresses developed in HDPE geogrids increase significantly when the pore pressure is applied, while it increases slightly when the breakage/slippage of reinforcement is considered, as shown in Figures 5-23(a and b).

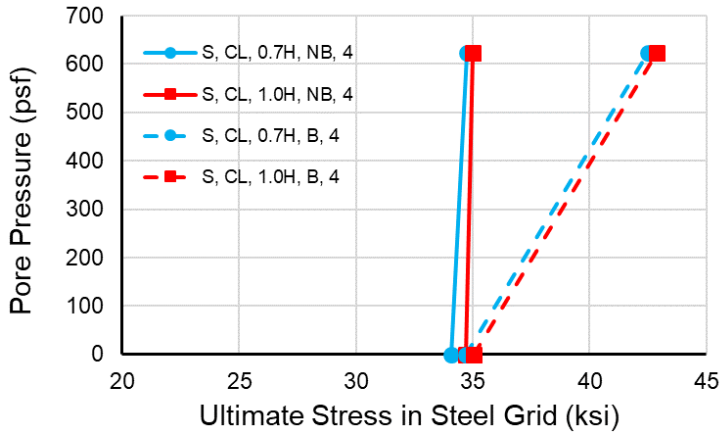

(a) Ultimate stress developed in reinforcement of MSE walls reinforced with steel grids, and consisted of cohesionless backfill soil and 4 ksi precast panels

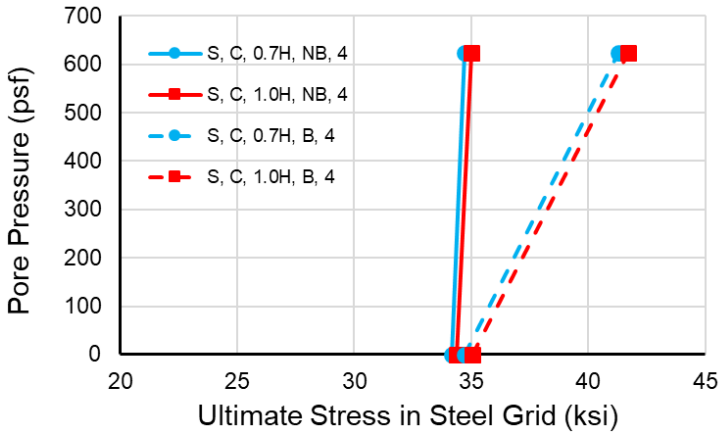

(b) Ultimate stress developed in reinforcement of MSE walls reinforced with steel grids, and consisted of cohesive backfill soil and 4 ksi precast panels

Figure 5-22 Ultimate stress developed in reinforcement of MSE walls reinforced with steel grids

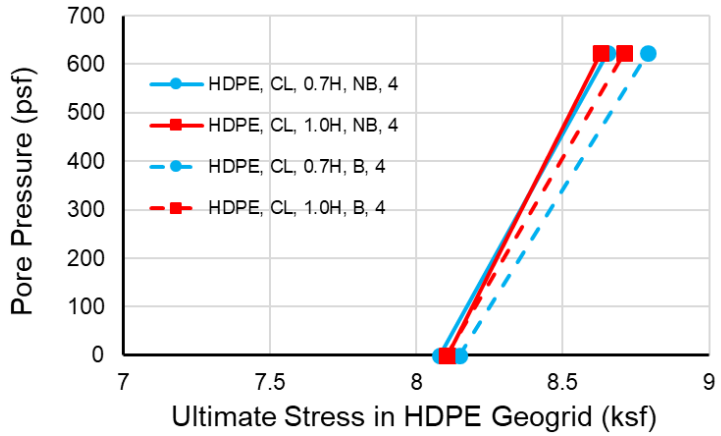

(a) Ultimate stress developed in reinforcement of MSE walls reinforced with HDPE geogrids, and consisted of cohesionless backfill soil and 4 ksi precast panels

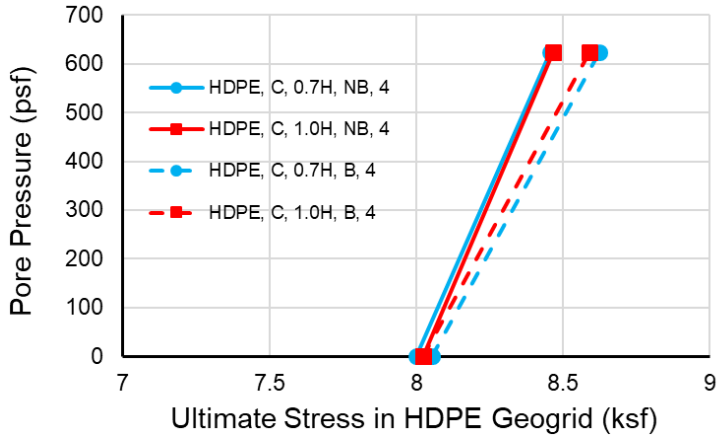

(b) Ultimate stress developed in reinforcement of MSE walls reinforced with HDPE geogrids, and consisted of cohesive backfill soil and 4 ksi precast panels

Figure 5-23 Ultimate stress developed in reinforcement of MSE walls reinforced with HDPE geogrids

The ultimate stresses developed in both reinforcement types were then compared with their respective yield and ultimate tensile strengths, as shown in Figures 5-24(a and

b). Figure 5-24(a) shows that the ultimate reinforcement stresses that occurred in steel grids have not reached their yielding strength, while Figure 5-24(b) shows that the ultimate reinforcement stresses that occurred in HDPE geogrids have surpassed their yielding strength, yet they have not failed due to rupture, as the ultimate tensile strength has not been reached.

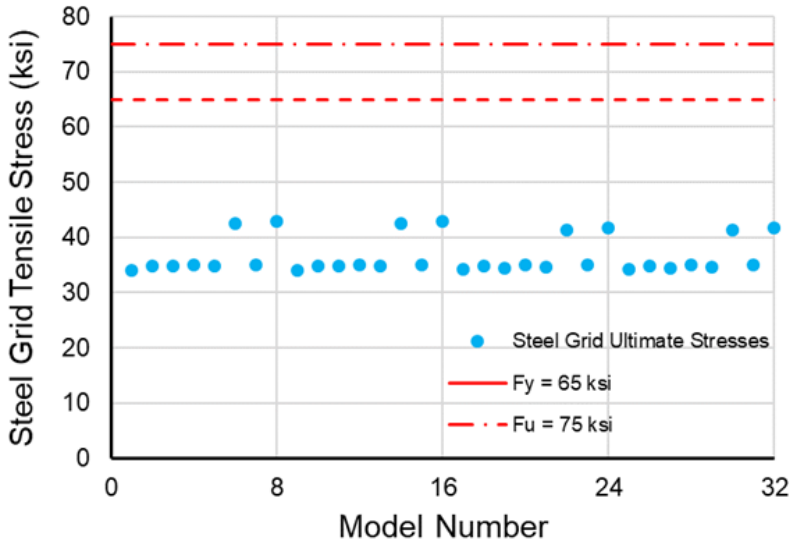

(a) Steel grid

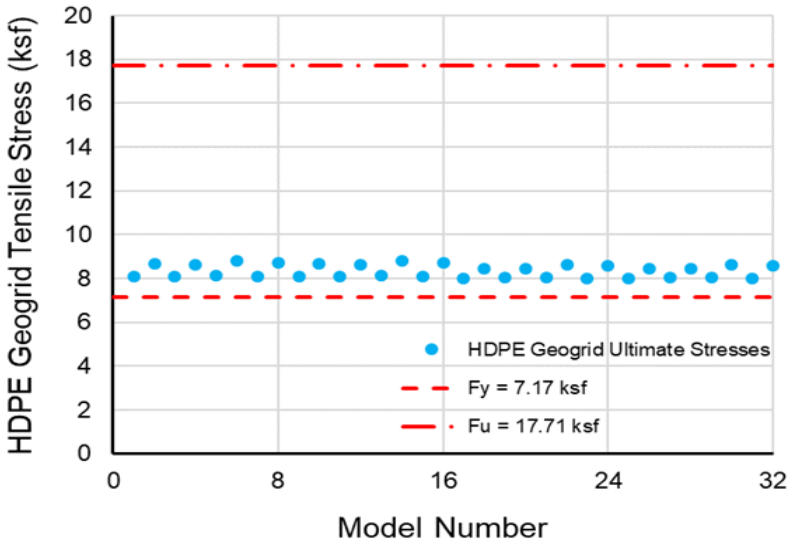

(b) HDPE geogrid

Figure 5-24 Stress comparison between developed reinforcement ultimate stress and reinforcement tensile strength for ABAQUS models reinforced with (a) steel grid, and (b) HDPE geogrid

Figures 5-25(a and b) show comparisons between the FHWA (2009) designed internal stability serviceability limits and developed reinforcement ultimate stresses from the ABAQUS models. Figure 5-25(a) shows a comparison regarding the steel grid reinforced models, and Figure 5-25 (b) shows a comparison regarding the HDPE geogrid reinforced models. The calculated maximum tensile forces in reinforcement layers using the FHWA (2009) code match quite well with the observed ultimate tensile forces conducted from the numerical models of both reinforcement types. These results also show that the code rupture limits are more conservative for the steel grid reinforced models than the HDPE geogrid reinforced models, and the code pullout limits are very

critical for steel grid reinforced models when pore pressure is applied, reinforcement length is taken as 0.7H, and breakage/slippage of reinforcement is considered (Figure 5-25(a)). On the other hand, Figure 5-25 (b) shows that the code pullout limits are conservative for HDPE geogrid reinforced models.

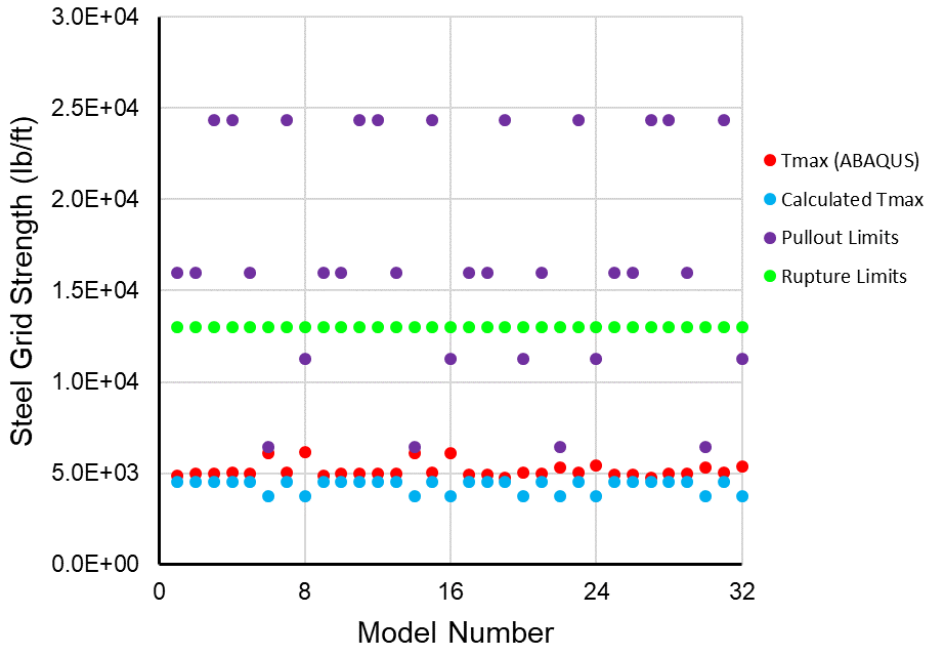

(a) Steel grid

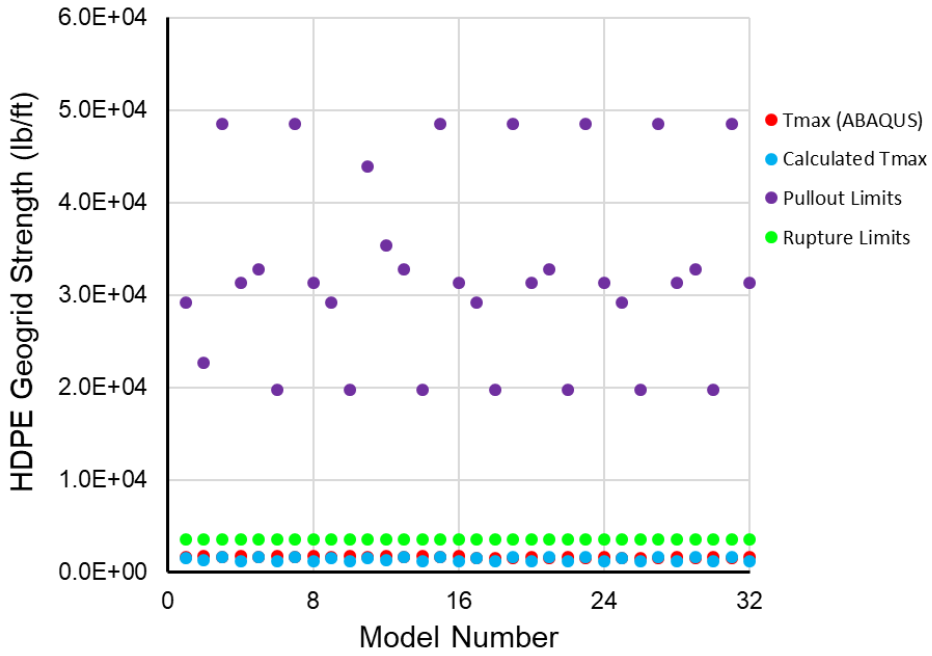

(b) HDPE geogrid

Figure 5-25 Stress comparison between the FHWA (2009) designed internal stability serviceability limits and developed reinforcement ultimate stress of the ABAQUS models reinforced with (a) steel grid, and (b) HDPE geogrid

Chapter 6
REGRESSION AND STRUCTURAL RELIABILITY ANALYSES

6.1 Regression Analysis

To assess the effect of the parametric study parameters on the MSE wall behavior; a regression analysis was carried out on the parametric study models. The six main parameters “Xs” that were chosen to investigate their effect on the out-of-plane movement “Y” are:

X_1 = reinforcement type (= -1 for steel grid and 1 for HDPE geogrid),

X_2 = pore pressure (=-1 for no applied pore pressure and 1 for applied pore pressure (624 psf)),

X_3 = reinforcement length (=-1 for 0.7H and 1 for 1.0H),

X_4 = reinforcement breaking/slippage (=-1 when breaking/slippage is not considered and 1 when breaking/slippage is considered),

X_5 = PCP compressive strength (=-1 for 4 ksi and 1 for 5 ksi), and

X_6 = backfill soil cohesion (=-1 for cohesionless and 1 for a cohesion of 418 psf).

6.1.1 Meaningful Relationship

There are several factors that may affect MSE wall movement. This section covers the main parameters that may affect the performance of MSE walls. The out-of-plane movement conducted from the ABAQUS numerical models of the parametric study was considered for the analysis and was assumed to be positive if it was moving away from the facing panels (out-of-plane movement). Initially, the investigated parameters were

compared individually with the wall movement in scattered plots, as shown in Figures 6-1(a through f). The Y-axes represent the out-of-plane movement obtained from ABAQUS, and the X-axes represent the values of the wall parameter, either taken as -1 or 1. These figures show that the out-of-plane movement of an MSE wall increases when the reinforcement type is HDPE geogrid, pore pressure is applied, the reinforcement length is taken as 0.7H, breakage/slippage of reinforcement is considered, or the backfill soil is cohesionless. However, the PCP compressive strength seems to have no effect on the wall movement as the values look even on both sides of the vertical axis shown in Figure 6-1(e). Furthermore, the reinforcement type, the pore pressure, and the reinforcement length appear to have a significant effect on the wall movement as the values vary significantly between the left and the right sides of the vertical axes.

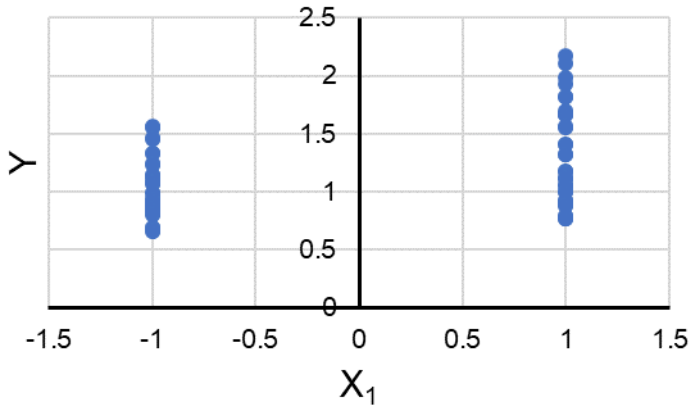

(a) Reinforcement type

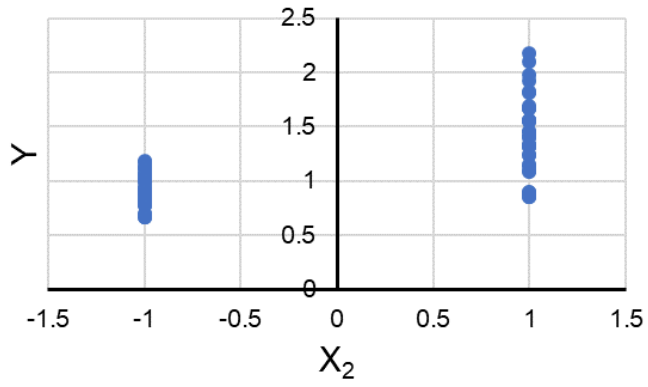

(b) Pore pressure

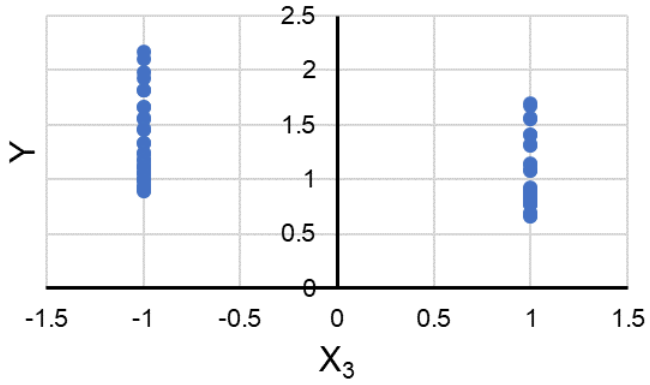

(c) Reinforcement length

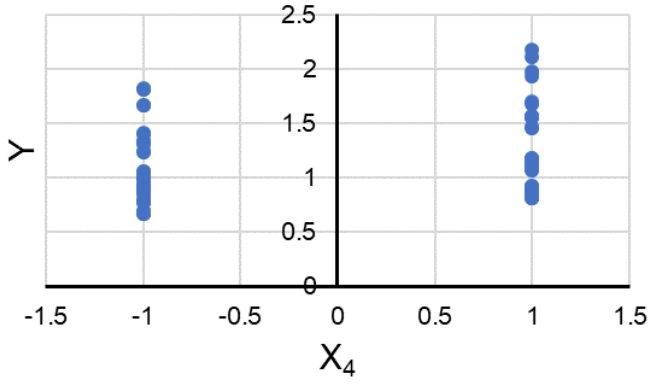

(d) Reinforcement breaking/slippage

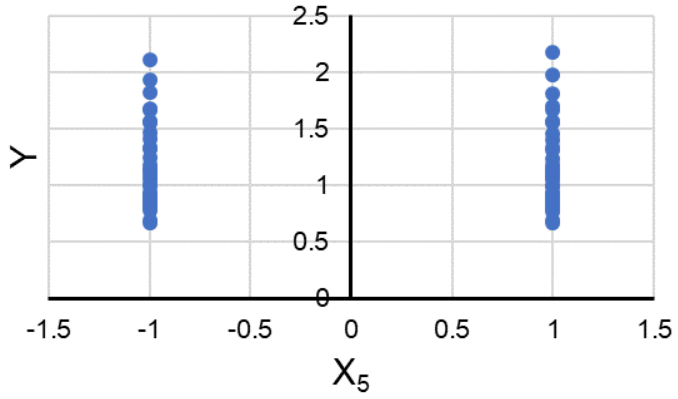

(e) PCP compressive strength

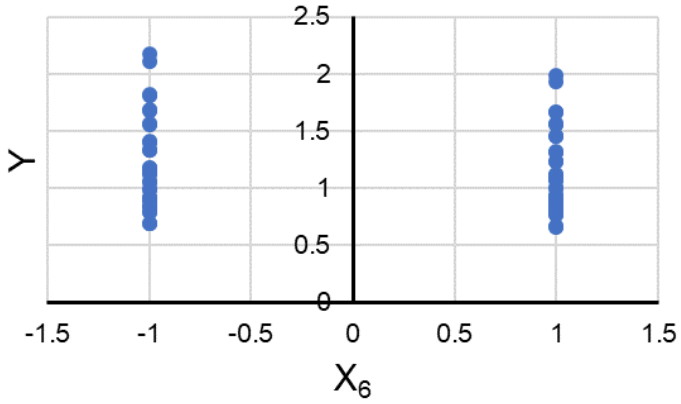

(f) Backfill soil cohesion

Figure 6-1 MSE wall parameters versus out-of-plane movement

6.1.2 Multi Linear Regression (MLR) Model

Based on the scatter plots shown in Figures 6-1(a through f), it was assumed that there was a relation between the wall movement and the wall parameters except for the

PCP compressive strength. Therefore, the MLR model was carried out by regressing the wall movement (Y), in inches, on the rest of the five parameters, as follows:

X_1 = reinforcement type (= -1 for steel grid and 1 for HDPE geogrid),

X_2 = pore pressure (=-1 for no applied pore pressure and 1 for applied pore pressure (624 psf)),

X_3 = reinforcement length (=-1 for 0.7H and 1 for 1.0H),

X_4 = reinforcement breaking/slippage (=-1 when breaking/slippage is not considered and 1 when breaking/slippage is considered), and

X_5 = backfill soil cohesion (=-1 for cohesionless and 1 for a cohesion of 418 psf).

A preliminarily model with five predictor parameters was assumed as follows:

$$\widehat{Y}_i = \beta_0 + \beta_1 X_{i1} + \beta_2 X_{i2} + \beta_3 X_{i3} + \beta_4 X_{i4} + \beta_5 X_{i5} + \in_i \quad (6.1)$$

where, $\widehat{Y}_i$ is the predicted value for model “i", and β is the estimated factor of a variable X. The regression analysis of the preliminary model was carried out using SAS software. 64 models were considered. The outputs of the regression analysis consist of the ANOVA Table and the fitted line parameters (Figure 6-2), and plots of the residual values (e_i) vs the Xs’ parameters and the predicted value ($\widehat{Y}_i$), as shown in Figures 6-3(a through f).

The SAS System

The REG Procedure
Model: MODEL1
Dependent Variable: y

Number of Observations Read	64
Number of Observations Used	64

Analysis of Variance

Source	DF	Sum of Squares	Mean Square	F Value	Pr > F
Model	5	8.13758	1.62752	101.51	<.0001
Error	58	0.92992	0.01603		
Corrected Total	63	9.06750			

Root MSE	0.12662	R-Square	0.8974
Dependent Mean	1.18005	Adj R-Sq	0.8886
Coeff Var	10.73020		

Figure 6-2 ANOVA Table and fitted line parameters of the preliminarily model

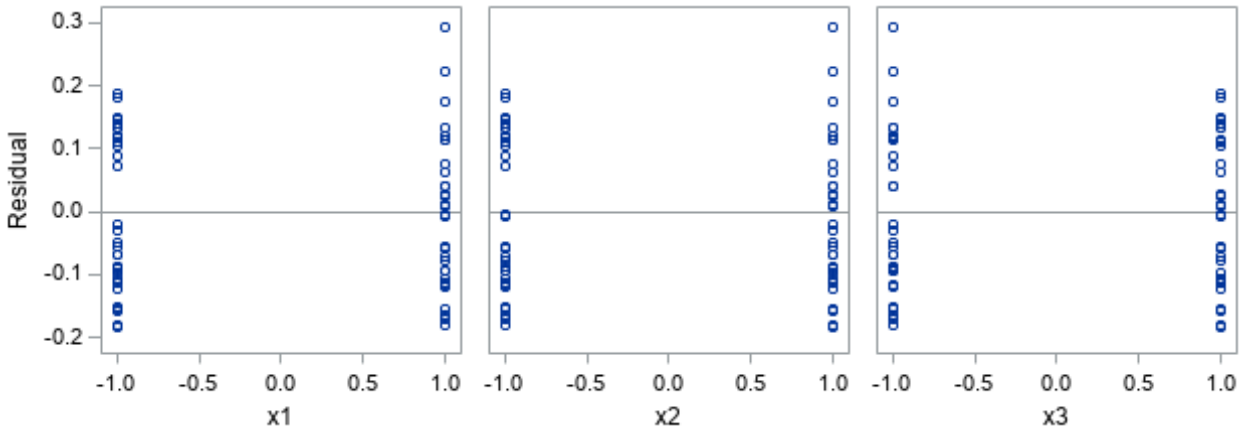

(a) e_i vs X_1 (b) e_i vs X_2 (c) e_i vs X_3

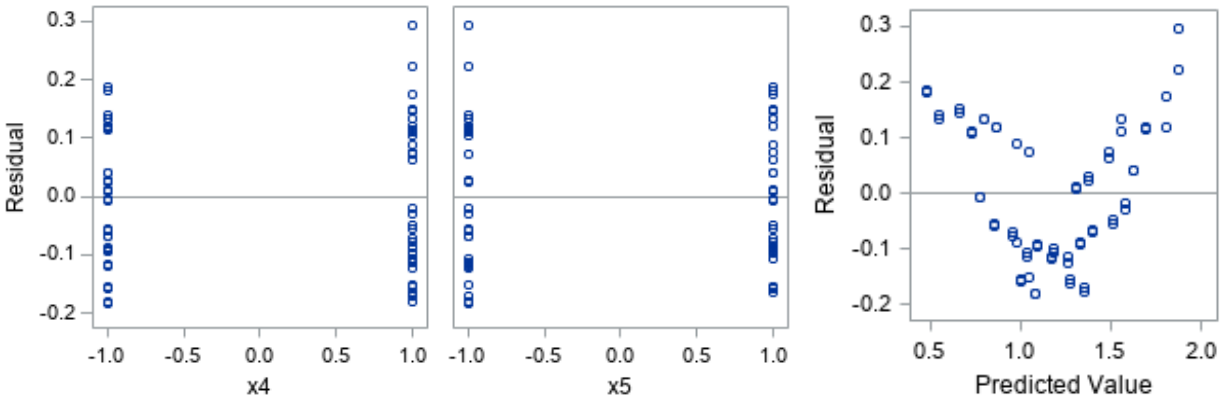

(d) e_i vs X_4 (e) e_i vs X_5 (f) e_i vs $\hat{Y}_i$

Figure 6-3 Residuals versus Xs and predicted values of the preliminarily model

Figures 6-3(a through e) show that the wall parameters have random relationships with the fitted line residuals. On the other hand, Figure 6-3(f) shows that there seems to be a pattern between the predicted values and the fitted residuals; thus, a polynomial model is needed in order to reduce the curvilinearity effect.

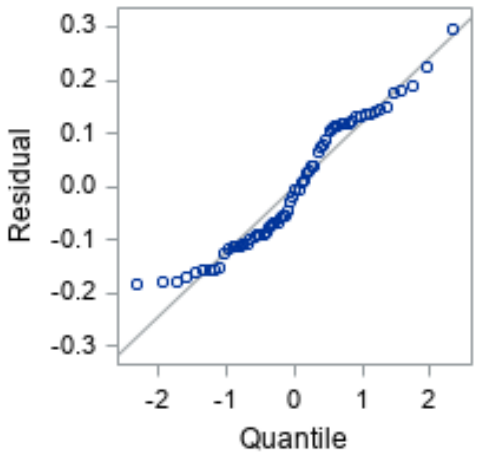

Figure 6-4 Normality plot of the preliminarily model

The normality plot shown in Figure 6-4 shows that most of the data is along the 45-degree line angle; therefore, it can be concluded that the error term is normally distributed or very close to normal.

The second iteration was performed by assuming a transformed model by taking the new Y_i' as the logarithm "Log" of Y_i to provide better accuracy for the fitted model. The model was assumed as:

$$\mathrm{Log}(\widehat{Y}_i) = \beta_0 + \beta_1 X_{i1} + \beta_2 X_{i2} + \beta_3 X_{i3} + \beta_4 X_{i4} + \beta_5 X_{i5} + \mathrm{Log}(\in_i) \quad (6.2)$$

The outputs of the regression analysis of the second iteration are shown in Figure 6-5. The new constant variance plot shown in Figure 6-6 shows that the curvilinearity has been reduced after transforming Y_i to Log(Y_i).

The SAS System

The REG Procedure
Model: MODEL1
Dependent Variable: y

Number of Observations Read	64
Number of Observations Used	64

Analysis of Variance

Source	DF	Sum of Squares	Mean Square	F Value	Pr > F
Model	5	5.58893	1.11779	178.00	<.0001
Error	58	0.36422	0.00628		
Corrected Total	63	5.95315			

Root MSE	0.07924	R-Square	0.9388
Dependent Mean	0.11791	Adj R-Sq	0.9335
Coeff Var	67.20789		

Figure 6-5 ANOVA Table and fitted line parameters of Log(Y_i) model

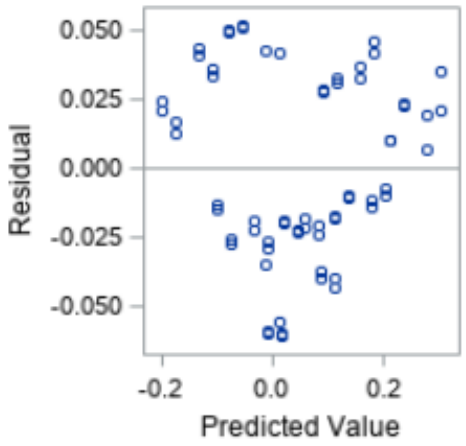

Figure 6-6 Constant variance plot of Log(Y_i) model

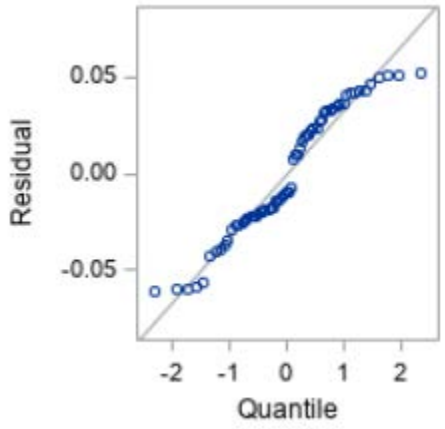

Figure 6-7 Normality plot of Log(Y_i) model

The same conclusion can be observed from Figure 6-7 as the majority of the data is along the 45-degree line angle. Therefore, the distribution of the error term is normally distributed or very close to normal.

The outliers were tested for the new model. The 64 models were found to be in the safe region from being outliers as the absolute of the R-student values are less than three, and the absolute of the DFFITS and DFBETAS values are less than one (Appendix B). However, Models 4, 5, 9, 12, 20, and 28 were eliminated from the model as they appear to be y-outliers by looking at the constant variance plot shown in Figure 6-6.

The last iteration was developed by regressing the Log(Y_i) on the rest of the 58 models. The outputs are shown in Figure 6-8. This figure shows that the P_r values of the predicted values are all less than the confidence interval “0.05”, which means that all the predicted values are significant and cannot be eliminated from the equation. Furthermore,

Figure 6-8 also shows that all the variance inflation factors “VIFs” are less than 10, and the average value “$\overline{VIF}$” equals to 1.015, which almost equals to 1. Therefore, it can be concluded that there is no multi-collinearity issue. Also, it shows that the R^2 value is equal to 0.9593. This means that 95.93% of the total variation in wall movement is explained by the new model.

The SAS System

The REG Procedure
Model: MODEL1
Dependent Variable: y

Number of Observations Read	58
Number of Observations Used	58

Analysis of Variance

Source	DF	Sum of Squares	Mean Square	F Value	Pr > F
Model	5	1.01372	0.20274	245.32	<.0001
Error	52	0.04298	0.00082645		
Corrected Total	57	1.05669			

Root MSE	0.02875	R-Square	0.9593
Dependent Mean	0.06133	Adj R-Sq	0.9554
Coeff Var	46.87788		

Parameter Estimates

Variable	DF	Parameter Estimate	Standard Error	t Value	Pr > |t|	Tolerance	Variance Inflation
Intercept	1	0.05662	0.00382	14.83	<.0001	.	0
x1	1	0.04536	0.00382	11.88	<.0001	0.98855	1.01158
x2	1	0.10036	0.00382	26.29	<.0001	0.97913	1.02131
x3	1	-0.05478	0.00382	-14.35	<.0001	0.97913	1.02131
x4	1	0.02926	0.00382	7.66	<.0001	0.98168	1.01866
x5	1	-0.01245	0.00378	-3.29	0.0018	0.99626	1.00376

Figure 6-8 Finalized model outputs

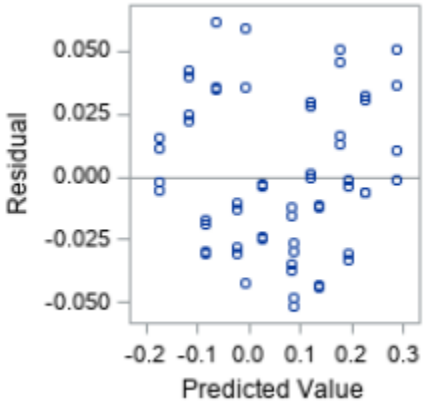

Figure 6-9 Constant variance plot of finalized Log(Y_i) model

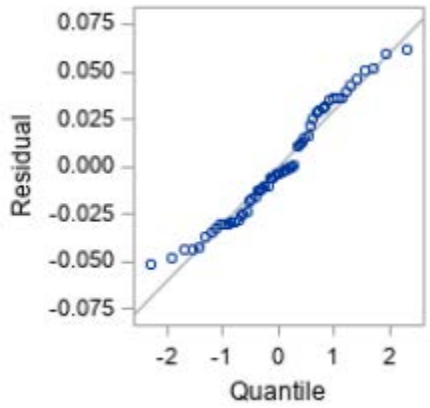

Figure 6-10 Normality plot of finalized Log(Y_i) model

Figure 6-9 shows that the errors become randomly distributed after removing the y-outliers, meaning that the curvilinearity issue no longer exists. Figure 6-10 shows that most of the observations fall along the 45-degree line, concluding that the normality is satisfied. Figures 6-11(a through e) show that the wall parameters have random relationships with the fitted residuals.

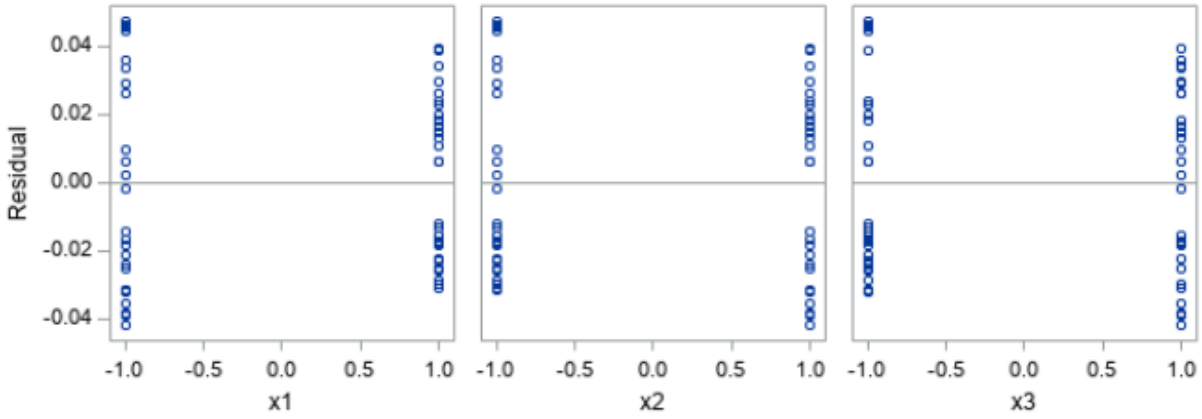

(a) e_i vs X_1 (b) e_i vs X_2 (c) e_i vs X_3

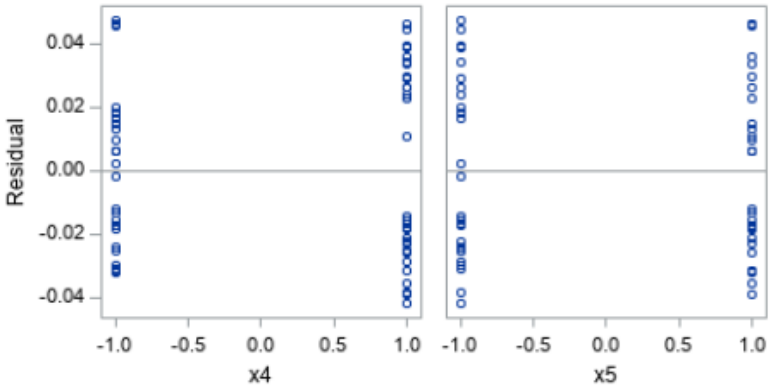

(d) e_i vs X_4 (e) e_i vs X_5

Figure 6-11 Residuals versus Xs if the finalized model

Figure 6-12 shows the correlation coefficient “r” values between the wall movement “Y” and the wall parameters “Xs”. The r value ranges between -1 and 1. Negative value means for every positive increase in one variable, a negative decrease of a determined proportion occurs in the other. If the r value is zero, for every increase or decrease in one variable, the other variable is not affected, meaning that these variables are not related. On the other hand, if the r value is positive, for every increase or decrease in one variable, the other variable increases or decreases accordingly. If the value is exactly 1 or -1, a

perfect correlation between the two variables exists. Figure 6-12 shows that the parameters of the reinforcement type, the pore pressure, and the reinforcement breakage/slippage have a positive relation with the wall movement, while the reinforcement length and the backfill soil cohesion have an inverse relation with the wall movement. When the reinforcement length is taken as 1.0H or the backfill soil has a cohesion value of 418 psf, the lateral wall movement tends to decrease. Figure 6-12 also shows that the pore pressure has a significant correlation with the wall movement.

Pearson Correlation Coefficients, N = 58 Prob > |r| under H0: Rho=0						
	y	x1	x2	x3	x4	x5
y	1.00000	0.33412 0.0104	0.81690 <.0001	-0.45211 0.0004	0.21500 0.1051	-0.11674 0.3828
x1	0.33412 0.0104	1.00000	0.03828 0.7754	0.03828 0.7754	-0.07669 0.5672	-0.03828 0.7754
x2	0.81690 <.0001	0.03828 0.7754	1.00000	-0.10476 0.4338	0.07156 0.5935	-0.03333 0.8038
x3	-0.45211 0.0004	0.03828 0.7754	-0.10476 0.4338	1.00000	0.07156 0.5935	-0.03333 0.8038
x4	0.21500 0.1051	-0.07669 0.5672	0.07156 0.5935	0.07156 0.5935	1.00000	-0.00239 0.9858
x5	-0.11674 0.3828	-0.03828 0.7754	-0.03333 0.8038	-0.03333 0.8038	-0.00239 0.9858	1.00000

Figure 6-12 Pairwise correlation matrix

6.1.3 Final MLR Model

The final model depends on the reinforcement type (X_1), the pore pressure (X_2), the reinforcement length (X_3), the reinforcement breakage/slippage (X_4), and the backfill soil

cohesion (X_5). This means in the MLR model, the lateral wall movement ($\widehat{Y}$), in inches, is affected by those variables according to their respective factors. The final fitted model is:

$$\mathrm{Log}(\widehat{Y}_i) = 0.05662 + 0.04536X_{i1} + 0.10036X_{i2} - 0.05478X_{i3} + 0.02926X_{i4} - 0.01245X_{i5} \quad (6.3)$$

where:

X_1 = reinforcement type (= -1 for steel grid and 1 for HDPE geogrid),
X_2 = pore pressure (=-1 for no applied pore pressure and 1 for applied pore pressure (624 psf)),
X_3 = reinforcement length (=-1 for 0.7H and 1 for 1.0H),
X_4 = reinforcement breaking/slippage (=-1 when breaking/slippage is not considered and 1 when breaking/slippage is considered), and
X_5 = backfill soil cohesion (=-1 for cohesionless and 1 for a cohesion of 418 psf).

As Equation 6.3 contains a logarithmic term, the fitted model becomes polynomial. This equation leads to the same conclusions obtained from the pairwise correlation matrix shown in Figure 6-12. When the reinforcement type is HDPE geogrid, pore pressure is applied, or the reinforcement breakage/slippage is considered, the lateral wall movement tends to increase. On the other hand, when the reinforcement length is taken as 1.0H or the backfill soil is cohesive, the lateral wall movement tends to decrease. Equation 6.3 shows also that the presence of pore pressure affects the wall movement the most as its respective factor is the highest compared to the other parameter factors.

6.2 Structural Reliability Analysis

The internal stability of steel grid reinforced MSE walls was investigated by performing structural reliability analysis using the Monte Carlo Simulation. The structural reliability is based on considering a model to be successful if its performance has met the requirement. The response of the random generated samples can be evaluated using the following formula:

$$g(x) = R - S \tag{6.4}$$

where g(x) is a random model, R is the uncertain resistance of that model, and S is the uncertain applied load on that model. The probability of failure is determined as the percentage of samples that have values of g(x) less than zero. This is because the applied loads of those models have exceeded their respective resistance capacities. R and S were considered in this research to follow normal distribution with mean and standard deviation (μ_R, σ_R) and (μ_S, σ_S), respectively.

6.2.1 Monte Carlo Simulation

A Monte Carlo Simulation approach was used to check for the ultimate limit states of the internal stability of steel grid reinforced MSE walls proposed by the FHWA (2009). The Monte Carlo Simulation is widely used since it has been developed in the 1930s. This method is an engineering tool than can be used for the statistical analysis of uncertainty in engineering problems. If a system parameter is known to follow a certain probability distribution, the performance of the system is studied by considering several possible values of the parameter, each following a specified probability distribution. This method

uses the principle of trial and error using a computer program by generating random number of models and calculating the percentage of models that fail. This method was used in this research using Matlab software.

After generating the random number of samples, the overall structural reliability can be evaluated as:

$$\text{Structural reliability} = \frac{\text{Number of successful samples}}{\text{Total number of samples generated}} \quad (6.5)$$

Thus, the probability of failure can be computed as:

$$\text{Structural probability of failure} = \frac{\text{Number of failed samples}}{\text{Total number of samples generated}} \quad (6.6)$$

6.2.2 Internal Stability Equations of MSE Walls

Steel grid reinforced MSE walls were investigated using the Monte Carlo Simulation. The ultimate limit states (ULS) of the FHWA (2009) internal stability checks of MSE walls were investigated.

The internal stability relies on resisting the wall against two failure modes, pullout and rupture of earth reinforcement. Both failure modes are designed to satisfy the maximum tensile forces developed in the earth reinforcement "T_{MAX}". T_{MAX} can be calculated as:

$$T_{MAX} = K_r[\gamma_r(z + h_{eq})S_V\ S_H] \quad (6.7)$$

where K_r is lateral earth pressure coefficient, γ_r is the backfill soil unit weight, z is the depth from the top of the wall, h_{eq} is an equivalent soil surcharge layer of height that equals to 2 ft., and S_V and S_H are the vertical and horizontal spacing of the earth reinforcement, respectively. The assessment of the uncertainty in T_{MAX} was investigated based on the uncertainties in K_r, γ_r, h_{eq}, S_V, and S_H. The K_r value varies at each reinforcement level based on the FHWA (2009) code mentioned in Section 2.3.1. The pullout resistance is developed from the interaction between the reinforcement layers and the adjacent soil particles, and can be calculated as:

$$R_{pullout} = F^* \alpha \gamma_r z L_e C b \quad (6.8)$$

where F* is a pullout resistance factor, α is a scale correction factor (equals to 1 for metallic reinforcement), L_e is the effective reinforcement length, C is the reinforcement effective area perimeter (equals to 2 for steel grids), and b is the reinforcement width. F* can be estimated for steel grids as:

$$F^* = 20\left(\frac{t}{S_t}\right) \quad \text{at the top of the structure} \quad (6.9)$$

$$F^* = 10\left(\frac{t}{S_t}\right) \quad \text{at a depth of 20 ft and below} \quad (6.10)$$

where t is the thickness of the transverse bar and S_t is the transverse spacing. The uncertainties in the pullout failure mode was assessed based on the uncertainties in F* and γ_r. Therefore, the pullout ultimate limit state at each reinforcement level of the steel grid reinforced MSE walls can be defined as:

$$R_{Pullout} - T_{MAX} = [2 F^* \gamma_r z L_e b] - K_r[\gamma_r(z + h_{eq})S_V S_H] \quad (6.11)$$

The rupture of the reinforcement depends on the tensile strength of the reinforcement and can be calculated as:

$$R_{rupture} = F_y A_C \quad (6.12)$$

where F_y is the yielding strength of the material and A_C is the designed cross-sectional area considering the corrosion loss. According to FHWA (2009), the steel grid reinforcement of MSE walls are typically coated with 18 mils (450 μm) of galvanization. This thickness was estimated based on the Coating Standard (ASTM A-884, 2019). The uncertainties in F_y and A_C were considered. Therefore, the rupture ultimate limit state at each reinforcement level can be calculated as:

$$R_{Pullout} - T_{MAX} = [F_y A_C] - K_r[\gamma_r(z + h_{eq})S_V S_H] \quad (6.13)$$

The uncertainties in theses parameters were assumed to be normally distributed that consist of mean values and coefficient of variance values of 5%.

The reliability analysis was carried out on 30 ft high MSE walls that consisted of different backfill soil unit weights (110 and 125 pcf), backfill soil friction angles (30^o and 34^o), vertical reinforcement spacing (1.5 and 2.5 ft), and horizontal reinforcement spacing (1.5 and 3 ft). The steel grid used for the investigation was W11xW11, which consisted of three longitudinal bars spacing at six inches and transverse bars spacing at 24 inches throughout the length of the reinforcement.

The structural reliability index “β” was considered in this research to assess the probability of failure of the studied models. The structural reliability index is often used to

indicate the probability of failure of a structure. Higher values of reliability index are considered for a structure whose failure would lead to serious consequences. Table 6-1 shows different values of reliability index and their respective probability of failure. The targeted reliability index value that was considered for this research was 2.5 with a probability of failure of 0.0062.

Table 6-1 Corresponding values of reliability index and probability of failure

Reliability index β	Probability of failure P_f
2.0	0.023
2.33	0.010
2.5	0.0062
3.0	0.0013
3.5	0.00023
4.0	0.000032

6.2.3 Structural Reliability Results

Figures 6-13 to 6-14 show a comparison of the reliability index of MSE walls consisting of different reinforcement spacing, and different friction angles and unit weights of the backfill soil. These MSE wall models have a height of 30 ft. The X-axes of these figures represent the depth of the reinforcement layers, measured from the top of the MSE walls. The reliability index is then computed at each reinforcement layer of these models.

The pullout ultimate limit states of MSE walls shown in Figures 6-13(a through d) indicate that the first few reinforcement layers are critical to pullout. These figures also show that increasing the reinforcement spacing significantly increases pullout failure, increasing the friction angle of the backfill soil slightly decreases pullout failure, while changing the backfill unit weight seems to have no effect on the MSE structural safety.

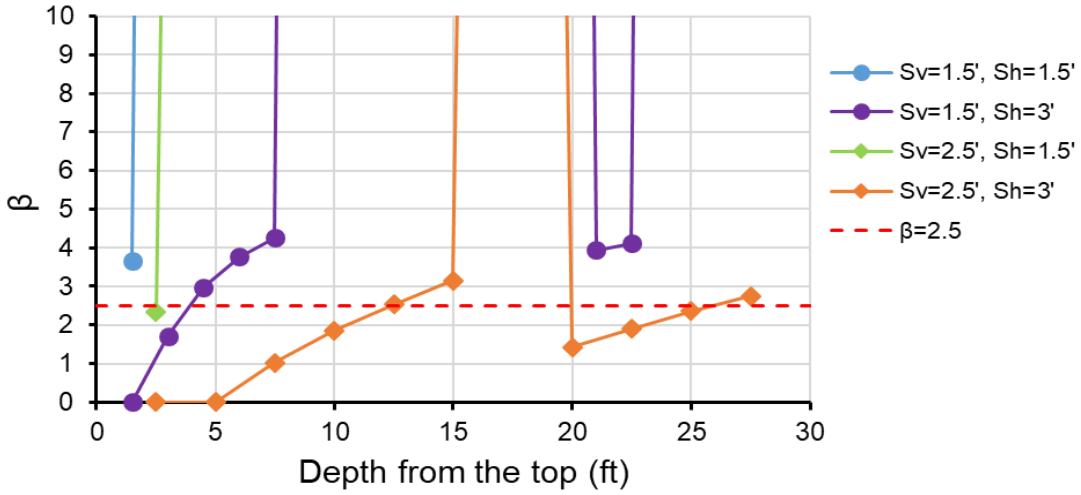

(a) H=30 ft, Ø=30º, and ɣ=110 pcf

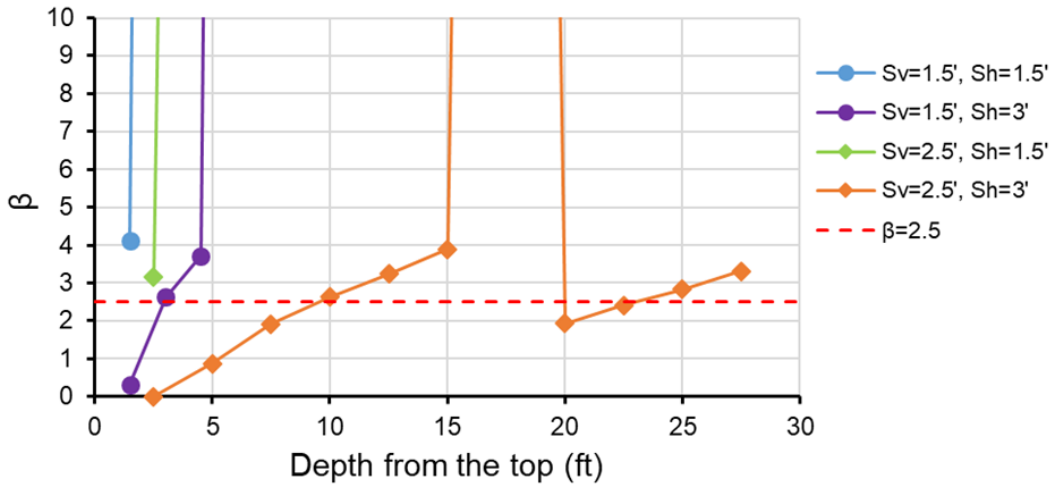

(b) H=30 ft, Ø=34º, and ɣ=110 pcf

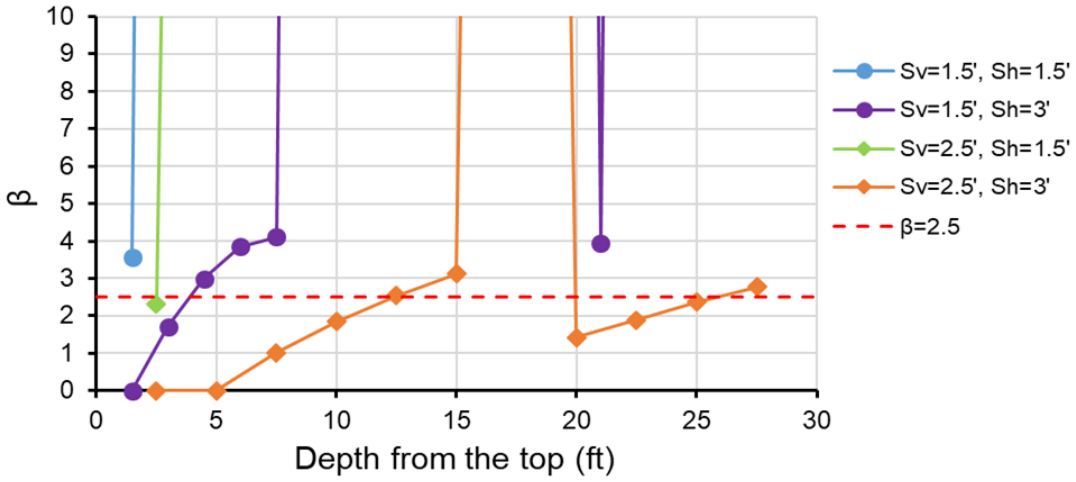

(c) H=30 ft, Ø=30º, and ɣ=125 pcf

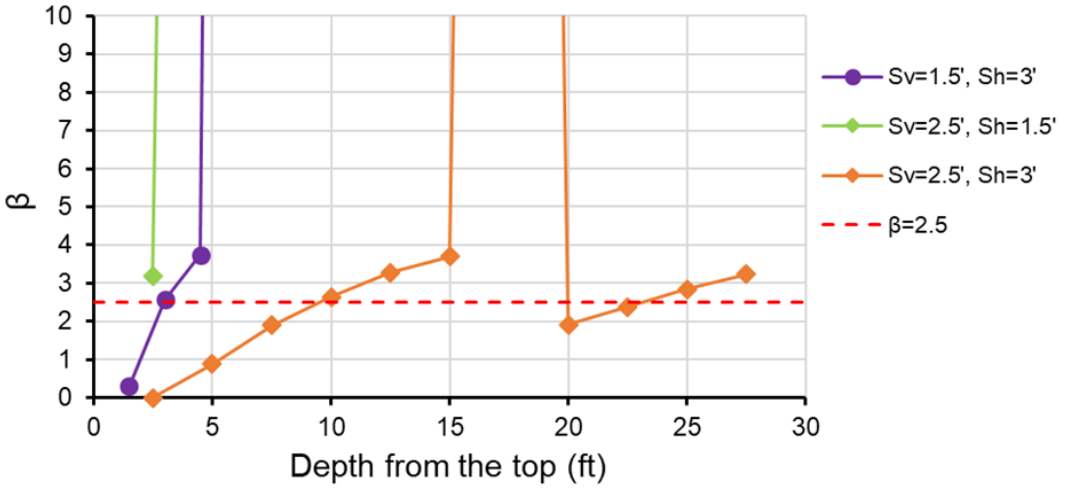

(d) H=30 ft, Ø=34º, and ɣ=125 pcf

Figure 6-13 Pullout ultimate limit states of MSE walls

Figures 6-14(a through d) show the rupture ultimate limit states of MSE walls. These figures show that only when the vertical and horizontal grid spacing are taken as 2.5 ft and 3 ft, respectively, the reinforcement layers at the very bottom become critical to

rupture. They also show that increasing the friction angle of the backfill soil slightly decreases rupture failure, while increasing the backfill unit weight increases the rupture failure. This is because the rupture limit state equation has the backfill unit weight in the load term, thus, it increases while increasing the reinforcement depth, while the resistance term remains in a constant range throughout the increase in reinforcement depth, as shown in Equation 6.13.

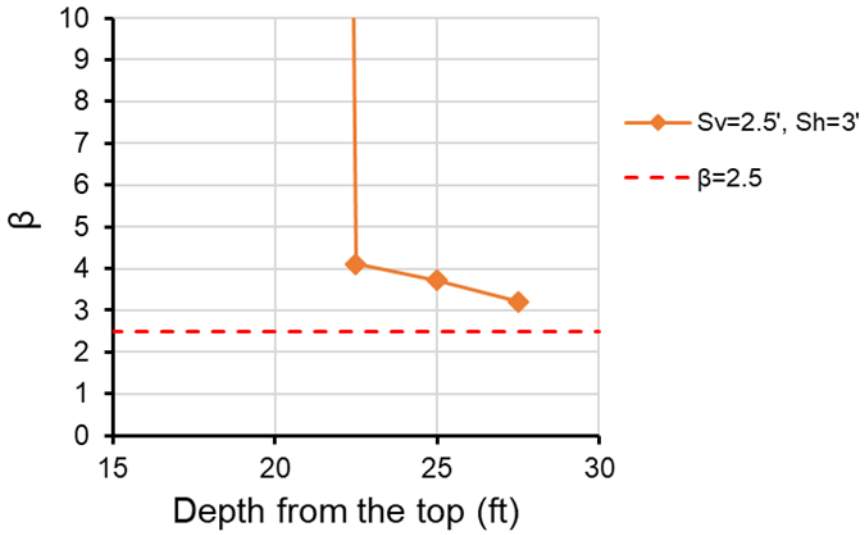

(a) H=30 ft, Ø=30^{o}, and ɣ=110 pcf

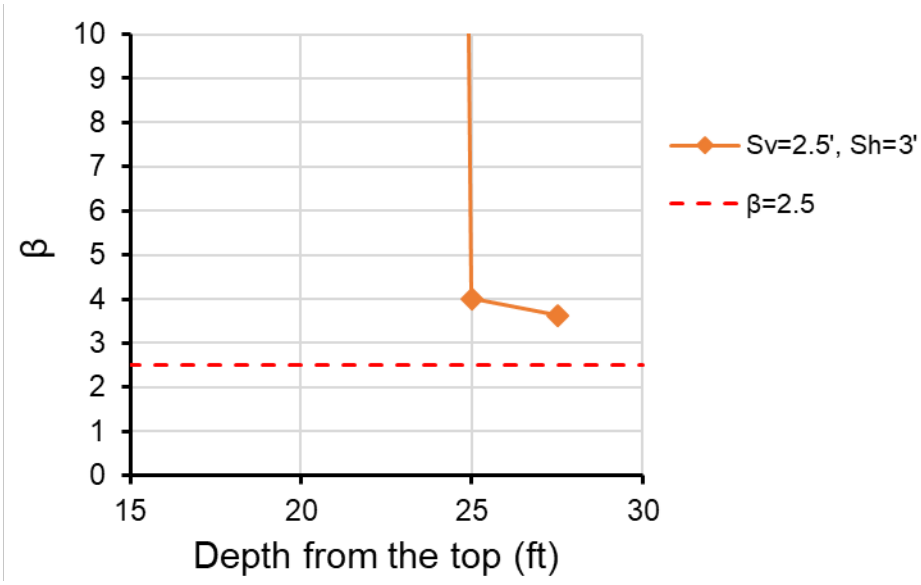

(b) H=30 ft, Ø=34º, and ɣ=110 pcf

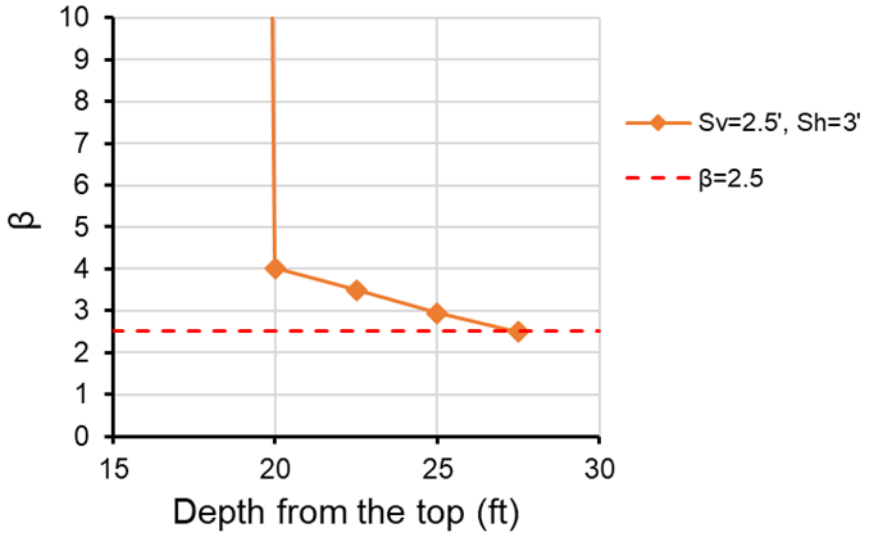

(c) H=30 ft, Ø=30º, and ɣ=125 pcf

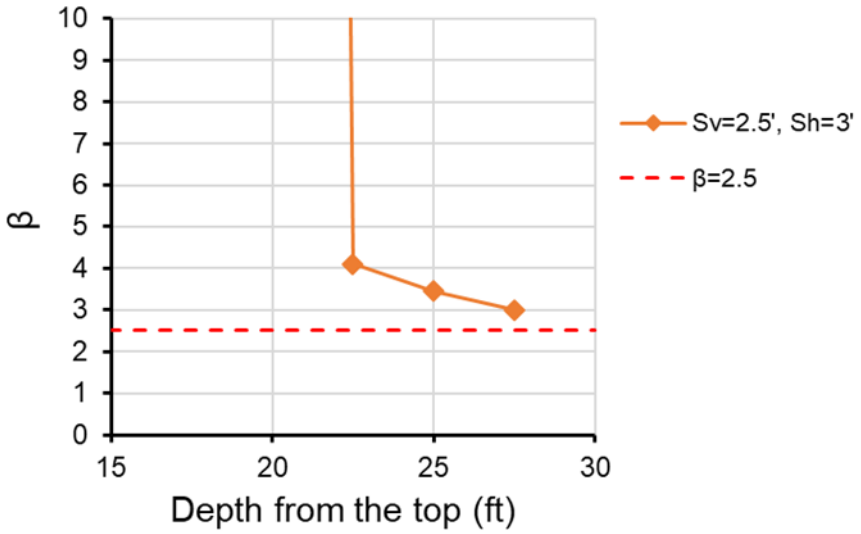

(d) H=30 ft, Ø=34º, and ɣ=125 pcf

Figure 6-14 Rupture ultimate limit states of MSE walls

Afterwards, the serviceability limit states for the pullout and rupture reduction factors of the FHWA (2009) were checked. The FHWA (2009) reduction factors for the pullout and rupture limit states for different types of MSE walls are shown in Appendix A. Based on the code, the load factor was taken as 1.35, while the reduction factors for the steel grid's pullout and rupture were taken as 0.9 and 0.65, respectively. These recommended factors were checked at different wall heights ranging from 20 ft to 100 ft to check whether it satisfies the targeted probability index, which is 2.5, or not. The most critical cases shown by Figures 6-13 and 6-14 were used for the comparison; for the pullout limit states, the MSE walls that consisted of backfill friction angle and unit weight of 30^0 and 110 pcf, respectively, and grid vertical and grid horizontal spacing of 2.5 ft and 3 ft, respectively (Figure 6-13(a)) were considered, while for the rupture limit states, The MSE walls were

generated based on the backfill friction angle and unit weight equal to 30^0 and 125 pcf, respectively, and grid vertical and grid horizontal spacing of 2.5 ft and 3 ft, respectively (Figure 6-14(c)).

The comparison is shown in Figure 6-15, and it shows that the pullout recommended factor by the FHWA (2009) is conservative for wall heights above 40 ft, and a modified reduction factor for the pullout limit state shall be applied according to the figure when wall heights are below 40 ft. On the other hand, Figure 6-15 shows that the rupture recommended factor by the FHWA (2009) is conservative for wall heights that are below 60 ft, while a modification factor for the rupture limit state is needed according to the figure when wall heights are above 60 ft.

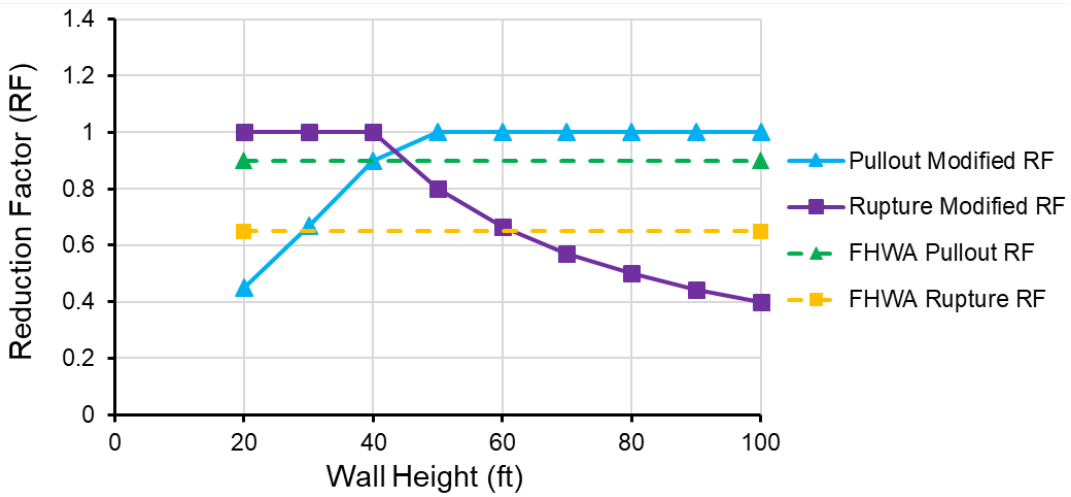

Figure 6-15 Comparison between the FHWA (2009) recommended reduction factors and the modified reduction factors

Chapter 7
CONCLUSIONS AND RECOMMENDATIONS

7.1 Summary

The current study was inspired by multiple MSE walls that are currently experiencing unexpected distress, such as deformations, settlement, widening of panel joints, and other types of distress associated with retaining walls. The three most critical MSE walls were selected for this study. Wall 264R is located south of the Bedford Euless Rd and Airport Freeway intersection in Hurst, Texas. Wall 179L is located at the intersection of NE Loop 820 and W Pipeline Rd in Hurst, Texas. Walls CC1-3 are a combination of walls supporting the abutment on the Southwest Blvd Bridge, located at the intersection of Chisholm Trail Pkwy and Southwest Blvd in Fort Worth, Texas. The construction of Walls 264R and 179L was completed between 1997 and 1998, while the construction of Walls CC1-3 was completed between 2012 and 2013.

A visual inspection of the monitored MSE walls was carried out in May 2017. During the field visits at Wall 264R, backfill leakage, wide gaps at panel joints, and bulging of the precast panels at the new section were observed. Extensive cracks were observed on the copings and the traffic barriers of Wall 179L, as well as water/backfill leakage near the manhole located at Wall 179L. For Walls CC1-3, differential movement between panels, opening of panel joints, and leakage of backfill material were observed.

Several non-destructive tests were performed on the critical walls. The 3D robotic laser scanner was used to check for the growing movement of the precast panels of the

MSE walls. Ground Penetrating Radar (GPR) and Infrared Camera were used to examine the integrity of the strips and determine if there was any rupture or delamination, respectively. The Resistivity Imaging (RI) technique was used to investigate the groundwater table and perched water zones behind the precast facing panels.

Five boreholes were conducted in March 2018, two at Wall 264R, two at Wall 179L, and one at Walls CC1-3, in order to check the integrity of the backfill soils with the standard specifications of TxDOT and ASTM, as well as to be used to validate the backfill soil modeling in ABAQUS. The backfill soils of Walls 264R and 179L are silty sand; therefore, Sieve Analysis, Proctor Compaction, and Triaxial tests were performed on the obtained soil samples. On the other hand, only Sieve Analysis and Angle of Repose tests were performed on the backfill soil of Walls CC1-3 as it consists of only aggregate.

A Finite Element Modeling (FEM) of the west side of Wall CC1 was created in ABAQUS CAE (ABAQUS 2016) software to simulate the geometric and material properties of the MSE wall as closely as possible. The objective of the numerical modeling was to develop a modeling framework to simulate the behavior of the actual MSE walls and conduct a parametric study to investigate the effect of the MSE wall parameters that may potentially lead to failure of an MSE wall. The parametric study was initiated using the Design of Experiments (DOE) using Minitab software and it was carried out using a 3D typical MSE wall using ABAQUS software. Six main parameters were chosen that consisted of two cases each for this study, resulting in 64 different models. These parameters are pore water pressure,

reinforcement type, reinforcement length, reinforcement breakage/slippage, and backfill soil cohesion. A regression analysis was then carried out using SAS software to assess the effect of the parametric study parameters on the MSE wall lateral movement. Afterwards, the internal stability of steel grid reinforced MSE walls was investigated by performing a structural reliability analysis using the Monte Carlo Simulation using Matlab software.

7.2 Findings and Conclusions

- The survey results show that Walls 264R and 179L are exhibiting a considerable out-of-plane movement. It also shows that there is a continuous settlement shown by Wall 264R.
- It can be noted that heavy rain events affect Wall 264R by causing out-of-plane movement and settlement as the movement spikes occurred when heavy rains took place. On the other hand, the survey data conducted at Wall 179L seems to have no correlation with precipitation. This could be caused by the manhole that is existed behind the precast panels of Wall 179L, which might leak water into the backfill soil at different times from the rain events.
- The crack meter readings show that Wall 264R is exhibiting settlement.
- The RI scans indicate that Walls 264R and 179L have poor drainage systems since they allow water pockets to be formed behind the precast panels during rain events, while Walls CC1-3 seem to have a good drainage system as the resistivity appeared to be low in both scans. These observations were also noted by laser scanning.

- The GPR scan data shows that the penetration depth and the resolution of the scan were heavily affected by the steel reinforcement in the pavement and the density of the reinforcement layers; thus, the underneath reinforcement layers could not be scanned using the GPR machine.
- The infrared camera scans show that the temperature distribution that is caused by the sunlight varies at the external surfaces of the concrete panels and it is higher than that at the front face of the backfill soil; therefore, the infrared waves could not pass through the concrete panels and the gaps between the panels and the backfill soil could not be detected.
- Based on the sieve analysis results, the backfill soils of Walls 179L and CC1-3 fall within the acceptable range of the TxDOT specifications, while the backfill soil of Wall 264R fails to meet the TxDOT specifications as it has excessive fine content.
- The Proctor Compaction test results show that the backfill soils of Walls 264R and 179L failed to achieve the optimum dry density value of 125 pcf, as all the values conducted from the test were less than the specified limit.
- The Triaxial test results revealed that the selected backfill soil of the new section (BH1 location) of Wall 264R has bad shear strength properties which might cause the poor performance of the wall.
- The Triaxial test results also indicate that the backfill soil of Wall 179L has met the minimum friction angle at both borehole locations.
- The angle of repose test results show that all the soil samples of Walls CC1-3 have met the minimum friction angle recommended by TxDOT specifications.

- The results of the numerical modeling of Wall CC1 show that stresses developed in the structural parts were within the material strength properties. The possible cause of the bad performance could be due the acute angle between Walls CC1 and CC2 which caused overlapping of steel grids, and bending of steel grids. Walls to be placed in front of bridge abutments should have a 1.5 ft minimum and 3 ft desirable clearance from back of wall panel to face of abutment cap (TxDOT (2018)).
- The parametric study results show that the overall lateral wall movement of HDPE reinforced MSE walls are higher by 0.5-0.75 inches than steel grid reinforced MSE walls.
- Based on the parametric study results, the lateral wall movement tends to increase for both types of earth reinforcement, steel grids or HDPE geogrids, when the pore pressure is applied, breakage/slippage of reinforcement is considered, or the reinforcement length is taken as 0.7H. However, the PCP compressive strength seems to have no effect on the lateral wall movement.
- These results also show that overall movement tends to decrease slightly when the backfill soil is cohesive. However, an MSE wall is not recommended to be built with a cohesive backfill soil. This is because it has poor permeability characteristics which may cause added pore water pressure.
- The results of the parametric study also indicate that the maximum developed stresses in earth reinforcement of both types of earth reinforcement, steel grids or HDPE geogrids, were not affected by the reinforcement length or the PCP

compressive strength. However, it tends to increase when pressure is applied or breakage/slippage of reinforcement is considered.

- By comparing the ultimate stresses developed in the reinforcement of the parametric study models to their respective pullout and rupture limits calculated based on the FHWA (2009) code, it was concluded that the rupture limits of the steel grid reinforced MSE walls are conservative, while for the HDPE geogrid reinforced MSE walls, it was found that the pullout limits are more conservative than the rupture limits. The pullout limits were found to be very critical for the steel grid type when the pore pressure is applied and the breakage/slippage of reinforcement is considered.
- Based on the regression analysis, the wall parameters that were found to be significant in the MLR model are the reinforcement type, the pore pressure, the reinforcement length, the breakage/slippage of reinforcement, and the cohesion of the backfill soil. The PCP compressive strength parameter was excluded from the regression model as it appeared to have no correlation with the lateral wall movement.
- A logarithmic term had to be introduced in the MLR model to better estimate the effect of the wall parameters on the lateral wall movement.
- The MLR equation shows that when the reinforcement type is a HDPE geogrid, the pore pressure is applied, or the reinforcement breakage/slippage is considered, the lateral wall movement tends to increase. On the other hand, when the reinforcement length is taken as 1.0H or the backfill soil is cohesive, the lateral wall movement tends to decrease. It shows also that the presence of pore pressure affects the wall

movement the most, as its respective factor is the highest compared to the other parameter factors.

- According to the structural reliability results, the pullout ultimate limit states of MSE walls indicate that the first few reinforcement layers from the top of an MSE wall are critical to pullout. It also shows that increasing the reinforcement spacing increases significantly the pullout probability of failure, increasing the friction angle of the backfill soil decreases slightly the pullout probability of failure, while changing the backfill unit weight seems to have no effect on the MSE structural safety.
- On the other hand, the rupture ultimate limit states show that only when the reinforcement spacing is high, the reinforcement layers that exist at the very bottom become critical to rupture. The results also show that increasing the friction angle of the backfill soil decreases slightly the rupture probability of failure, while increasing the backfill unit weight increases the rupture probability of failure.
- The comparison of the serviceability limit states of the pullout and rupture reduction factors of the FHWA (2009) measured from multiple wall heights shows that the pullout recommended factor by the FHWA (2009) is conservative for wall heights above 40 ft, and a modified reduction factor for the pullout limit state shall be applied when the wall heights are below 40 ft. On the other hand, it shows that the rupture recommended factor by the FHWA (2009) is conservative for the wall heights that are below 60 ft, while a modification factor for the rupture limit is needed when the wall heights are above 60 ft.

- The structural reliability results were found to be in good agreement with the results conducted from the parametric study, as the modeled MSE wall height used for the parametric study is 30 ft. The parametric study results show that the pullout limits are critical for the steel grid type MSE walls, while the structural reliability results show that when the wall height is taken as 30 ft, the recommended pullout factor, which is 0.9, is not sufficient and a reduced reduction factor for the pullout shall be applied.

7.3 Future Research

- Long-term evaluation using the 3D robotic laser scanner, SX10, can be conducted on the MSE walls to determine any ongoing movements of the precast panels.
- The MSE walls can be instrumented during the construction phase using strain gauges installed at the earth reinforcement to check for the accuracy of the MSE wall design methods.
- Different wall parameters for the parametric study can be considered to evaluate their effect on the wall movement and the developed stresses in earth reinforcement.
- A regression analysis can be developed on the ultimate tensile stresses of earth reinforcement obtained from a parametric study generated on modeled MSE walls.
- HDPE reinforced MSE walls can be investigated using the structural reliability analysis method.

Appendix A

RESISTANCE FACTORS, Φ, FOR TENSILE AND PULLOUT RESISTANCE FOR MSE WALLS

Reinforcement Type and Loading Condition			Resistance Factor
Metallic reinforcement and connectors	Strip reinforcements [A]		
		Static loading	0.75
		Combined static/earthquake loading	1.00
		Combined static/traffic barrier impact [B]	1.00
	Grid reinforcements [A, C]		
		Static loading	0.65
		Combined static/earthquake loading	0.85
		Combined static/traffic barrier impact [B]	0.85
Geosynthetic reinforcement and connectors		Static loading	0.90
		Combined static/earthquake loading	1.20
		Combined static/traffic barrier impact [B]	1.20
Pullout resistance of tensile reinforcement (metallic and geosynthetic)		Static loading	0.90
		Combined static/earthquake loading	1.20
		Combined static/traffic barrier impact [B]	1.00

Notes:

A. Apply to gross cross-section less sacrificial area. For sections with holes, reduce gross area in accordance with AASHTO (2007) Article 6.8.3 and apply to net section less sacrificial area.

B. Combined static/traffic barrier impact resistance factors are not presented in AASHTO.

C. Applies to grid reinforcements connected to rigid facing element, e.g., a concrete panel or block. For grid reinforcements connected to a flexible facing mat or which are continuous with the facing mat, use the resistance factor for strip reinforcements.

Appendix B

OUTPUT STATISTICS OF THE MLR MODEL

The REG Procedure
Model: MODEL1
Dependent Variable: y

Output Statistics											
						DFBETAS					
Obs	Residual	RStudent	Hat Diag H	Cov Ratio	DFFITS	Intercept	x1	x2	x3	x4	x5
1	0.0517	1.6001	0.0938	0.9410	0.5146	0.2101	-0.2101	-0.2101	-0.2101	-0.2101	-0.2101
2	-0.009587	-0.2903	0.0938	1.2140	-0.0934	-0.0381	0.0381	-0.0381	0.0381	0.0381	0.0381
3	0.0167	0.5067	0.0938	1.1922	0.1630	0.0665	-0.0665	-0.0665	0.0665	-0.0665	-0.0665
4	-0.0600	-1.8710	0.0938	0.8566	-0.6018	-0.2457	0.2457	-0.2457	-0.2457	0.2457	0.2457
5	-0.0558	-1.7325	0.0938	0.9002	-0.5572	-0.2275	0.2275	0.2275	0.2275	-0.2275	0.2275
6	-0.007115	-0.2154	0.0938	1.2189	-0.0693	-0.0283	0.0283	-0.0283	0.0283	-0.0283	0.0283
7	0.0363	1.1096	0.0938	1.0774	0.3569	0.1457	-0.1457	-0.1457	0.1457	0.1457	-0.1457
8	-0.0208	-0.6315	0.0938	1.1746	-0.2031	-0.0829	0.0829	-0.0829	-0.0829	-0.0829	0.0829
9	0.0509	1.5720	0.0938	0.9495	0.5056	0.2064	-0.2064	-0.2064	-0.2064	-0.2064	-0.2064
10	-0.0105	-0.3182	0.0938	1.2118	-0.1023	-0.0418	0.0418	-0.0418	0.0418	0.0418	0.0418
11	0.0127	0.3843	0.0938	1.2059	0.1236	0.0505	-0.0505	-0.0505	0.0505	-0.0505	-0.0505
12	-0.0610	-1.9021	0.0938	0.8467	-0.6118	-0.2498	0.2498	-0.2498	-0.2498	0.2498	0.2498
13	0.0414	1.2704	0.0938	1.0359	0.4086	0.1668	-0.1668	-0.1668	-0.1668	0.1668	-0.1668
14	-0.009623	-0.2914	0.0938	1.2139	-0.0937	-0.0383	0.0383	-0.0383	0.0383	-0.0383	0.0383
15	0.0336	1.0260	0.0938	1.0975	0.3300	0.1347	-0.1347	-0.1347	0.1347	0.1347	-0.1347
16	-0.0245	-0.7451	0.0938	1.1556	-0.2396	-0.0978	0.0978	-0.0978	-0.0978	-0.0978	0.0978
17	0.0504	1.5585	0.0938	0.9535	0.5013	0.2046	-0.2046	-0.2046	-0.2046	-0.2046	0.2046
18	-0.0171	-0.5195	0.0938	1.1906	-0.1671	-0.0682	0.0682	-0.0682	0.0682	0.0682	-0.0682
19	0.0240	0.7288	0.0938	1.1585	0.2344	0.0957	-0.0957	-0.0957	0.0957	-0.0957	0.0957
20	-0.0591	-1.8409	0.0938	0.8661	-0.5921	-0.2417	0.2417	-0.2417	-0.2417	0.2417	-0.2417
21	-0.0350	-1.0693	0.0938	1.0872	-0.3439	-0.1404	0.1404	0.1404	0.1404	-0.1404	-0.1404
22	-0.0118	-0.3571	0.0938	1.2085	-0.1149	-0.0469	0.0469	-0.0469	0.0469	-0.0469	-0.0469
23	0.0431	1.3255	0.0938	1.0208	0.4263	0.1741	-0.1741	-0.1741	0.1741	0.1741	0.1741
24	-0.0183	-0.5564	0.0938	1.1857	-0.1789	-0.0731	0.0731	-0.0731	-0.0731	-0.0731	-0.0731
25	0.0495	1.5268	0.0938	0.9630	0.4911	0.2005	-0.2005	-0.2005	-0.2005	-0.2005	0.2005
26	-0.0180	-0.5455	0.0938	1.1871	-0.1755	-0.0716	0.0716	-0.0716	0.0716	0.0716	-0.0716
27	0.0206	0.6252	0.0938	1.1756	0.2011	0.0821	-0.0821	-0.0821	0.0821	-0.0821	0.0821
28	-0.0600	-1.8701	0.0938	0.8568	-0.6015	-0.2456	0.2456	-0.2456	-0.2456	0.2456	-0.2456
29	0.0429	1.3162	0.0938	1.0234	0.4233	0.1728	-0.1728	-0.1728	-0.1728	0.1728	0.1728
30	-0.0143	-0.4320	0.0938	1.2010	-0.1390	-0.0567	0.0567	-0.0567	0.0567	-0.0567	-0.0567
31	0.0406	1.2463	0.0938	1.0424	0.4008	0.1636	-0.1636	-0.1636	0.1636	0.1636	0.1636
32	-0.0219	-0.6644	0.0938	1.1694	-0.2137	-0.0872	0.0872	-0.0872	-0.0872	-0.0872	-0.0872
33	-0.0224	-0.6813	0.0938	1.1666	-0.2191	-0.0895	-0.0895	0.0895	0.0895	0.0895	0.0895
34	0.0236	0.7175	0.0938	1.1605	0.2308	0.0942	0.0942	0.0942	-0.0942	-0.0942	-0.0942
35	-0.0258	-0.7853	0.0938	1.1482	-0.2526	-0.1031	-0.1031	0.1031	-0.1031	0.1031	0.1031
36	0.0325	0.9926	0.0938	1.1051	0.3192	0.1303	0.1303	0.1303	0.1303	-0.1303	-0.1303
37	-0.0397	-1.2177	0.0938	1.0499	-0.3916	-0.1599	-0.1599	0.1599	0.1599	-0.1599	0.1599
38	0.0206	0.6250	0.0938	1.1756	0.2010	0.0821	0.0821	0.0821	-0.0821	0.0821	-0.0821

39	-0.0262	-0.7978	0.0938	1.1459	-0.2566	-0.1048	-0.1048	0.1048	-0.1048	-0.1048	0.1048
40	0.0413	1.2670	0.0938	1.0368	0.4075	0.1664	0.1664	0.1664	0.1664	0.1664	-0.1664
41	-0.0236	-0.7188	0.0938	1.1603	-0.2312	-0.0944	-0.0944	0.0944	0.0944	0.0944	0.0944
42	0.0223	0.6778	0.0938	1.1672	0.2180	0.0890	0.0890	0.0890	-0.0890	-0.0890	-0.0890
43	-0.0272	-0.8265	0.0938	1.1403	-0.2658	-0.1085	-0.1085	0.1085	-0.1085	0.1085	0.1085
44	0.0311	0.9474	0.0938	1.1152	0.3047	0.1244	0.1244	0.1244	0.1244	-0.1244	-0.1244
45	-0.0428	-1.3160	0.0938	1.0235	-0.4233	-0.1728	-0.1728	0.1728	0.1728	-0.1728	0.1728
46	0.0351	1.0715	0.0938	1.0867	0.3446	0.1407	0.1407	0.1407	-0.1407	0.1407	-0.1407
47	-0.0291	-0.8878	0.0938	1.1279	-0.2855	-0.1166	-0.1166	0.1166	-0.1166	-0.1166	0.1166
48	0.0462	1.4218	0.0938	0.9937	0.4573	0.1867	0.1867	0.1867	0.1867	0.1867	-0.1867
49	-0.0191	-0.5807	0.0938	1.1822	-0.1868	-0.0763	-0.0763	0.0763	0.0763	0.0763	-0.0763
50	0.0100	0.3041	0.0938	1.2130	0.0978	0.0399	0.0399	0.0399	-0.0399	-0.0399	0.0399
51	-0.0135	-0.4100	0.0938	1.2034	-0.1319	-0.0538	-0.0538	0.0538	-0.0538	0.0538	-0.0538
52	0.0286	0.8715	0.0938	1.1313	0.2803	0.1144	0.1144	0.1144	0.1144	-0.1144	0.1144
53	-0.0374	-1.1450	0.0938	1.0686	-0.3683	-0.1503	-0.1503	0.1503	0.1503	-0.1503	-0.1503
54	0.007040	0.2131	0.0938	1.2190	0.0685	0.0280	0.0280	0.0280	-0.0280	0.0280	0.0280
55	-0.0193	-0.5866	0.0938	1.1814	-0.1887	-0.0770	-0.0770	0.0770	-0.0770	-0.0770	-0.0770
56	0.0326	0.9950	0.0938	1.1046	0.3200	0.1306	0.1306	0.1306	0.1306	0.1306	0.1306
57	-0.0202	-0.6141	0.0938	1.1773	-0.1975	-0.0806	-0.0806	0.0806	0.0806	0.0806	-0.0806
58	0.009986	0.3024	0.0938	1.2131	0.0973	0.0397	0.0397	0.0397	-0.0397	-0.0397	0.0397
59	-0.0147	-0.4458	0.0938	1.1995	-0.1434	-0.0585	-0.0585	0.0585	-0.0585	0.0585	-0.0585
60	0.0273	0.8317	0.0938	1.1393	0.2675	0.1092	0.1092	0.1092	0.1092	-0.1092	0.1092
61	-0.0402	-1.2330	0.0938	1.0459	-0.3966	-0.1619	-0.1619	0.1619	0.1619	-0.1619	-0.1619
62	0.0190	0.5780	0.0938	1.1826	0.1859	0.0759	0.0759	0.0759	-0.0759	0.0759	0.0759
63	-0.0220	-0.6694	0.0938	1.1686	-0.2153	-0.0879	-0.0879	0.0879	-0.0879	-0.0879	-0.0879
64	0.0363	1.1101	0.0938	1.0773	0.3570	0.1458	0.1458	0.1458	0.1458	0.1458	0.1458

Sum of Residuals	0
Sum of Squared Residuals	0.06870
Predicted Residual SS (PRESS)	0.08364

References

- Abaqus, V. (2014). 6.14 Documentation. Dassault Systemes Simulia Corporation, 651.
- Abdel-Mohti, A., & Khodair, Y. (2014). Analytical investigation of pile–soil interaction in sand under axial and lateral loads. International Journal of Advanced Structural Engineering (IJASE), 6(1), 54.
- Abdelouhab, A., Dias, D., & Freitag, N. (2011). Numerical analysis of the behaviour of mechanically stabilized earth walls reinforced with different types of strips. Geotextiles and Geomembranes, 29(2), 116-129.
- Adams, M. T., & Nicks, J. E. (2017). Development of a Risk Assessment for MSE Wall Projects. In Geotechnical Frontiers (pp. 94-101).
- Allen, T. M., Bathurst, R. J., Holtz, R. D., Walters, D., & Lee, W. F. (2003). A new working stress method for prediction of reinforcement loads in geosynthetic walls. Canadian Geotechnical Journal, 40(5), 976-994.
- Allen, T., Christopher, B., Elias, V., & DeMaggio, J. (2001). Development of the simplified method for internal stability design of mechanically stabilized earth walls (No. WA-RD 513.1,). The Department.
- Almomani, M., & VISITOR, Y. S. (2018). EVALUATION OF FIBER REINFORCED POLYMER (FRP) STRENGTHENING FOR DETERIORATED BRIDGE BENT CAPS (Doctoral dissertation).
- Alzamora, P. E., Enrique, D., & Anderson, S. A. (2009). Review of mechanically stabilized earth wall performance issues (No. 09-2745).
- Ambauen, S. J. (2014). Numerical simulation of mechanically stabilized earth walls for parametric evaluation of behavior under surcharge loading.

- American Association of State Highway and Transportation Officials. (2016a). “Manual for Bridge Evaluation, 2nd Edition, with 2011, 2013, 2014, 2015, and 2016 Interim Revisions.” C3, Washington, DC.
- American Association of State Highway and Transportation Officials. (2016b). AASHTO LRFD Bridge Design Specifications, Customary U.S. Units, 7th Edition, with 2015 and 2016 Interim Revisions, Farmington Hills, MI.
- Armour, T. A., Bickford, J., & Pfister, T. (2004). Repair of failing MSE railroad bridge abutment. In GeoSupport 2004: Drilled Shafts, Micropiling, Deep Mixing, Remedial Methods, and Specialty Foundation Systems (pp. 380-394).
- ASTM International. (2019). A884/A884M-19 Standard Specification for Epoxy-Coated Steel Wire and Welded Wire Reinforcement.
- Bathurst, R. J., Miyata, Y., Nernheim, A., & Allen, A. M. (2008). Refinement of K-stiffness method for geosynthetic-reinforced soil walls. Geosynthetics International, 15(4), 269-295.
- Bathurst, R. J., Nernheim, A., & Allen, T. M. (2009). Predicted loads in steel reinforced soil walls using the AASHTO Simplified Method. Journal of Geotechnical and Geoenvironmental Engineering, 135(2), 177-184.
- Bell, J. R., Stilley, A. N., & Vandre, B. (1975). Fabric retained earth walls. In Engineering Geology & Soils Engineering Symp Proc (Vol. 13).
- Berg, R. R., Christopher, B. R., Samtani, N. C., & Berg, R. R. (2009). Design of mechanically stabilized earth walls and reinforced soil slopes–Volume I (No. FHWA-NHI-10-024). United States. Federal Highway Administration.
- Budge, A. S., Bay, J. A., & Anderson, L. R. (2006). Calibrating vertical deformations in a finite element model of an MSE wall. In GeoCongress 2006: Geotechnical Engineering in the Information Technology Age (pp. 1-5).

- Chalermyanont, T., & Benson, C. H. (2004). Reliability-based design for internal stability of mechanically stabilized earth walls. Journal of Geotechnical and Geoenvironmental Engineering, 130(2), 163-173.
- Ghazavi, M., Hosseini, M., & Mollanouri, M. (2008). A comparison between angle of repose and friction angle of sand. In The 12th International Conference for International Association for Computer Methods and Advances in Geomechanics (IACMAG) (pp. 1-6).
- Chen, D. H., Nazarian, S., & Bilyeu, J. (2007). Failure analysis of a bridge embankment with cracked approach slabs and leaking sand. Journal of Performance of Constructed Facilities, 21(5), 375-381.
- Christopher, B. R. (1993). Deformation response and wall stiffness in relation to reinforced soil wall design.
- Ehrlich, M., & Mitchell, J. K. (1994). Working stress design method for reinforced soil walls. Journal of geotechnical engineering, 120(4), 625-645.
- Elias, V., Christopher, R., & Barry, P. E. (1997). Mechanically Stabilized Earth Walls and Reinforced Soil Slopes Design and Construction Guidelines: FHWA Demonstration Project 82, Reinforced Soil Structures WSEW [ie MSEW] and RSS. Federal Highway Administration.
- Fishman, K. L., Withiam, J. L., & Gladstone, R. A. (2010). Metal Loss for Metallic Reinforcements and Implications for LRFD Design of MSE Walls. In Earth Retention Conference 3 (pp. 844-853).
- Hatami, K., & Bathurst, R. J. (2005). Development and verification of a numerical model for the analysis of geosynthetic-reinforced soil segmental walls under working stress conditions. Canadian Geotechnical Journal, 42(4), 1066-1085.

- Helwany, S. M., Wu, J. T., & Froessl, B. (2003). GRS bridge abutments—an effective means to alleviate bridge approach settlement. Geotextiles and Geomembranes, 21(3), 177-196.
- Hossain, M. S., Kibria, G., Khan, M. S., Hossain, J., & Taufiq, T. (2011). Effects of backfill soil on excessive movement of MSE wall. Journal of Performance of Constructed Facilities, 26(6), 793-802.
- Huang, B., Bathurst, R. J., & Hatami, K. (2009). Numerical study of reinforced soil segmental walls using three different constitutive soil models. Journal of Geotechnical and Geoenvironmental engineering, 135(10), 1486-1498.
- Kibria, G., Hossain, M. S., & Khan, M. S. (2013). Influence of soil reinforcement on horizontal displacement of MSE wall. International Journal of Geomechanics, 14(1), 130-141.
- Kim, D., & Salgado, R. (2011). Load and resistance factors for internal stability checks of mechanically stabilized earth walls. Journal of Geotechnical and Geoenvironmental Engineering, 138(8), 910-921.
- Kim, D., Bhowmik, S. K., & Willmer, J. L. (2010). A case history of MSE wall failure: Finite element modeling and evaluation. In GeoFlorida 2010: Advances in Analysis, Modeling & Design (pp. 2232-2242).
- Lee, W. F. (2000). Internal stability analyses of geosynthetic reinforced retaining walls (Doctoral dissertation, University of Washington).
- Liu, H., & Won, M. S. (2009). Long-term reinforcement load of geosynthetic-reinforced soil retaining walls. Journal of geotechnical and geoenvironmental engineering, 135(7), 875-889.
- Lubliner, J., Oliver, J., Oller, S., & Oñate, E. (1989). A plastic-damage model for concrete. International Journal of solids and structures, 25(3), 299-326.

- Mahmood, T. (2009). Failure analysis of a mechanically stabilized earth (MSE) wall using finite element program plaxis.
- Martin, O. (2010). Comparison of different constitutive models for concrete in ABAQUS/explicit for missile impact analyses. JRC Scientific and Technical Reports.
- Meyerhof, G. (1953). The bearing capacity of foundations under eccentric and inclined loads. In Proc. of the 3rd Int. Conf. on SMFE (Vol. 1, pp. 440-445).
- Mitchell, J. K., and W. C. Villet. (1987). Reinforcement of earth slopes and embankments. NCHRP Rep. (290). Washington, DC: Transportation Research Board, National Research Council.
- Neely, W. J., & Tan, S. L. (2010). Effects of second-order design factors on the behavior of MSE walls. In Earth Retention Conference 3 (pp. 522-530).
- Obaidat, Y. (2011). Structural retrofitting of concrete beams using FRP-debonding issues. Lund University.
- Reddy, D. V., & Navarrete, F. (2008). Experimental and analytical investigation of geogrid MSE walls. In From Research to Practice in Geotechnical Engineering (pp. 277-291).
- Riad, M. (2017). Quantitative Non-destructive Evaluation (NDE) of FRP Laminate-Concrete Bond Strength (Doctoral dissertation).
- Samtani, N. C., & Alexander, D. E. (2005). Remediation of a failing MSE wall by jet grouting. In Innovations in Grouting and Soil Improvement (pp. 1-15).
- Scarborough, J. A. (2005). A tale of two walls: Case histories of failed MSE walls. In Slopes and Retaining Structures under Seismic and Static conditions (pp. 1-12).
- Schlosser, F. (1978). History, current development and future developments of reinforced earth. In Proceedings of the Symposium on Soil Reinforcing and Stabilizing

Techniques, sponsored by New South Wales Institute of Technology and the University of Sidney, Australia (pp. 5-28).

- Simulia, D. S. (2011). Abaqus 6.11 theory manual. Providence, RI, USA: DS SIMULIA Corp.
- Tarawneh, B., Al Bodour, W., & Masada, T. (2017). Inspection and Risk Assessment of Mechanically Stabilized Earth Walls Supporting Bridge Abutments. Journal of Performance of Constructed Facilities, 32(1), 04017131.
- Texas Department of Transportation. (2017). Concrete repair materials. Departmental Material Specification DMS4655.
- Texas. Department of Transportation. (2014). Standard Specifications for Construction and Maintenance of Highways, Streets, and Bridges: Adopted by the Texas Department of Transportation, November 1, 2014. Texas Department of Transportation.
- Timilsina, S. (2018). In-Service Performance Evaluation of Fire and Impact Damaged Bridges with CFRP Laminate Strengthening (Doctoral dissertation).
- Vidal, H. (1969). The principle of reinforced earth. Highway research record, (282).
- Xu, B., Zhang, W., Mei, J., Yue, G., & Yang, L. (2019). Optimization of Structure Parameters of Airfield Jointed Concrete Pavements under Temperature Gradient and Aircraft Loads. Advances in Materials Science and Engineering.
- Yoo, C., & Kim, S. B. (2008). Performance of a two-tier geosynthetic reinforced segmental retaining wall under a surcharge load: full-scale load test and 3D finite element analysis. Geotextiles and Geomembranes, 26(6), 460-472.
- Zevgolis, I. E., & Bourdeau, P. L. (2008). Stochastic modeling of redundancy in Mechanically Stabilized Earth (MSE) walls. In GeoCongress 2008: Geosustainability and Geohazard Mitigation (pp. 1179-1186).

Biographical Information

Zaid Momani received his Bachelor of Science degree in civil engineering from University of Jordan, Jordan in 2015 and his master's degree in Structural Engineering from University of Jordan, Jordan in 2016. His graduation project was on designing an eight-story building based on ribbed slabs. His Master's thesis was on Influence of Openings on Shear Walls Using the International Building Code (IBC)". His research interest includes improving the public safety of earth retaining wall structures and evaluating the performance special concrete mixes such as Ultra High Performance-Fiber Reinforced Concrete "UHP-FRC".